Aalto University
MASTER'S THESIS 2018

Feasibility study of renovation of a residential building in near zero-energy building

Mykhailo Prisikar

Thesis submitted in partial fulfillment of the requirements for the degree of Master of Science in Technology.
Otaniemi, 28 May 2018

Supervisor: Prof. Matti Lehtonen
Advisor: D.Sc. (Tech.) John Millar

Aalto University
School of Electrical Engineering
Master's Programme in Automation and Electrical Engineering

Aalto University

Abstract

Aalto University, P.O. Box 11000, FI-00076 Aalto www.aalto.fi

Author
Mykhailo Prisikar

Title
Feasibility study of renovation of a residential building in near zero-energy building

School School of Electrical Engineering

Master's programme Automation and Electrical Engineering

Major Electrical Power and Energy Engineering **Code** ELEC3024

Supervisor Prof. Matti Lehtonen

Advisor D.Sc. (Tech.) John Millar

Level Master's thesis **Date** 28 May 2018 **Pages** 13+60 **Language** English

Abstract

In this feasibility study, a renovation of a residential building in near zero-energy building was studied.

For this purpose, a selection of available on the market solar and wind energy conversion systems was taken. The shortlisted systems were, then, compared along key criteria that define their fit and efficiency for application in on-site energy generation. The consumption and electricity prices used for the purposes of this study were forecasted for the entire project period. These forecasts, together with the results from the energy conversion systems comparison, were then implemented in a simulation model that extrapolates over the period of 25 years the performance of various alternatives for the renovation of the residential building.

Based on the simulation results, the most efficient, and, therefore, optimal, configuration of renewable energy sources for the studied site, in terms of maximum on-site generation, is the use of a combination of wall and roof-installed photovoltaic panels. Moreover, the energy storage option is not feasible for any of the simulated configurations. Finally, the electricity purchase contract for the building should be based on the spot market price formation.

The overall implementation of the optimal configuration requires EUR 70387.97 of initial costs. The total net present cost is equal to EUR 201503.00, whereas the levelized cost of electricity is equal to EUR 0.117. During the project implementation, 50344.48 kWh will be purchased from the grid and 36461.58 kWh will be sold, yielding 13882.90 kWh of net purchase. The fraction of renewables in the overall consumption, during the entire project, will be 55.16 percent. The payback period of the system configuration exceeds the project implementation period.

The study was funded by Aalto University Student Union (AYY).

Keywords near zero-energy building, renewable energy generation, wind energy conversion, solar energy conversion, energy consumption, electricity market price

1 CONTENTS

SYMBOLS AND ABBREVIATIONS

Symbols

A	*swept area of the rotor [m²]*
$A_{weibull}$	*scale parameter*
$C_{annual,total}$	*total annual cost [€/yr]*
d	*distance [m]*
E	*vertical irradiance [W/m²]*
$E_{defferable}$	*deferrable load served [kWh/yr]*
E_{gap}	*gap's energy of the material (1.12 eV for crystalline Si)*
$E_{grid\ sales}$	*energy sold to grid [kWh/yr]*
E_{load}	*AC load served [kWh/yr]*
E_{served}	*total electrical load served [kWh/yr]*
$F_{t,T}$	*futures price*
G	*effective irradiance [W/m²]*
G_{ref}	*reference irradiance [W/m²]*
I	*current of cell [A]*
I_D	*diode current [A]*
I_O	*inverse saturation current [A]*
I_{ph}	*photocurrent [A]*
i	*discount rate [%]*
k	*Boltzmann's constant (1.381 E-23) [J/K]*
k	*von Karman's constant (0.40)*
$k_{weibull}$	*shape parameter*
L	*Monin-Obukhov length [m]*
muI_{SC}	*temperature coefficient of the photocurrent [°C]*
N_{cs}	*number of cells in series*
P_{air}	*power in the airflow [W]*
$P_{t,T}$	*risk premium*
P_{wt}	*power extracted by the wind generator rotor [W]*
q	*charge of the electron (1.602·E-19) [C]*
R_{poject}	*project lifetime [yr]*
R_s	*series resistance [ohm]*
R_{sh}	*shunt resistance [ohm]*
T	*temperature [°C]*
T_c	*effective cell's temperature [°K]*
$T_{c\ ref}$	*reference cell's temperature [°K]*
u, U	*air speed [m/s]*
u_*	*air friction speed [m/s]*
V	*output voltage [V]*

V_w	*the speed of the free wind [m/s]*
y_t	*data on which the ARMA model is to be applied.*
z_0	*roughness length of the surface*
α	*elevation angle*
β	*tilt angle*
γ	*azimuth*
γ	*diode quality factor*
ε	*weighted sum of errors*
ρ	*air density (1.225) [kg/m³]*
φ_1, φ_2	*AR coefficients*

Abbreviations

AC	*alternating current*
CRF	*capital recovery factor*
DC	*direct current*
HAWT	*horizontal axis wind turbines*
HIRLAM	*high-resolution model*
IEA	*International Energy Agency*
ISC	*short-circuit current*
LCOE	*levelized cost of energy*
MPP	*maximum power point*
MPPT	*maximum power point tracking*
NPC	*net present cost*
NPS	*Nord Pool Spot*
NREAP	*National Renewable Energy Action Plan*
nZEB	*near zero-energy building*
PV	*photovoltaic*
PWM	*pulse width modulation*
RC	*roughness classes*
RES	*renewable energy sources*
RIX	*ruggedness index*
Si	*silicon*
STC	*standard testing conditions*
SWT	*small wind turbine*
VAT	*value added tax*
VAWT	*vertical axis wind turbines*
VOC	*open-circuit voltage*

2 INTRODUCTION

2.1 BACKGROUND AND FOCUS OF THE STUDY

To prevent global warming and climate change, Directive 2009/28/EC sets targets to reduce CO2 emissions by 2020 to 20%. [1] The main ways of reducing CO2 emissions is to increase the energy efficiency and the renewable energy generation. Buildings are responsible for 36% of the global greenhouse gas emissions and 40% of the overall electricity consumption. [2] Energy Efficiency Buildings Directive 2010/31 EU 2010 was signed by European Parliament, with the aim to set the main objectives and goals: starting from 2020, all buildings to be built must be nearly zero-energy buildings (nZEB) and implement onsite renewable energy generation sources. [3] nZEB is defined by Directive as the high energy performance building, that can cover its energy needs by nearby or onsite generation. [3] In addition, the Directive requires buildings that will be renovated in the near future to consider the possibility of transformation of the old building in nZEB. In Finland, the Directive is implemented in a shape of National Building Code [4], D3 Energy Management in Buildings Directive [4] and in the Land Use and Building Act. [5]

The main purpose of this thesis is to study and determine the cost-effective ways of renewable energy sources (RES) use in the renovation of buildings in nZEB in the urban area. The study building is selected among Aalto University Student Union's (AYY) real-estate that should be renovated during next years. The selected building is an eight-floor student dormitory with 64 apartments situated in Helsinki at Turkismiehentie 8. The reason why this building was selected is that it represents the common Finnish buildings, built in 70's from concrete, so this study can be extrapolated to similar buildings for further renovation projects and studies.

Other tasks of this study are to compare the solar and wind generation capabilities in the urban area and compare them to residential consumption profile. Since the studied site is already connected to the electricity grid, different types of energy supply, as well as long-term electricity price forecasting, will be studied. The feasibility study will optimize electricity trading and consumption options to achieve the most cost-optimal RES solution.

The objective if this thesis is to study closely the modern simulation and optimization software for RES design and planning. Another important goal is to determine the future directions and goals of further researches. At the time of writing this study, the author has not found such detailed studies comparing solar and wind-based energy generations in the urban environment in the long-term scale.

2.2 SCOPE AND STRUCTURE

The study will cover a 25-year period. The forecast of electricity consumption and its cost is made from 2019 to 2044. Historical data for modeling and time series are used until the end of 2016. 2017 is used to test the model for its correlation with real-data values. The resolution of the data is an hour, respectively one year will be represented

by 8760 hours, 365 days. there are no adjustments for leap years for the sake of model simplicity, consistency and comparability among the years.

This study considers RES exclusively in the form of photovoltaics and a wind energy conversion. The choice is based on rapid development and as a consequence, a significant reduction in prices for photovoltaics. Wind turbines will be considered as small wind turbines (SWT) that can be installed on-site. Heat pumps will not be considered in the study since they are mostly used in space heating and cooling systems. Other RES, such as solar concentrating, geothermal and biomass are not considered since they cannot be installed in the immediate vicinity of the study site or their installation may be complicated and time consumed.

The study considers only electricity consumption of the studied site and as a consequence does not takes into account the consumption of heating. The ratio between generation and consumption also will not take into account the heating energy obtained from the district heating.

Chapter 2 is the introductory part and describes the problem and the structure of the study. The feasibility study consists of three main parts: on-site generation simulations, consumption analysis and forecast, and the electricity price formation. Please, see details in Appendix 1. On-site energy generation part consists of Chapters 3 and 4. Chapter 3 describes the solar energy conversion systems. The chapter will guide through the basic principles of solar panels operation, selection, and orientation. Based on meteorological synthetic data and the studied area visualization, the hourly based generation volumes will be generated. This chapter will discuss the installation and generation of photovoltaic (PV) panels on the roof and on one of the building's walls. In addition, this chapter will cover the inverter selection and system concepts. Chapter 4 describes the wind energy conversion systems. Topographical analysis, wind speed modeling, turbine selection and positioning will be introduced in this chapter. The outcome of the simulation is the hourly generated energy from the selected turbine, installed on the roof of the studied site.

The consumption of the studied building is discussed in Chapter 5. During this chapter, the time-series model will be created, that, as a result, will be able to predict the consumption of electricity during the project. Seasonal fluctuations and other behavioral patterns are taken into account.

During the study, it will be revealed that the on-site energy generation should be insufficient to fully cover the electricity consumption over the year. It will also be established that a certain amount of energy could be sold to the grid as surplus. In order to streamline the relationship between energy sellers and studied site, Chapter 6 calculate the long-term electricity price forecast and considered two types of contracts: long term fixed price contract and market-driven contract.

Chapter 7 uses the data from the previous chapters to determine the most optimal RES system configuration. The selected configuration will be optimized and sensitivity

analysis will be conducted. This chapter will also discuss an economic analysis for the project.

3 SOLAR ENERGY GENERATION SIMULATION

3.1 CHAPTER INTRODUCTION

This chapter will study the feasibility of solar energy conversion at the studied site. The whole process will be divided into the preparation and the simulation parts. Simulation part will present the results for further analysis.

The preparation part will consist of the following steps. The metrological data collection and hourly synthetic data generation will determine the solar irradiation. The selection of PV panels, guided by working principles of PV cells and comparison study will select the appropriate PV panel for the system. The justification of layout and interconnection of panels determine the system interactions. This step will also introduce the visualization of the studied site. The last step is the selection of inverters that will be used in PV system. The simulation process will be done in PVSyst software. The results of the simulation are the hourly resolution data of energy generation from wall-mounted and roof-mounted PV systems. This establishes the technical feasibility of the on-site electricity generation.

The major elements of the PV system are the panels, mounting rack tables, cabling, inverters and storage systems if necessary. [6] Mounting rack tables should be taken into account during the simulation since they increase the length of the panel row that should be fitted within site dimensions. The cabling selection is out of the scope of this study so it will not be introduced in this paper, nevertheless, estimated cable losses have been taken into consideration during the simulation process.

The study will utilize all applicable space for PV panel installation that could be found useful during the project. Furthermore, economic balance of the project will be taken into account as one of the main criteria, since the aim of the whole project is to study the feasibility of nZEB.

3.2 PREREQUISITES FOR SOLAR ENERGY GENERATION

Solar power is the cleanest as well as most considerable sustainable energy resource existing. It offers the possibilities to supply a vital percentage of all RES in the nearest future. [7] As reported by the International Energy Agency (IEA), solar power is likely to be the major electric source by 2050. [8]

Figure 1 shows the average annual solar irradiation among European countries. Finland's irradiation is similar to that of Germany, a region that is among the leading marketplaces for photovoltaics. Nevertheless, Finnish government grants 20-25% of

the total fixed costs of the project for housing companies and residential properties. Single houses can apply for the tax deduction from the total installation work. [9]

Based on the National Renewable Energy Action Plan (NREAP), the installation of RES will be raised in Finland by 9.5 % from 2005 to 2020, at the time it ought to be 38 % from the total electricity consumption. [10] This is applicable also to solar energy. At the present, the share of energy from the sun is around 0.01 percent of the total energy generation in the country. [11]

The amount of solar irradiation is almost identical in Southern Finland as in Central European countries; however, a majority of the radiation (1170 kWh/m² annually) is referred in the southern part of Finland during May to August, which shows a great interest in PV development in Finland. [12] The market growth of grid-connected PV systems grew from 8 MW of capacity in 2015 up to 20 MW in 2016. [10]

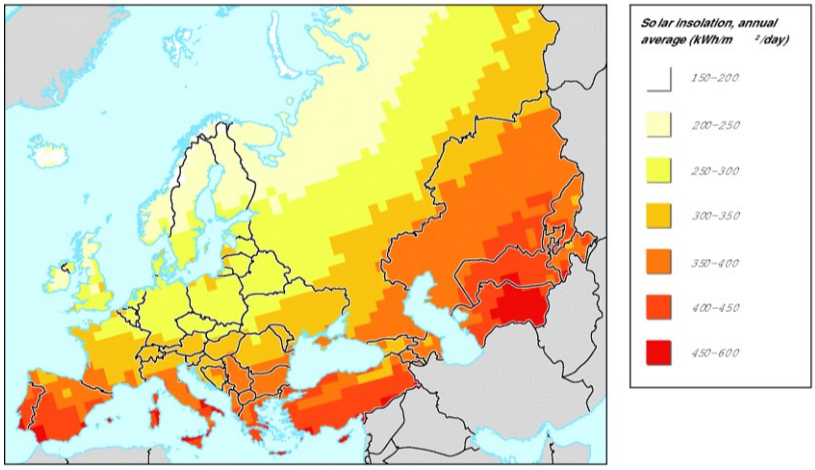

Figure 1: Solar insolation map, the quantification of energy per surface area on the ground [13]

3.3 METHODOLOGY

Chapter 3 study procedure is based on the PVSyst software's guideline. [14]

The PVSyst software selection is based on a comparison of three different products that are able to simulate the PV system: SAM 2017.9.5 by the National Renewable Energy Laboratory [15], the PVLib by Sandia National Laboratories [16] and the PVSyst by University of Geneva [14].

The System Advisor Model is a freeware application that is easy to use but it cannot perform the appropriate shading calculations, does not have a big database of system parts, and cannot perform the panels positioning and interconnection optimization. The PVLib is a freeware software but does not offer any graphical user interface, because PVLib is a plugin for Python or Matlab and, as a consequence, all commands should be done by script coding. This makes it difficult to learn and use all its features. The PVSyst is a shareware product with 30 days' trial period, that includes various

reporting and testing tools. PVSyst is able to simulate shadings and optimize the panel's interconnection.

3.3.1 Finland meteorological characteristics

Since PV energy generation strongly depends on the climate and weather, the reliable meteorological data is the key role for precise electricity generation prediction. This section will introduce the main parameters of irradiance calculations for temperature analysis, which will be used later in energy generation simulations.

The total solar irradiation on the Earth's surface is composed of *direct* and *diffuse* irradiation. The direct irradiance or beam radiation is observed directly from the position of the sun during the day. The direct radiance casts an intense shadow on objects. The diffuse irradiance as in opposition to the direct irradiance, has no specified direction because it is scattered by the atmosphere. [17]

The proportion between diffuse and direct irradiation can differ significantly. This proportion is based on the time of the day and the cloud conditions. When the sky is clear, the direct irradiation prevails on the total irradiation. On cloudy days, the total irradiation is more or less completely diffused. In Finnish weather conditions, especially at winter, the diffuse irradiation dominates in the total irradiation. [18] The amount of irradiation reflection from the ground is called the albedo. Since different surfaces reflect different amounts of radiation, this coefficient varies depending on the location and time of year. For simulation purposes, the albedo coefficient for studying site selected to be 0.20 during the year, and for winter season it will rise to 0.40 due to snow refection. [19] It is assumed, that snow will not block PV panels during the project, because the panels will be cleaned at all time. These cleaning costs are included in the maintenance costs in the simulation, covered in Section 7.2.1.

The climate conditions of the area are ultimately dependent upon the radiation power of the sun, as well as its allocation and temporal variations. Because of cloud cover, the highest possible yearly radiation phases tend to be achieved before perihelion, typically in early June. The daily highest irradiation typically starts before noon, because of cloud cover. According to the Finnish Meteorological Institute, the total annual amount of sunrays is maximum (approximately 1900 hours annually) in the southern part and lowermost (1300 hours annually) in eastern Lapland. [20]

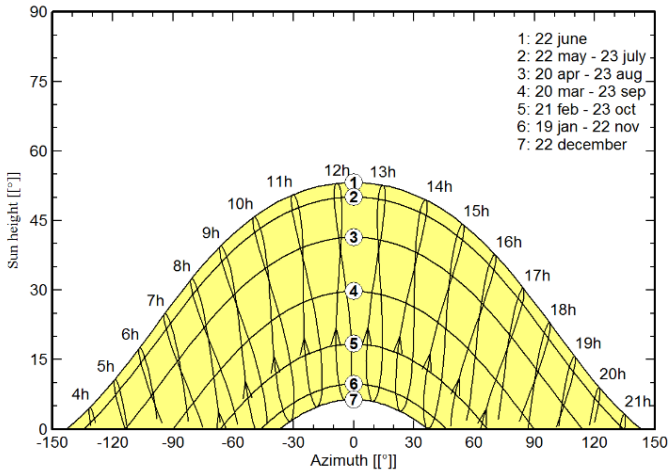

Figure 2: Solar paths at Lat. 60.20N, long. 24.92E [21]

Cloud cover is common in Finland in autumn and winter, expanding from the northwest towards the southeast; around 65% to 85% of the sky is then covered in cloud. In addition, there are overcast days, when the mean cloud covers over 80% of the sky than clear days when the mean cloud cover under 20% of the sky, or partially cloudy days. Clear period takes place commonly in May and June, while minimum frequently in November and December. The average hours of sunlight in Helsinki vary from 0:34 for every day in December to 9:48 every day in July. The typical number of hours of sunlight in Helsinki are 1802 hours per year (of a total potential 4383 hours) with an average of 4:56 of sunlight per day. It is sunny 41.1% of daylight hours. The other 58.9% of daylight hours are usually cloudy and or with shade, haze or lower sun intensity. Figure 2 shows the solar paths during the year, where the sun is in the highest position on 22nd of June and in the lowest position on 22nd of December. This also means that, during the summer time, the sun stays in the sky much longer than at winter time that leads to higher rates of energy generation by PV panels during the summer season. [20]

3.3.2 Synthetic meteorological characteristics generation

The precise PV energy generation simulation needs an hourly resolution meteorological data. Synthetic generation delivers hourly data based on monthly values. This transformation is necessary given that the numerous simulation procedures require to be calculated as instant and pseudo instant values as hourly average and not all needed data is available in hour resolution.

The synthetic meteorological characteristics for simulation were gathered based on Meteonorm 7.1 database. [21] The data was collected at the Helsinki-Ilmala meteorological station at 60.20˚N and 24.92˚E, which is approximately 4 km from the studied area. The data consists of 1964 – 1998 monthly data points each of them representing irradiation, temperature and the wind velocity, which proceed from averages over several years. The synthetic data generation is done by the Meteonorm algorithm which is a part of the PVsyst software. The algorithm is based on the model

suggested by Collares-Pereira [22] for irradiance calculations and Scartezzini [23] for temperature analysis.

The compiled synthetic data consists of four main values:

- *Global horizontal irradiation*. The algorithm adjusts the Markov matrices [24] to consider local conditions which include the turbidity. The output of hourly value from day-to-day values will depend on the Collares-Pereira algorithm. [14]
- *Diffuse horizontal irradiation*. For a synthetic generation, the algorithm utilizes the DirInt model [25] to split global irradiation into diffuse and beam. At the end of every thirty-day period, the diffuse values are renormalized to be able to correspond with the monthly diffuse. This is achieved as a result of a correction when each individual hourly value is adjusted by the ratio between the particular 30-day values with the as-generated-hourly-cumulative 30-day diffuse rate. [14]
- *Ambient temperature*. The temperature needs to be continuous, thus temperature series are generated by 24-hour stochastic slopes, with constraints on the 30-day average value. Throughout the day, temperature acts much rather similar to a sinusoid. The amplitude of this sinusoid is the global day-to-day irradiance and a few hours phase shift. [26, 27] The correlation variables for amplitude and phase shift are based on European area typologies. [28] The PV panels characteristics is temperature sensitive in about 0.4%/°C. [14]
- *Wind velocity*. The wind velocity is required for the estimation of PV modules temperature throughout the operation. The wind on its own is not essential for solar energy generation, therefore this particular model is designed to present a rough approximation of 30-day average as well as wind distributions. This wind speed interpolation must not be utilized for wind energy generation since data is not accurate enough but is a rough approximation. [14]

3.3.3 Photovoltaic cell operating principle

The basic main operating principle of the PV cell is based on the equivalent circuit on Figure 3. This Shockley's one-diode model is used for a cell of a panel and for the whole model. [14]

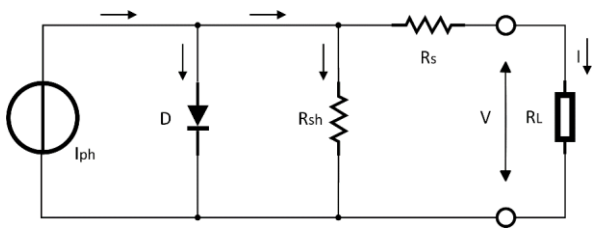

Figure 3: PV cell equivalent circuit

More complex models, which include two different diodes are not used since all future calculations are based on basic input parameters from manufacture sheets that are not

as accurate as the parameters gained from the laboratory tests. Based on that, a small variance in cells will not make a huge impact on the output data. One-diode model considers the two diodes as identical, where the γ coefficient adjusted from 1 to 2, describes the mix between the diodes. [14]

The equation [14] for the one-diode model is described by:

$$I = I_{ph} - I_o \left[\exp\left(\frac{q(V+IR_S)}{N_{cs}kT_c\gamma}\right) - 1\right] - \left[\frac{V+IR_S}{R_{sh}}\right] \quad (1)$$

I_{ph} is determined by irradiance and the temperature of the panel. The one-diode model assumes that I_{ph} is generally proportional to the solar irradiance. The temperature influence is minimal but positive based on parameters stated above. Thus for any situation, the I_{ph} will be calculated based on the reference conditions values: G_{ref} and T_{ref}. [14] and described by:

$$I_{ph} = \left[\frac{G}{G_{ref}}\right] \times \left[I_{ph\,ref} + mul_{SC}(T_c - T_{c\,ref})\right] \quad (2)$$

The diode's reverse saturation current is fluctuated with the PV panel temperature [14], as outlined by:

$$I_o = I_{o\,ref}\left[\frac{T_c}{T_{c\,ref}}\right] \times exp\left[\left(\frac{qE_{gap}}{\gamma k}\right) \times \left(\frac{1}{T_{c\,ref}} - \frac{1}{T_c}\right)\right] \quad (3)$$

3.3.4 Electrical design of photovoltaic cell

For evaluation and selecting between different photovoltaic cells or the actual panels with each other, equal testing conditions are specified. Based on that the I-V cell characteristics are then calculated so the cells could be equally treated. Such standard testing conditions (STC) are part of the IEC 60904/DIN EN 60904 standards [29]:

- Vertical irradiance equals to 1000 W/m²;
- temperature of cell equals to 25°C with ± 2°C tolerance;
- defined light spectrum with the spectral distribution according to IEC 60904-3.

It is good to note, that PV systems almost never run under STC conditions but efficiency is always stated by the manufacturer under such conditions. Generally, the I-V curve is defined by next several values [29]:

- The *maximum power point* (MPP) is the highest power that cell could generate. This value is specified by the maximum product of voltage and current;
- the *short-circuit current* (I_{SC}) is roughly 5 - 15% higher than the MPP current for the crystalline cell;
- the *open-circuit voltage* (V_{OC}) is roughly about 0.6 V.

3.3.5 Irradiation and temperature effects

The power generation along with the I-V curves of PV modules rely upon temperatures and irradiance. Throughout the day, the irradiance varies higher than the temperature. [27] The change in irradiance impact the module current most of all due to the fact that the current is in direct dependency with the irradiance. In cases where irradiance falls by fifty percent, the generated electric power also decreases by fifty percent.

Most PV panels are connected in series, and this is because voltage is stable under such configuration. The stability of voltage is explained by the fact that fluctuating irradiance does not affect voltage. Temperature changes, which do affect voltage, do not change significantly throughout the day. [30]

Generally speaking, the panel voltage depends on the panel temperature. The change in voltage of the PV panel determines the overall system voltage, furthermore the whole PV system layout. [31]

The effects of panel temperature and solar irradiance on the PV panel are shown in Figure 4. As observed from Figure 4 (left), the V_{OC} increases logarithmically by raising the solar radiation, while the I_{SC} raises linearly. The impact of the photovoltaic panel temperature on the panel properties is presented in Figure 4 (right). The major impact of the increased panel temperature is on V_{OC}, which reduces linearly with the panel temperature, therefore the panel efficiency decreases. As is shown in Figure 4 (left), the I_{SC} raises insignificantly with the rise of the panel temperature. [26]

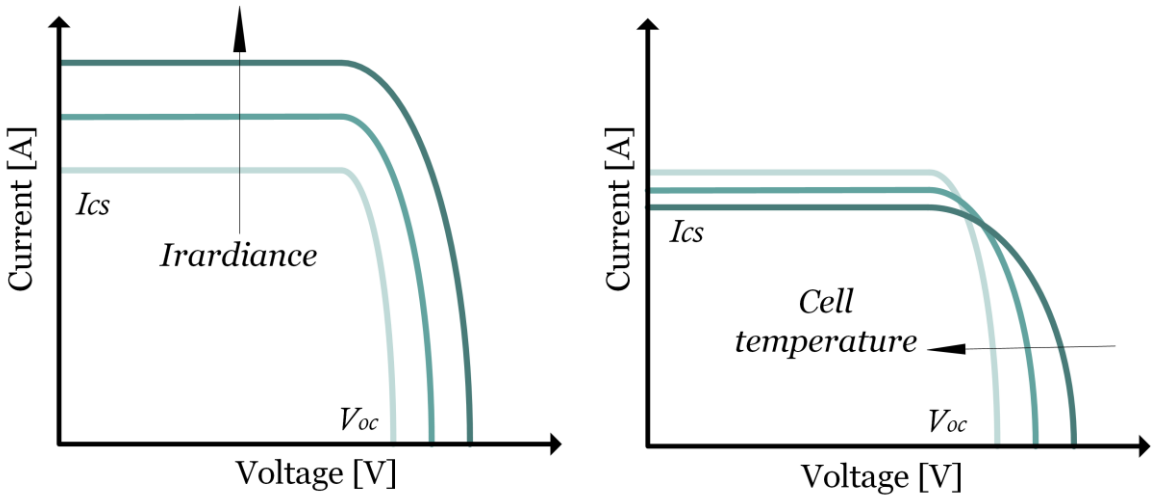

Figure 4: Effects of irradiation and cell temperature on PV cell characteristic (left) increased irradiance and (right) increased the temperature

Various sized cells gain various I-V shape. I_{SC} of the cells is directly proportional to the height and width of the panel. Thus, larger PV cell will be more powerful. The dimensions of the cell have no impact on V_{OC}. [32]

3.3.6 Types of photovoltaic technology

The flat type panels represent 99% of the total PV market and the others are PV concentrators. The main material for PV panes is silicon that has the maximum efficiency at the market. Nearly 90% of all panels are produced from *monocrystalline* (mono-Si) or *polycrystalline* silicon (poly-Si). [26] [31] [33] The rest of the commercially available PV panels are made from amorphous silicon (a-Si), cadmium telluride (CdTe) or copper indium gallium selenide (CIS/CIGS). A huge rise in the manufacturing of mono-Si and poly-Si modules has triggered a massive decrease in price in the last couple of years. [31] [33] [34]

The mono-Si is regarded as the most accessible PV cell material in the world. The average market share for the latest available date (2016) for mono-Si PV panels is 25%. [33] The major benefit of mono-Si is the comparatively high efficiency, ranges from 15% to 19%. In recent years, the efficiency of monocrystalline silicon is about 26%, however, such efficient panels are relatively expensive. [33] The major downside of the mono-Si crystals is the higher manufacturing price, which results from the slow-moving, complicated as well as energy-demanding production process. [31] [35]

The production technique of the poly-Si cells is simpler compared to the production technique of the mono-Si cells, making the poly-Si cells more affordable for the customer. [34] However, the efficiency of a poly-Si cell is a bit lower, around 16% [35].

For grid-connected solar systems, solar cells made from mono-Si and poly-Si are generally used [31], so the selection process will be handled only over these two types of photovoltaic technology.

3.3.7 Selection of photovoltaic panels

A PV cell is commonly 0.1 – 0.4 millimeters thick with 10 by 10 centimeters dimensions. [30] By itself PV cell is able to generate approximately 0.5 V. To achieve higher voltages, several PV cells are interconnected in series. Panel current, therefore, is determined by multiplying the amount of parallel PV cells with the current of a PV cell. Such interconnected PV cells form a PV panel. Common industrial panels provide rated power of 150-330 W, therefore such powers generated at 20-40 V voltage levels of and currents of 7-9 A. [31]

The PV modules include a number of fundamental properties that may be grouped. Electrical, mechanical, and economic factors are the three main criteria that are commonly used in PV panel selection. [36] [37] The fundamental electrical properties, consequently, are efficiency, rated power, temperature V_{OC} and I_{SC}. The fundamental mechanical properties involve the type of cell, dimension, weight, and mounting specifications as well as the requirements specific to the installation area. The economic property is the price of one installed watt. [38]

The selecting of solar panels was based on a comparison of 189 modules from different manufacturers that are certified to be used in EU and Finland. Those panels were distributed by customer ratings so panels with at least three reviews were selected for the following comparison. All characteristics were gained from the manufacturer's

datasheets and the prices were gained from biggest EU PV wholesales websites [39] [40] [41] [42], where the cheapest price on the same module was selected. Appendix 2 shows ten most preferable panels that could be used in a study.

Every panel is suitable for on-roof or on-wall installation. Every panel could withstand high wind flow and snow mass on top of it. [43] All compared PV modules are manufactured for outdoor use for more than 25 years. All panels are manufactured under European specifications and requirements and guarantee the reliability of the unit for the product lifetime. [34] [31]

The AXIpremium AC-290M/156-60S [44] panel was selected to be the best choice among the panels in Appendix 2 for the studied site, due to the following conclusions:

- Due to several types of research, mono-Si *cell type* performs better at lower temperatures e.g. at cold climate, while poly-Si cells are more suited for a dry and warm climate. [45] [37] It was observed that an increase in temperature decreased the efficiency of mono-Si panels lower than of poly-Si panels. [46] Studies showing that the gap between performances stated in datasheets and those measured is more accurate for poly-Si panels then for mono-Si panels. [47] The other important factor is that the system consisting of mono-Si panels is 35% lighter, compared to poly-Si panels. [37] Hence, the selected mono-Si panel is the most suited for a studied site.
- The *rated power* shows the output power of the panel at STC. This value cannot be used for determining the proper panel due to the fact that power relies on the dimensions of the panel. [46] The dimensions of compared panels vary, this is why it is more important to answer the question of how many panels could fit the site. The rated power value was used for one-watt price calculations.
- Based on datasheets, the *rated power characteristic* was calculated to show the efficiency for 400 W/m² annual solar irradiation which is the average value for the studied site. The selected panel has highest characteristics at annual irradiation and cell temperature. [30]
- *V_{OC} and I_{SC}* values are in the same rage for each panel. V_{OC} and I_{SC} values will be used in the Section 3.3.9 at inverter selection part.
- Due to the fact that compared panels supply different rated power, the *price* of one installed watt was calculated by dividing the price of one panel on the rated power. The economic aspect could be the most convincing during the project approval, so the price of the selected panel is reasonable and is the cheapest among compared panels.
- The panels installation will be along the width of the building, so panels will be turned to the South and as many as possible panels should fit in 15060 – 15780 cm width. Based on the previous statement, twelve AXIpremium AC-290M/156-60S modules can fit, where the most competitors could fit only 8 or 9 panels in a row.
- According to manufacturer datasheet [44], the selected panel will not degrade lower than 80% after 25 years of operation, which is the best result among the

competitors at *performance warranty* value. This value takes into account only the Si degradation of the PV panel.

The main I-V curve characteristics, as well as the relationship between irradiation and temperature impacts of AXIpremium AC-290M/156-60S panel, are shown in Figure 5. According to numerous researches [48] [49] [50] [51], outdoor-installed PV panels generate less energy every year due to glass wearing, delamination, bubbles and cracks. On average, all the factors reduce energy production by 2% per year.

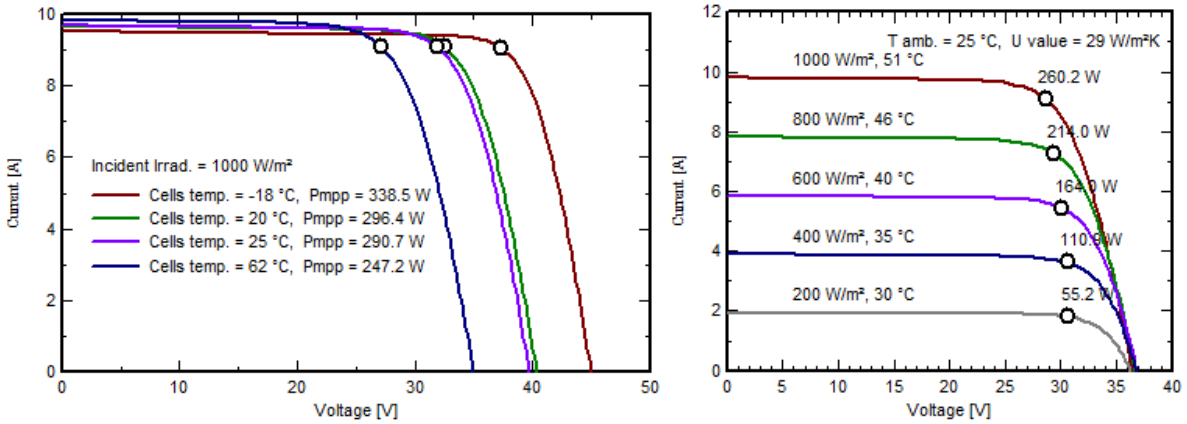

Figure 5: AXIpremiun AC-290M/156-60S panel I/V characteristics (left) under different temperature and (right) under different irradiation values

3.3.8 Positioning and orientation of photovoltaic panels

After selecting the appropriate panel model, the next step is to define the position, tilt angle and the distance of selected PV panels. Wrong selection of such parameters could cause undesirable shadings and as a result a reduction in energy generation.

The shading pattern and array design are important elements that impact the mismatch losses. German Federal Ministry for the Environment states that shading is a number one issue for causing decreased yields and efficiency decreasing of up to 30% in PV systems. [48] The proper placements of the PV modules in the system influence the photoelectric current going through a string, and, therefore, if not performed properly, result in mismatch losses. Based on this, special attention should be payed to the positioning and interconnection of the panels in the system in order to avoid losses.

3.3.8.1 Tilt angle selection

Finland, situated in the northern hemisphere, experiences a solar radiation that is coming from the south. There is obviously a deviance during the year, however theoretically PV panels should be facing as close to the true south as possible. According to the building prints, four sides of the building are directed on 27°, 117°, 207° and 297° from the south. Since that, sides of the building that are not facing as close as possible to the south are not feasible for PV panel installation. [49] Based on that, the roof and a side with azimuth γ equal 27° from the south will be used. To

increase the maximum number of installed PV panels, installation tables should be mounted parallel to the selected side of the building. [50]

A precise understanding of the sun's route is crucial for determining solar irradiance as well as the PV system's yield. The altitude of the sun is determined at the *solar altitude* and the *solar azimuth*. South is typically given as 0°. East angle is recorded with a negative sign (east = -90°). To the west, the angle has no sign (west = 90°). [30]

The solar irradiance intensity mostly depends upon the elevation angle α. [51] It is determined from the horizon line. While the sun moves through the sky, the elevation angle changes during the daytime and changes throughout the year.

Every time when the sun's altitude is perpendicular to the Earth the sunbeam uses the shortest way through the atmosphere. When the sun is at a flat angle, the way through the Earth's atmosphere becomes longer. This leads to higher absorption as well as a scattering of solar radiation which leads to a reduced radiation intensity. [30] Figure 6 shows the different elevation angles on during the year in Helsinki. The maximum solar elevation angle α of = 53.3° is reached on 21 June. The lowest α of = 6.4° is reached on 21 December. During the equinox, α reaches 30.1°. [52]

The intensity of the solar irradiation on the PV panel is characterized by the panel's tilt and azimuth angle against the position of the sun. The optimal array positioning depends on the consumption schemes, weather condition, climate, shadings of the site, and the latitude. [53]

The optimum efficiency for northern hemisphere can be achieved by "the rule of thumb" which states that the PV panel's tilt angle is 10° - 15° less the location latitude [31] [50]. However, "the rule of thumb" is not applicable in the case when the site is exposed to high diffuse irradiation or shadings from nearest panels and structures. [54]

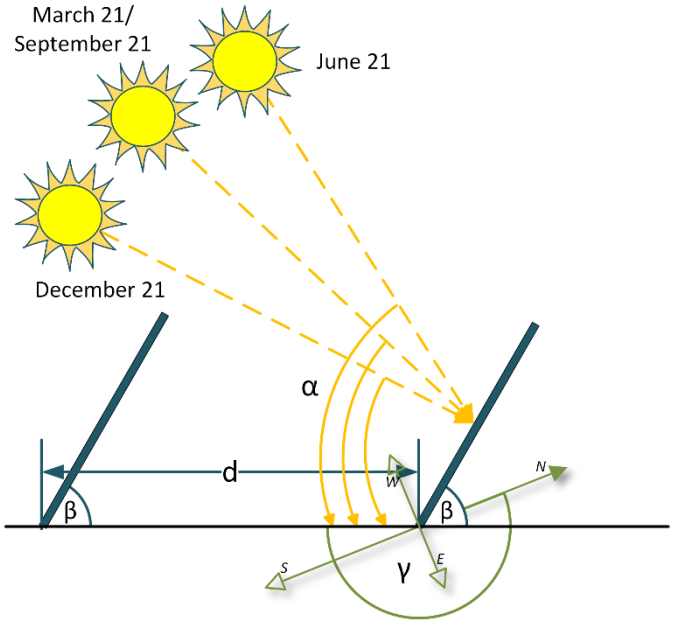

Figure 6: Tilt angle and panels position under different solar periods

With the fixed tilt angle of the panel, the maximum electricity output over the year varies as a result of the various lengths of daylight hours period between seasons, since the summer sun in the zenith is much higher compared to the sun in winter. [30] The position of the sun during the year and the angle α between sun and panels are shown in Figure 6.

Since the difference in α angle during the year significantly varies, the tilt angles of roof and wall mounted panels were simulated in PVSyst software. The simulation studies the behavior of the panel during the year in minute resolution. The outcome of simulation is the annual effective irradiation on the panel as well as the annual losses from shadings. The simulations were processed for a single panel in 0° - 90° interval for roof mounted panel, where β equals 0° is stated as a roof angle. For the wall-mounted panel, β equals 0° is the wall angle that equals to 90°. The simulation was performed per each β degree, so 180 total simulations. Figure 7 represents the results of the tilt angle simulation for both installation sites.

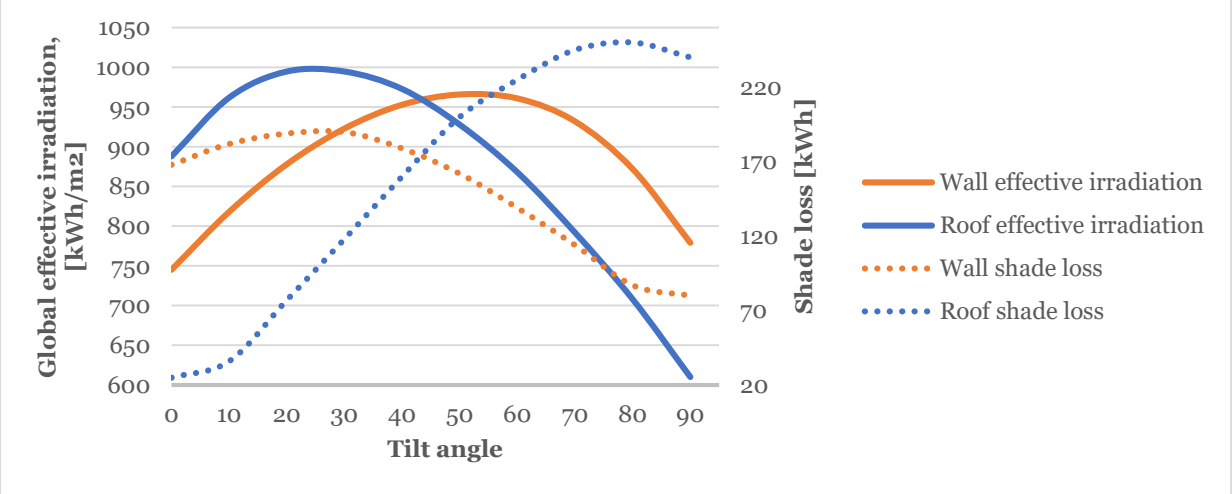

Figure 7: Tilt angle simulation results

Based on the simulations, the fixed tilt angle β for wall mounted panels is 53°. The highest global effective irradiation for the fixed tilt angle of roof-installed panels accrued when β equals 15°. These angles show the best effective irradiation during the year as so as acceptable shade losses.

3.3.8.2 Shading effect on the photovoltaic panel

The shading can result in an impact on the PV array efficiency since shading of 5-10 % of the PV array is capable of reducing the electricity generation by over 80 %. [30]

The shading could be *global* or *near shadings*.

The global shadings are the horizon shadings that could shade the whole panel area since the producers of shadings are large regarding the sizes of the PV panel. The examples of global shadings producers are buildings, hills and trees, and shrubs. In case of the global shading, the array receives mainly diffuse solar radiation. The global shading extremely hard to prevent.

Near shadings, represent factors that shades only a segment of the array. Near shadings includes shadings from pipes, antennas, and nearby panels. [31] Electrically the near shadings represent mismatch, since the system current in a panel string is driven by the lowest current panel. The huge energy generation cut of a PV array is an effect of mismatch loss, and it is the difference in MPP of the array and the sum of MPP of the affiliate PV modules [55]. Mismatch losses are the result of variation in module specifications as well as due to partial shading [56]. The mismatch induced in particular PV modules that are exposed to near shading patterns is called *partial shading*. This partial shading effect is prevalent in the case when several PV modules are linked in array. The losses incurred are considered to be a consequence of the incoherence between the PV array MPP and MPP of an individual module, existences of multiple peaks in the output peaks, triggering of by-pass diodes combined with their on-state losses, or, alternatively, a result of the reverse currents. [57] [58]

If a PV module is located in the shadow of a physical object (e.g. a tree or a near structure), the module's I-V characteristic curve depends on by the bypass diode characteristics. Without the bypass diode, the total current from the module would be determined by the cell that is in shadow. The bypass diode is the reason why the maximum current flows through non-shaded cells. [30]

3.3.8.3 Global shading analysis

Nearby structures, trees, and shrubs, as well as far-away high architectural structures, may shade the panels, or at least result in horizon darkening. Shading from the building includes direct shadows that could be especially decisive. For shading analysis, the three-dimensional scene was built. Figure 8 represents the visualization of surroundings in 150 meters radius around the studied building with all structures that are more than 3 meters tall. The visualization was done in PVSyst Shading Visualization Tool. The overall scene, including trees, was based on visual inspection of the site. The surrounded structure proportions and heights were gained from the Municipal Register of the City of Helsinki [59]. The distance between the structures was gained from the Helsinki city plan [60]. The mean deviation in heights and distances is ± 0.1 meters. The same visualization will be used during shading analysis and mutual shading optimization.

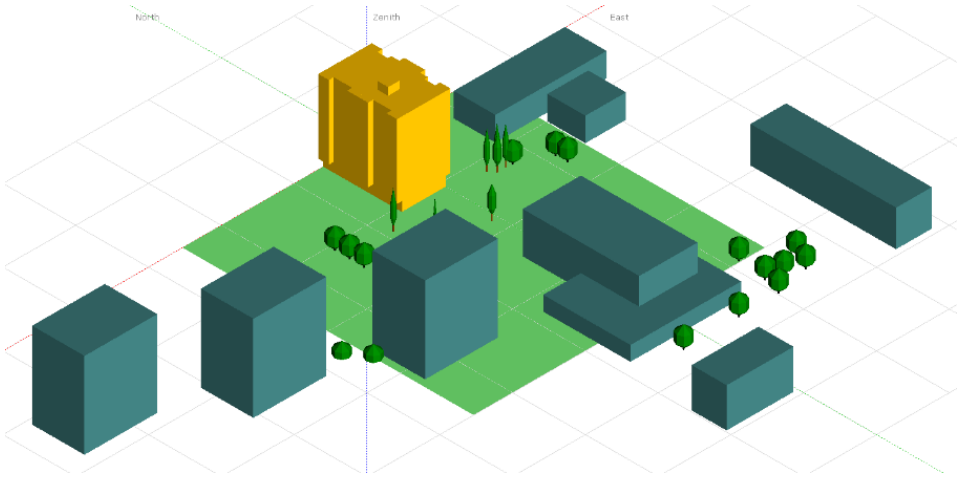

Figure 8: Studied site 3D visualization

When it is not possible to reduce shading by moving panels, the shading effect is reduced by planning the way modules are interconnected. Different interconnection systems of PV panels will be discussed in Section 3.3.9.2.

3.3.8.4 Near shading optimization

With a rack-mounted PV panel, self-shading of the panels can be a result of the front panels. Space preferences, as well as shading losses, were minimized during optimization process of the tilt angles and distances between the panel rows.

To be able to evaluate the shading due to the distance between the panels, a shading analysis is carried out. Since installation surface is limited by the wall and roof dimensions, the distance between panels can increase or decrease the total number of panels that could be fitted. Decreased irradiation due to a low distance between panels can generate the same amount of electricity with a lower number of panels but with a longer distance between them. The compromise between panel distances and a total number of panels was simulated for 1 – 2 meters range with a 0.1-meter step. This brings 10 simulations for each installation site, where a number of installed panels depends on the distance between panel tables and maximum surface utilization.

Wall-mounted 136 panels form 17 rows, with 8 panels in each. Since every row will cast uniform partial shading on the lower row, all panels in a raw will generate almost similar power. Based on that, every row should form a string and all strings will form an array. The V_{MPP} of array at 62˚C which is the highest panel temperature at summer, is 218 V. The V_{MPP} of array at 20˚C which is an average annual panel temperature is 261 V. The highest V_{MPP} could be achieved at the lowest temperature -18˚C with V_{OC} equals 360 V.

The roof-mounted panels are not forming easily recognizable rows. Therefore, the trial method was used to form 204 panels into 17 strings, for reducing the effect from near and self-shading to the minima.

The V_{MPP} of each array at 62˚C equals 381 V. The V_{MPP} of the array at 20˚C equals 456 V. The V_{OC} at -18˚C equals 629 V.

3.3.9 Inverter selection

PV panels are joined together by series and parallel connectivity to create an electrically and mechanically bigger unit, called the PV electric power generator. [30] The series-connected panels are referred to as a string. [31] The amount of series-connected modules characterizes the system voltage of the grid-connected system, which corresponds to the input voltage of the associated inverter. A correctly selected inverter should utilize the energy generated by PV panels in a most efficient way.

3.3.9.1 Main inverter considerations

The basic principle of the inverter is to convert DC into AC that could be used by the building electrical system or transferred by transmission or distribution lines. [61]

Inverters could be stand-alone or grid connected. [20] The basic principle of a standalone inverter is to convert DC into AC only for onsite needs. The grid-connected inverter can synchronize generated AC voltage level and the frequency with the grid. [9] The grid-connected inverters should match with International Electrotechnical Commission (IEC), Institute of Electrical and Electronics Engineers (IEEE), national or European electrical codes. The most significant, design, usage and connection standards are IEC 61727, IEEE 1547–2003, IEEE 929–2000. [62] PV arrays are connected to the inverter by the disconnecting switch which allows safe repairs and maintenance. The over-current protection equipment is installed on each the AC and DC side by fuses or circuit breakers. [13]

The inverter working characteristics are determined by the V_{OC} and I_{SC} of the PV array. [6] The system output is defined by the output power rating of the inverter so it could cut the array output down if it exceeds the inverter limitations. [31] Since two possible implementations of PV installations are studied, wall-mounted and roof-mounted PV arrays; thus, the power rate of the selected inverters should be defined separately for both cases.

It is common that the maximum efficiency of the inverter is greater than 95%. [61] The fluctuations of the operating point of the inverter change the overall inverter efficiency. The best performance of inverters is between 30% and 50% of the rated capacity of the inverter. [63] In cases where the operating point raises this array, its efficiency falls. The efficiency of the inverter cuts down radically while the operating point is under 10 % of the rated capacity. [6]

The system that does not exceed 5kWp (or with the size up to 50m^2) is typically a single phase system. [31] Any larger systems should work as a three-phase system. This also means that the system should be connected to the three-phase distribution system. Based on the pulse width modulation (PWM) working principle of modern inverters, any inverter could be programmed in a way when multiple single-phase inverters will be used in three-phase systems without additional costs. [61]

The studied building is situated in an urban area, therefore, connected to the electricity distribution grid. To be able to sell surplus electricity, grid-connected inverters should be used. In addition, grid-connected inverters will increase energy security and reliability of electricity supply. In conditions of incapability of covering peak periods of consumption by onsite generation, electricity will be supplied from the grid. Consuming the electricity that was generated on site will decrease the total transmission costs, which will be discussed in more detail in Section 6.2.1.

3.3.9.2 System concepts

The system concepts are identified by central or decentralized system concepts. The connection of panels forming strings and their parallel connectivity needs to be optimally matched with the inverter parameters and interconnection. [64] Inverters are available as a *central inverter*, which means only one inverter for the entire system,

various central inverters that are working as a master-slave principle, *string inverters* when they have connected with each other, and inverter as an *individual module* for each PV panel**.** [30]

Central inverter concept. In the LV systems, several panels linked in series in a string are connected to a single inverter. This central inverter concept is shown in Appendix 3 (upper left). The main advantage of central inverter concept is that due to the lower currents smaller diameter cable could be utilized which bring the cost reduction of the system. The negative aspects of this concept are power losses since Maximum Power Point Tracking (MPPT) is not correlated with each panel, losses in the string diodes, therefore, resulting high currents in the system. Relatively high cable sections must be implemented to minimize the ohm losses which will increase the total cost of the entire system. [64] Based on those facts, the concept is almost never used. [30]

Master-slave concept. Bigger systems usually utilize a central inverter concept in accordance with the master-slave principle, which is shown in Appendix 3 (upper right). The master inverter operates in low solar irradiance ranges. With higher solar irradiance, the next inverter, called "slave" is hooked up. [30] The benefit of this concept is the fact that every inverter will operate at its highest efficiency regardless of the solar irradiation range. Nevertheless, the investment expenses increased in comparison with central inverters. According to the literature review [64] [65] [62] master-slave concept is not commonly used neither efficient in average sizes PV systems [66].

Module inverter concept. A key for maximum system efficiency and performance is the inverters that are optimally revised to the PV panels. The ideal case when every single PV panel always performs at MPP. The highest MPP achieves when PV panel and the inverter is a single unit. Such panel inverter devices called micro inverters. [30] These devices are so compact they can be kept in the panel junction box. Module inverter concept is shown in Appendix 3 (lower left). A further advantage is a simplicity with which the PV systems could be extended. It is frequently stated that the downside of module inverters is lower efficiency. [64] [67] The main drawback of module inverters is the price since every module needs its own inverter and such inverters are still quite high-priced yet. [65]

Subarray and string inverter concept. Systems that exceed 3kW output power usually designed with string inverters. [65] [30] Typically, PV array forms one string. Medium-sized PV systems utilize multiple strings plugged into the inverter, which forms a sub-array concept, shown in Appendix 3 (lower right). String inverter concept allows best power-related adjustment to the fluctuated irradiance factors and partial shadings. [30] [64] String inverters utilization offers simpler installation, tending to significant decrease of installation costs. [30]

Considering the fact that inverters are connected straight to the module strings, the main advantages besides cost reductions are unnecessary junction boxes, DC central cable and minimizing the cabling due to series interconnection. [30] [6]

Based on the above, the sub-array and string inverter concept was chosen for the study. Roof and wall installed panels influence completely different shadings patterns, have different panel distance and tilt angle, and as a result, form a different number of panels in the string. Considering this fact, two different types of inverters will be selected for roof and wall mounted panels.

3.3.9.3 Inverter sizing and selection

Numerous research papers and inverter manufacturers state that the inverter array power ratio should be in the order of 1.0 to 1.2 [65] [30] [67] Nevertheless, the inverter size selection should take into account an acceptable overload loss, [14] in addition, it is necessary to consider the annual losses, tilt, orientation and site conditions. The inverters were selected from the poll of the market available inverters that were included in the PVSyst software. The main comparison parameters were the input maximum voltage, output power, and the efficiency curves.

AE 1TL-2.3 by Advanced Energy Inc. [68] was chosen as the string inverter for wall mounted panels. The nominal AC output power equals 2.3kW. Figure 9 (left) shows the inverter power distribution, where the inverter to array power ratio equals 1.01 which means that almost all generated energy could be utilized. Figure 9 (right) shows that no overload loss occurred in wall PV system. The nominal output AC power of wall-mounted panel's inverters equals 39.1 kW. Appendix 4 shows the detailed electrical layout between wall-mounted panels and inverters. Every color represents one array e.g. one inverter.

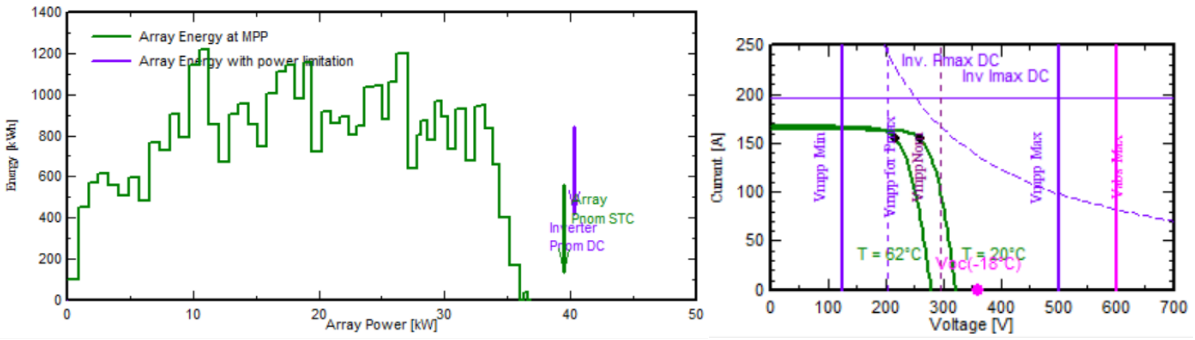

Figure 9: Wall inverter characteristics: (left) output distribution and (right) array voltage sizing

For the roof-mounted arrays, the AE 1TL-3.0 by Advanced Energy Inc. [68] inverter was selected. Figure 10 (left) and Figure 10 (right) shows the main characteristics of the selected inverter. The nominal AC output power of AE 1TL-3.0 inverter equals 3.07 kW. This inverter has 98.1% efficiency so for utilizing such efficient characteristics, the inverter-to-array power ratio is oversized with 1.18 ratio. Considering that the inverter is over-sized, it will run more frequent in its lower range, therefore the overall performance is will be higher rather than a nominal working condition. [61] Appendix 5 shows the detailed electrical layout between roof-mounted panels and inverters.

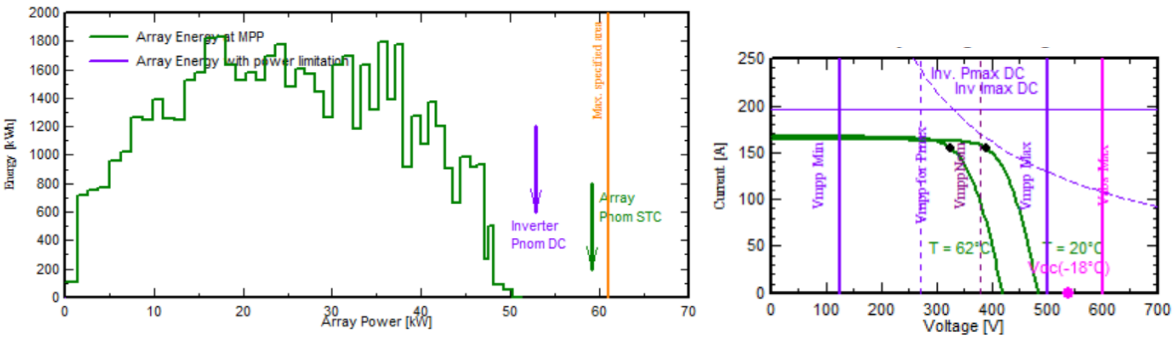

Figure 10: Roof inverter characteristics: (left) output distribution and (right) array voltage sizing

3.4 SIMULATION RESULTS

3.4.1 Meteorological analysis results

Based on synthetically generated data, the peak of horizontal solar irradiation is in summer at 465.4 kWh/m², which is almost a half of 961.5 kWh/m² annual horizontal irradiation. Figure 11 represents the horizontal global irradiation distribution by a number of hours during the year. The most of the hours are with low irradiation during the year. The peak of horizontal diffuse irradiation is either in summer is 224.5 kWh/m² while the annual horizontal diffuse irradiation is 476.35 kWh/m². The highest temperature of 18.70 ˚C occurred in July and the lowest temperate of -4.64 ˚C occurred in February. These values determine that almost half of all power should be generated during summer. Since the testing site is a student dormitory, where students tend to leave their apartments for a vacation during summer, storage systems and selling electricity to the grid will be discussed in Chapter 6. The synthetically generated data correspond with the basic statistical data from Finnish Metrological Institute, so it can be used in following simulation processes. [69]

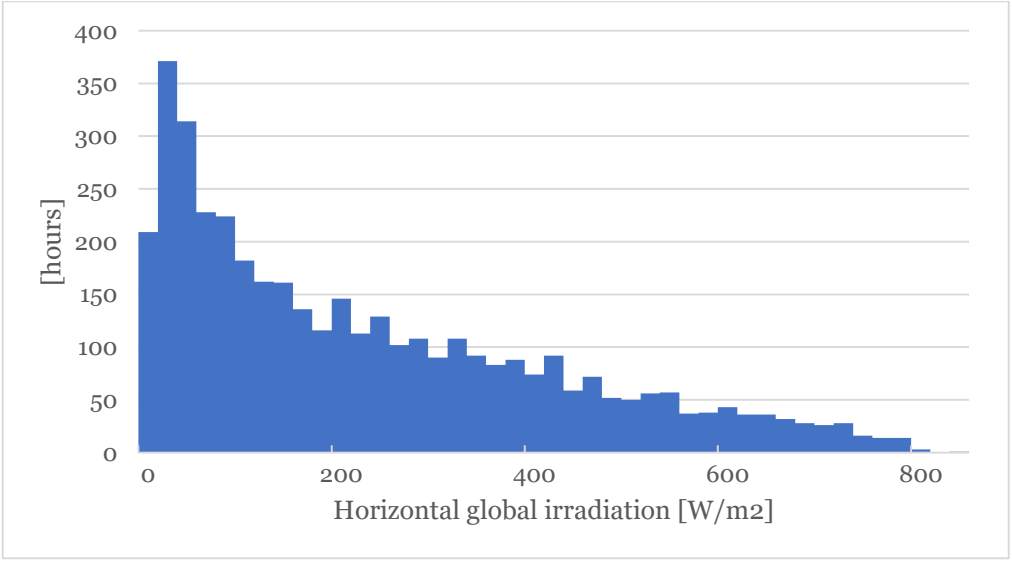

Figure 11: Horizontal global irradiation distribution

3.4.2 Positioning and orientation simulation results

Based on the self-shading simulation, the optimum distance for the wall-mounted panels is 1.5 meters. This distance allows installing 136 panels. It is also good to mention, that the annual generation curve of wall mounted panels are not changing dramatically with a different number of panels. So if the maximum generation is not the goal but the financial side of the project is a priority, the better way is to install fewer panels but with a longer distance between them.

Since the surface of the roof is not rectangular, the change of a total number of panels during simulation is not linear. Shorter distance between panels doubles the losses due to the self-shading effect. The annual generation peek of roof-mounted panels is observed when the distance between panels is 1.3 meters and the total number of installed panels is 204 panels. Any other parameters will only decrease the overall efficiency of energy generation.

The results of self-shading simulations are shown for wall-mounted PV panels in Figure 12 (left) and for roof-mounted PV panels in Figure 12 (right). Figures showing the increase of loss due to the shorter distance between panels.

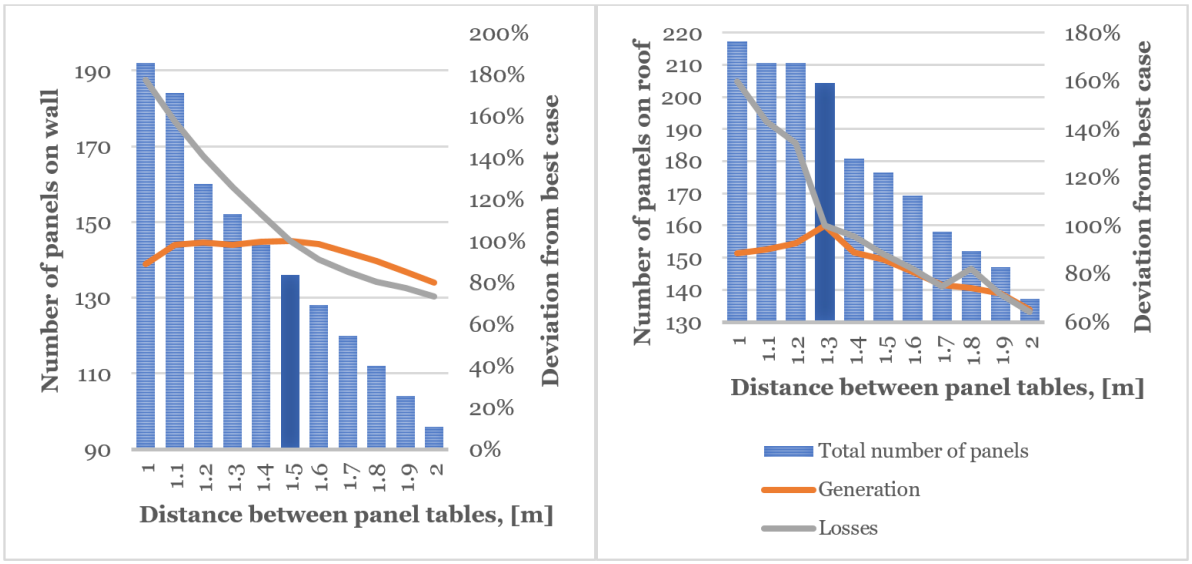

Figure 12: Distance simulation results (left) wall-mounted (right) roof-mounted PV panels

The overall visualization of selected panels, is shown in Figure 13 (left) for the wall-mounted panels and on Figure 13 (right) for the roof-mounted panels at 1st of May. The comparison between different configurations, as well as the wind turbine configuration, will be handled in Chapter 7.

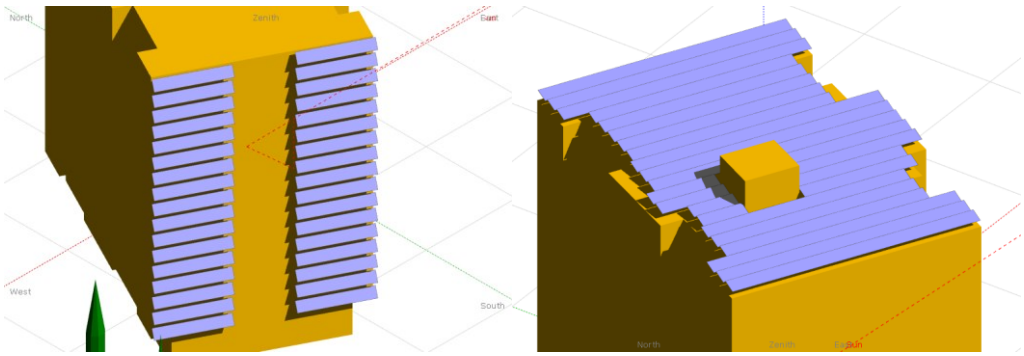

Figure 13: Visualization of panels at noon 1st of May (left) wall-mounted PV panels and (right) roof-mounted PV panels

Based on positioning and orientation optimization, the total number of wall installed panels is 136 pieces and 204 pieces for roof installation. The azimuth of panel's orientation is equal to the building south orientation which equals 27˚. The tilt of wall and roof panels is respectively 53˚ and 15˚. The distance between each raw is 1.5 and 1.3 meter.

3.4.3 System simulation results

The optimal PV panels positions are on the roof and on the south wall of the studied site with 27˚ azimuth. AXIpremium AC-290M/156-60S manufactured by mono-Si technology with the rated efficiency of 290W were selected for roof and wall installation.

Wall-mounted PV system consists of 136 panels with 53˚ tilt angle, where 8 panels in series are forming 17 parallel strings. Every string is equipped with AE 1TL 2.3 2.3 kW inverter. The total PV area equals 221m² which equal 39.44 kW of rated power at STC. The global wiring ohmic losses equal to 25mOhm. Wall-mounted PV system is able to generate 29537 kWh at first year, with the capacity factor (CF) of 8.6%. The CF represents the ratio between the actual yield and the nominal yield of the system and in comparison to the studies is reasonable for wall-mounted panels. [70] [14] The averaged PV array losses are of 1.01 kWh/kWp/day. Inverter losses are of 0.09 kWh/kWp/day. The average produced energy is of 2.05 kWh/kWp/day. The highest peak of energy production is in May is of 4222 kWh. The lowest energy production occurred on December is of 338 kWh. The averaged power output of the wall-mounted system is 3.37 kWh.

Roof-mounted PV system consists of 204 panels with 15˚ tilt angle, where 12 panels in series are forming 17 parallel strings. Every string is equipped with AE 1TL 3.0 3.0 kW inverter. The total PV area equals to 332m² which equal 59.16 kWp of rated power at STC. The global wiring ohmic losses equal to 37mOhm. Roof-mounted PV system is able to generate 43313 kWh at first year, with the CF of 9.0%. The averaged PV array losses are of 0.65 kWh/kWp/day. Inverter losses are of 0.07 kWh/kWp/day. The average produced energy is of 2.24 kWh/kWp/day. The highest peak of energy production is in July is of 8684 kWh. The lowest energy production occurred on

December is of 134 kWh. The averaged power output of the roof-mounted system is 5.52 kWh. Figure 14 shows the 12 months averaged power output for both PV systems.

Although, some researches [75] [76] demonstrate bias towards the spring months, the meteorological data from Metheonorm, used as input, do not demonstrate such bias, and, therefore, the model does not inheret such a bias either. It is also important to note that the researches and meteorogical data [77] [78] [79] that do not favor the spring months are not that uncommon.

High collection losses accure due to the non-ideal azimuth of the building and due to the fixed tilt angle. Tracking plates could decrease the collection loss but increase the installation and maintain costs. The tilt angle was optimized by the respect to the yearly irradiation yield and not the summer, that is why the June is the worst performance ratio month for the wall-mounted system.

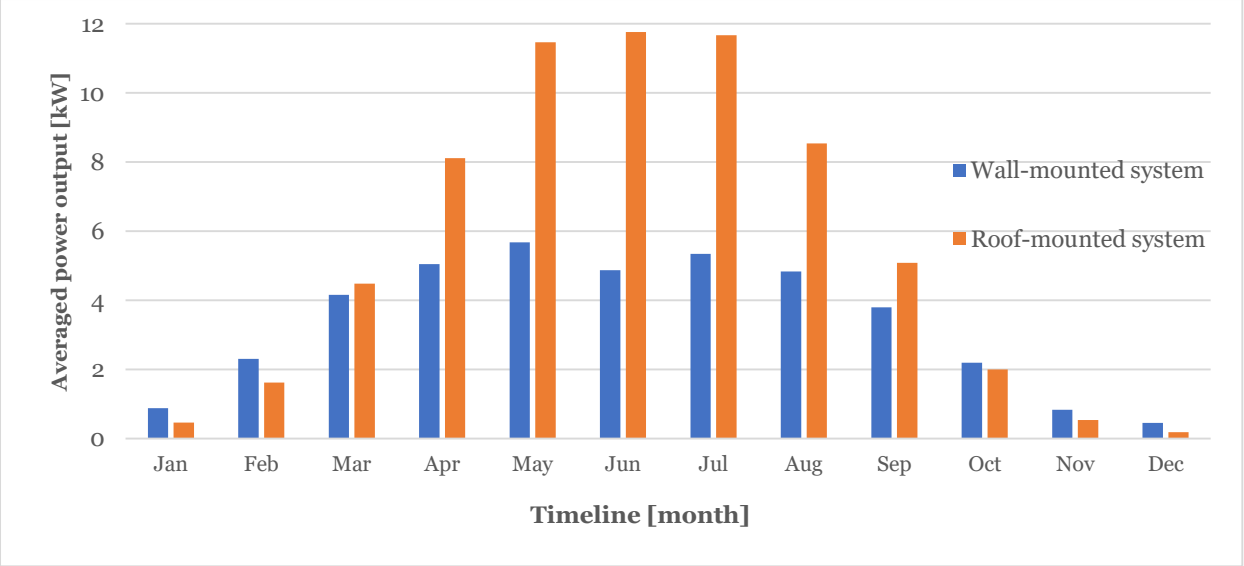

Figure 14: Monthly averaged power output of wall and roof-mounted systems

4 WIND ENERGY GENERATION SIMULATION

4.1 CHAPTER INTRODUCTION

This chapter will study the feasibility of wind energy conversion at the studied site. The whole process will be divided into a preparation and a simulation parts.

The preparation part will consist of the following steps. Topographical analysis will study the terrain, roughness and their influence on the studying site. Wind flow modelling will perform the wind distributions based on the topographical analysis. Wind distributions is the basis for the energy generation calculations of the selected turbine. The simulation process will be done in WAsP software. The results of the simulation are the hourly resolution data of energy generation from selected wind turbine. This establishes the technical feasibility of the on-site electricity generation.

The simulation part will present the results for further analysis.

The major components of the wind turbine system are the turbine, tower, cabling, inverters and storage systems, if necessary. [71] The cabling selection is out of the scope of this study, so it will not be introduced in this paper. Nevertheless, estimated cable losses have been taken into consideration during the simulation process.

Economic aspects of the project will be taken into account as one of the main criteria, since the aim of the whole project is to study the feasibility of nZEB.

4.2 PREREQUISITES FOR WIND ENERGY GENERATION

In spite of significant benefits of distributed renewable energy sources, small wind turbine (SWT) electrical power generation is, however, still, an underdeveloped form of total energy production. [72] For this scenario to be realized, SWTs should be installed in metropolitan areas near the end consumer.

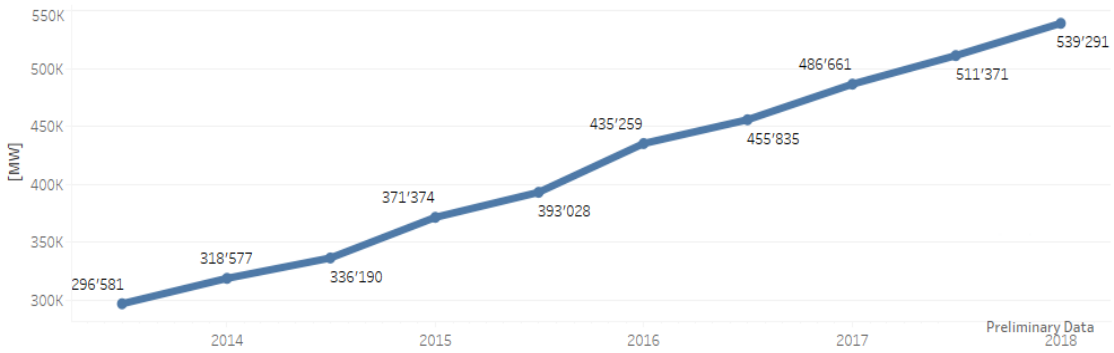

Figure 15: World total wind turbine installed capacity 2013-2017 [73]

The world total wind turbine installed capacity time-series is shown in Figure 15. The global wind turbine capacity by the end of 2017 reached 539291 MW, from which 52552 MW were added in 2017. This corresponds to an increased rate of 10.8 %. All global wind generators, installed by the end of 2017 may produce around 5 % of the world's power demand. [73] The Finnish wind capacity was raised from 1 005 MW in

2015 to 1 539 in 2016. [74] Wind turbines produced 2.06 TWh from 68.6 TWh of total energy production in Finland. [75] The big offshore windmills are the main producers of the wind energy. In many cases, it is more justified to produce electricity on offshore, but in case of nZEB, it is better to consider an urban wind energy generation, such as the SWT. [75]

The IEC in 61400-2 standard defines SWT as a wind turbine with an up to 200 m^2 rotor swept area, corresponding to a rated power of 50 kW, generating at a voltage level below 1 000 V AC or 1 500 V DC. [76]

The registered SWT capacity installed throughout the world has exceeded over 830 MW at the end of 2014. This represents a growth of 109% in comparison with 2013 (749 MW of capacity). [73] The SWTs market in Finland saw an increase in the number of installations in 2014, where the cumulative installed capacity of the SWTs growth up to 115 kW in 2014 [73]. There are few studies concerning SWTs in Finland. However, based on global trends, the urban usage of small turbines should radically grow in the next decades. [77] This study does not take into consideration the condition of the rooftop to withstand the dynamic and static forces from the tower and turbine, noise disturbance, vibration and visual acceptance of turbine since that is not the main topic of study.

It is difficult to state, that SWTs can replace large turbines or even conventional technologies of energy generation, but it serves a good example of complimentary generation. SWTs are also viewed, in a combination with solar PV energy production. Even at night, when PV panels cannot produce energy, SWT can do that. SWTs can encourage individuals and business sectors to consume a clean, zero-emission energy.

4.3 METHODOLOGY

Chapter 4 study procedure is based on the WAsP software's guidelines. [78]

The WAsP software selection is based on a comparison of three different products that are able to simulate the wind turbine system: WindPro 3.1 by EMD International A/S is a shareware application with limited functional during trial period, designed for simple energy estimation. However, it is capable of noise and shadow calculations. WAsP 11.3 by DTU Wind Energy Risø Campus is a shareware software, with free license for academic use, designed to calculate and optimize wind farm energy production and to generate wind resource maps. WAsP has no visualization module. WindSim 8.0 by WindSim AS is a shareware software with limited map resolution capability in trial period. The program can simulate the wind farm operation and estimate the energy generation.

Since all of the above perform the main task well, WAsP has been selected for its better compatibility with wind atlas and topographical files.

4.3.1 Topographical analysis

The effects of the topography have a big impact on the wind flow, so it is important to describe the surrounding characteristics as accurate as possible. In the real life, those effects cannot be separated from each other, but for better description of the overall condition, the topography effects could be divided into three main effects [78]:

- terrain orography
- the roughness of the surrounding terrain
- close-by sheltering obstacles

Each of effects will be studied based on open-sourced data and, as a result, will form height contour data and roughness data of the studied site. As the result, the surrounding map will be created that further will be used in site wind data analysis.

4.3.1.1 Effect of terrain orography

Height variations can take the effect on the wind flow at the studied site. According to a study [79], a 5% change in elevation can increase the average wind speed for up to 5% and as a consequence results in 15% increase of wind power flow. The information about height and terrain elevation is described by the elevation map.

The elevation map should extend up to 10 by 10 km around the studied site and the height contour resolution should be less than 10 m in close proximity to the studied site. [78] The elevation map was built on the data provided by National Land Survey of Finland. [80] The data is based on a model depicting the elevation of the ground where the baseline value is the sea level. The grid resolution of the model is 2 by 2 m with the Class I 0.3 m elevation accuracy. This data was processed and converted by WAsP map Editor Software, to fulfill the input parameters of the simulation. Figure 16 shows the elevation map with the circle on approximately 2 km radius of the studied site. The average elevation of the studied radius is 18 m with the 37 m peek on the south and 36 m on the east. The studied building is situated on 26 m terrain elevation.

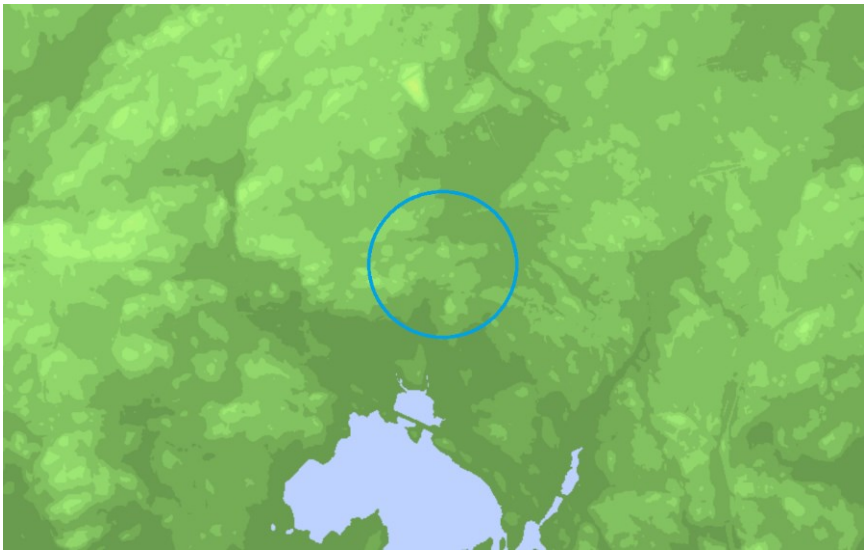

Figure 16: Marttila district area elevation map [80]

4.3.1.2 Roughness estimation

Since the Earth is not just an elevated surface but it is full of different terrains, such as oceans, forests, fields and other different obstacles, all this should affect the wind speed and flow. [78]

The wind flow at height of 1km is not affected by the terrain surface. The lower atmospheric levels will be affected by the friction with terrain surface and obstacles. The result of the friction is the wind speed deceleration on the bottom of the atmosphere levels. The influence of the terrain surface and obstacles on the wind flow is called the roughness. [78]

The terrain surface roughness can be divided into classes and lengths. Roughness classes and lengths are properties of the surface for analyzing the landscape for wind turbine installation. Appendix 6 shows terrain roughness classes (RC). The lower RC class, the lower the friction between wind flow and terrain is, the better this area is intended for wind turbine installation. [78] For instance, the sea surface classifies as the smoothest surface, so the RC value equals to zero. That is why the offshore wind power plants are so common.

The height above zero points represents Z_0, the roughness length, where the wind flow equals zero. The Z_0 could be considered as a climatologic parameter since roughness of the site could be changed due to snow cover and vegetation. The RC could be referred by meters in terms of the Z_0 [81] equations:

$$RC = 1.699823015 + \frac{\ln Z_0}{\ln 150}; \quad for\ Z_0 \leq 0.03 \tag{4}$$

$$RC = 3.912489289 + \frac{\ln Z_0}{\ln 3.3333}; \qquad for\ Z_0 > 0.03 \tag{5}$$

The studied site is situated far away from the dense city development with rare medium height buildings. A large area is filled with trees and shrubs. The terrain is rough an uneven but will be covered by snow for around 4 months annually. [20] Based on that, the 5 km radius area around the studied site is referred to 3rd roughness class with roughness length, Z_0 equals 0.3 m. These terrain characteristics will be used during area site wind climate simulations.

4.3.1.3 Shelter sub-model

The studied site is surrounded by variable heights obstacles. Most of the obstacles are already taken into account by the roughness class. But obstacles, like apartment buildings or large trees, could be unevenly distributed across the urban area and will not represent the whole area. Based on this, it is insufficient to describe the site area only by a roughness class. In order to take into account all mentioned effects, the shelter sub-model is used. [78] The shelter sub-model corrects the roughness profile due to unevenly distributed obstacles since, near a structure wind flow is highly influenced by a barrier appearance. Such effect could extend the wind speed up to

three times of the height of the structure. [81] The wind flow could be influenced up to forty times of the height of the structure. [81]

Based on the stated above, the shelter sub-model was built. It consists of heights from obstacles in 1 km radius across the studied site. The sub-model is based on a three-dimensional point-like laser scanned data from the National Land Survey of Finland database [80] and a three-dimensional map of the city of Helsinki. [60] Figure 17 (left) shows the shelter sub-model map. The lowest obstacles are marked with the light green color, these are private houses. The dark green color represents the medium height obstacles. The purple color represents the highest obstacles, these, actually, are the apartment buildings on the west of the studied site. The studied building itself is one of the highest structures in 1 km radius. Figure 17 (right) shows the Shelter sub-model in terms of roughness delimitation between buildings and trees. The red color represents the buildings and the green color represents trees.

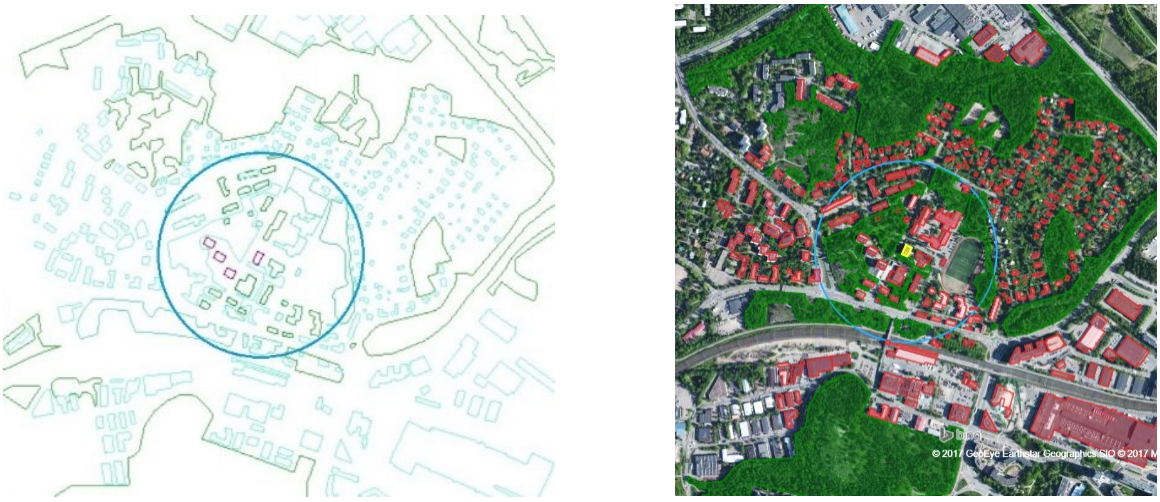

Figure 17: Visualization of shelter sub-model map (left) and roughness delimitation map (right), based on [82]

The shelter sub-model will specify the environment around the studied site and will lead to more accurate simulation results.

4.3.1.4 Turbulence influence

While the wind flows through steepness or ruggedness structures, the flow becomes distorted and generates turbulence. Figure 18 is showing such flow disturbances from a different view. [83] Both figures display the wind flows above a steepness structure. The strength of the wind flow is represented by means of the scale of the arrows. Short arrows, as well as the blue color, symbolize poor wind flow. The longer the arrows the larger the speed. The region with the yellow arrows has the strongest wind with a mainly permanent direction. Figure 18 show that wind turbine should be positioned near to in the center of the rooftop where the wind is the strongest as well as the turbine is beyond the spots with turbulence.

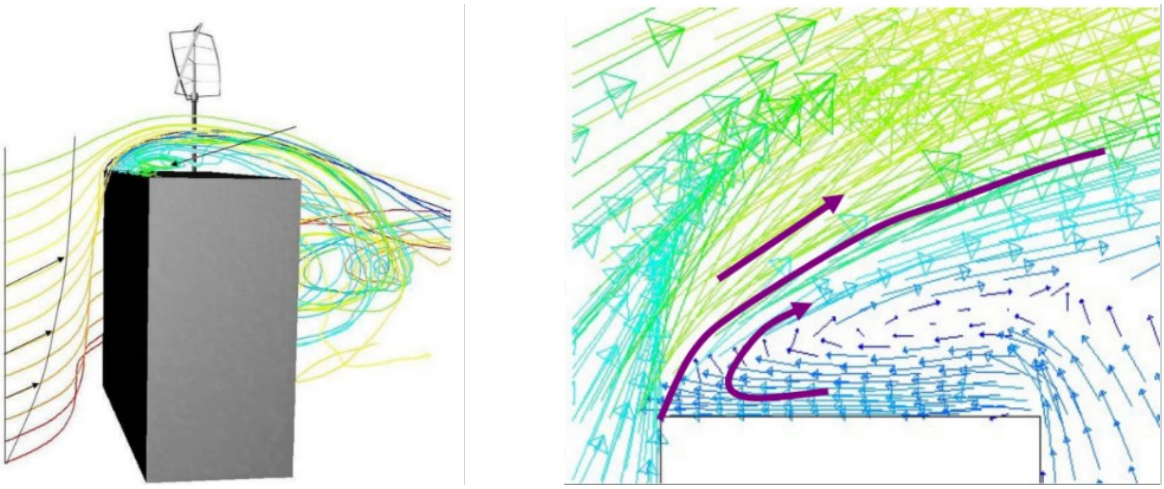

Figure 18: Turbulence from perspective view (left) [83] and en face (right) [83]

When the wind turbine is exposed to high turbulence, rotor blades can fail because of fatigue. [84] The middle of the plain roof provides much better performance than any other installation places. [85]

As a consequence, the result of turbulence is the appearance of vortices at the edges of the roof. [84] Air flows are pushed by the construction and cause an effect, called *a separation bubble* [84] which can be clearly seen in Figure 18. This leads to the fact that at the edge of the roof wind speed drops and such places should be avoided when installing wind turbines. Depends on the form of the building, roof structure and the angle of the roof-top, wind speed can vary by 70%. [84] Since the wind speed reducing turbulences are the result of those roof parameters, the wind turbine should be installed on the highest place of the rooftop, at least 30% above from the height of the building. [86]

The steepness or ruggedness of the area is determined by the ruggedness index (RIX) and it is defined as the fraction of the area within a certain distance from the studied site. [87] This index is measuring the extent of flow separation.

- If the RIX index is ~0%, the flow is following the surface without a disturbance.
- If the RIX index is >0%, the flow separation bubble may occur.

Figure 19 on left is showing the RIX index for the 240° wind direction at the height of turbine installation. Since nearest tall structures are steepness, the separation bubble may occur near the studied site, when the wind is blowing from 240° direction, which is underlining by the high red color between those buildings and the studied building. It could be clearly seen that even higher RIX index occurred behind the wind turbine

which is produced by the wind turbine by itself and could lead to waking phenomena in case of several wind turbines on one site. [81]

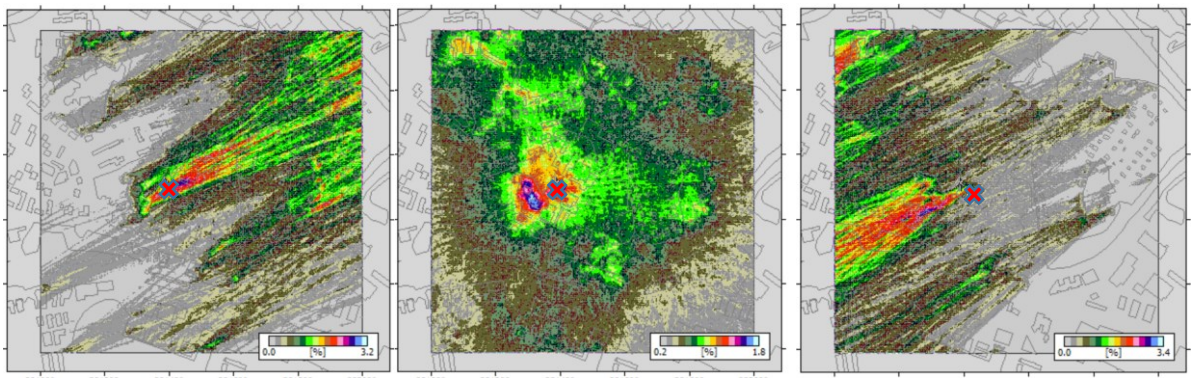

Figure 19: RIX distribution from 240° (left), 60° (right) and overall distribution (middle)

Figure 19 in the middle shows the RIX index distribution for all wind directions at the wind turbine installation height. As it was stated before, tall structures with steepness roofs producing the separation bubble. Figure 19 shows separation bubble at the studied site with 240° wind direction. The higher tower will not get rid of this phenomena. Never the less, the winds from other sides, except for the west side of the studying building, will be less influenced by the separation bubble since there are no tall structures. As the example, the RIX index distribution from the 60° is shown on the right of Figure 19.

The perfect position of a wind turbine in a sophisticated urban area depends on the elevation of the location where it will be installed. The wind turbine should be positioned at the roof in such a way, so the total swept area is clear as possible of turbulence and separated rooftop wind flows.

4.3.2 Wind flow modeling

After the topographical analysis of the studied site, where all near obstacles and roughness are identified, the wind flow model can be developed. For the area wind flow model, interpolated wind limited area models will be used. Based on a combination of the topographical analysis and area wind flow map the oleographic sub model will be developed. The further simulation will bring the Weibull probability wind distribution around the swept area of the wind turbine.

The global wind pattern is a result of variations in temperature across the globe in addition to the Earth's rotation. The most intensive air movement occurs from the equator streaming to the west up to the northern and southern tropic latitudes where wind is changing its direction to the east to Arctic and Antarctic latitudes, forming two natural wind tunnels. West direction wind speed is higher than east direction wind speed. This trend is impacted by the Earth's terrain configuration. [88]

Due to the fact that the wind speed and direction are not a constant value but instead a changing phenomenon, it is important to describe the change of wind by the probability vector of a certain speed and direction. Unfortunately, no analytical

solutions are applied, so numerical methods should be used instead. The task of simulation is to evaluate how the meteorological variables will vary with respect to topographical conditions. [89]

4.3.2.1 Wind climate estimation.

The concept underlying the numerical modeling of the atmosphere is the fact the atmosphere can be characterized by the values of the meteorological variables at a finite set of discrete points. [89] These points are defined in a three-dimensional grid with predefined spatial coordinates. The distance between points is called the spatial resolution of the grid. Since the atmosphere configuration is stratified, different spatial resolutions can be used for vertical and horizontal atmosphere modeling. [81] [89] That is why, based on the height of the wind turbine it is important to select the right resolution grid, especially for SWTs, that are typically installed very close to the surface in terms of the whole atmosphere.

Numerical weather prediction models could be global, as shown in Figure 20 (left), or limited area models for a particular territory, as seen in Figure 20 (right).

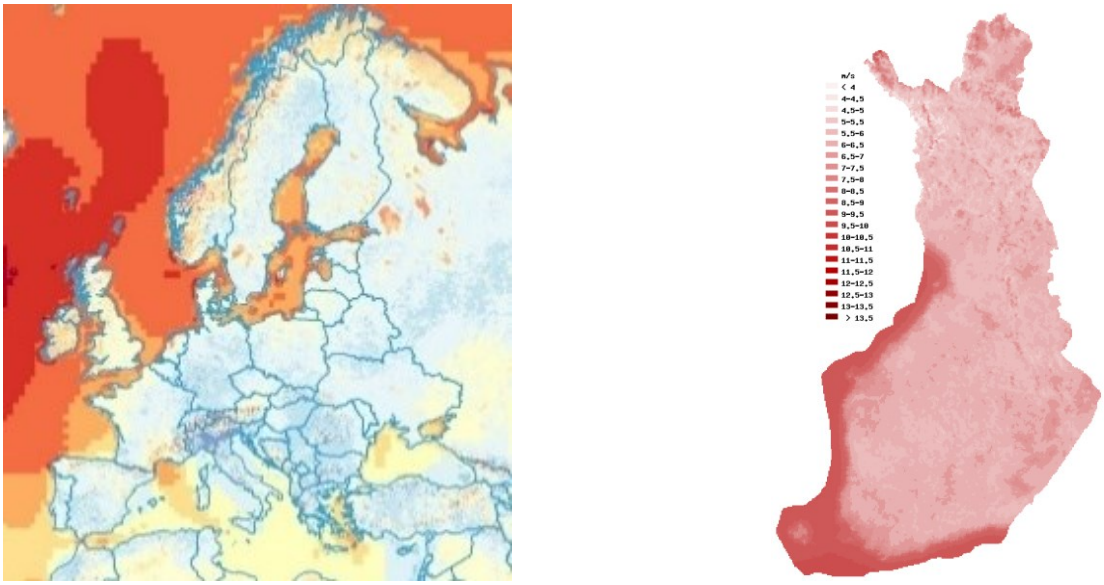

Figure 20: Global (left) [90] and limited numerical weather prediction models [91]

The limited area model could be as a part of the global model or as an additional high-resolution model (HIRLAM) inside a global. The HIRLAM describes almost every European country. HIRLAM obtains its lateral frame factors from the European Centre for Medium-Range Weather Forecasting global atmospheric model. [89] Finnish HIRLAM is called Finnish Wind Atlas was done by Finnish Meteorological Institute in cooperation with Risø DTU National Laboratory for Sustainable Energy. [91]

The Wind Atlas is based on computer modeling and represents average monthly wind conditions without distribution into wind direction sectors in a 250 by 250 m² grid

area, and with distribution into 12 wind directions in 2500 by 2500 m² grid area, both for 50 and 100 meters' height. [91]

4.3.2.2 Interpolation of wind atlas climatology dataset

The typical single geographical point interpolation forecast method [71] is to utilize the closest climatology dataset or at least most representative one. For this purposes, the grid was downscaled to three equidistant data points. Directional distributions were interpolated by Fourier splines and the attributes that are independent of wind direction are interpolated by Bezier surfaces. [92] Properties independent of direction, such as the distance from each climatological dataset to the studied site, are forecasted by linear interpolation instead than by third-order Bezier polynomial equation. [78]

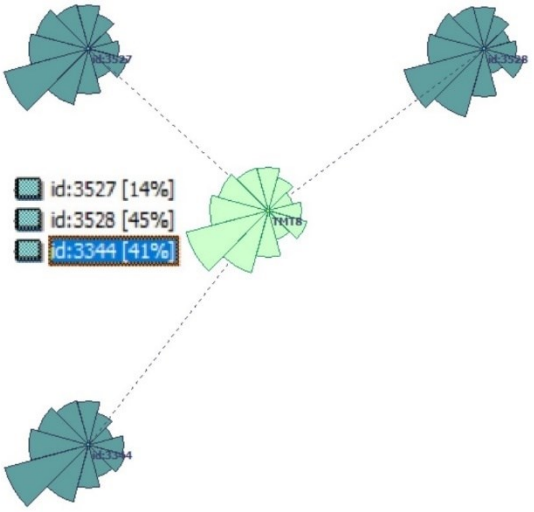

Figure 21: Wind atlas climatology interpolation visualization

Figure 21 shows the closest climatological data sets as so as their wind speed and directions. The resulting dataset is shown in the middle of figure and represents the overall interpolation attributes.

This data will be used in orographic sub-model, where the climatological data will be applied on the topographical analysis, to compute the wind behavior at the height of wind turbine.

4.3.2.3 Orographic sub-model

Since the interpolated climatological data describes the wind flow on a particular 50 meters' height, the data should be corrected by the orographic sub-model to correspond with the height of the installed wind turbine. [81] The sub-model uses a polar representation horizontal grid, which comes from the wind turbine installation site i.e. the interpolated climatology data set. The utilization of the orographic sub-model in WAsP is done in such a way, that the highest resolution will be at the studied site and decreases with the factor of 1.06 radially. [81]

The surface layer wind profile in roughness terrain is described by the equation:

$$u(z) = \frac{u_*}{k}\left(\ln\frac{z}{z_0} - \varphi\left(\frac{z}{L}\right)\right) \tag{6}$$

Where Karman's constant k is set to 0,40 and $\varphi\left(\frac{z}{L}\right)$ is the empirical stability function that compensates the for lower wind speed with the heat flux from the surface. [78] This transformation is done since the wind speed data is not referred to the wind speed at wind turbine installation height.

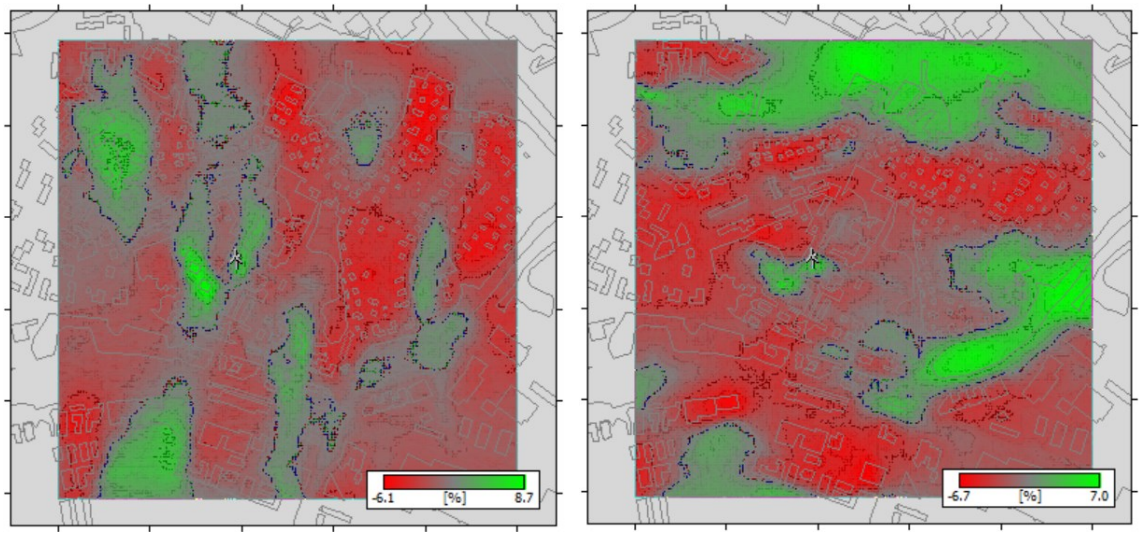

Figure 22: Orographic sub-model spatial study site view for the west (left) and south (right) winds

Figure 22 shows the interpolated climatological data for the turbine height for the west and south winds influenced by the orography lift.

4.3.2.4 The statistical model of wind estimation

Wind motion around the Earth is a stochastic phenomenon. The data in climatology dataset is averaged over the calendar months and can be explained by the statistical model. The statistical model describes the wind speed and the wind directions as a frequency distribution. This model is described by the two-parameter Weibull distribution function [85], which is shown in the equation [81]:

$$h(u) = \frac{k_{weibull}}{A_{weibull}}\left(\frac{u}{A_{weibull}}\right)^{k_{weibull}^{-1}} exp\left(-\left(\frac{u}{A_{weibull}}\right)^{k_{weibull}}\right) \tag{7}$$

The Weibull distribution function describes the fraction of time the wind speed is between u and $u + \Delta u$ for a given Δu.

- Factor $A_{weibull}$is the scale parameter, describes the number of days with high wind speed. The higher $A_{weibull}$ factor is, the higher number of windy days is. This factor can give the main concept of the wind situation on the site.
- Factor $k_{weibull}$ is the shape parameter, describes the shape of the curve. The lower $k_{weibull}$ factor is, the bthe roader wind speed distribution is, which means the high variety of speed ranges. $k_{weibull}$ scale factor stays in 1.6 to 2.4 rage.
- The unit of h stated as a percentage of hours per year per m/s.

The plot in Figure 23 represents a helpful as well as a practical view of the average wind speed with a variety of $k_{weibull}$ scale.

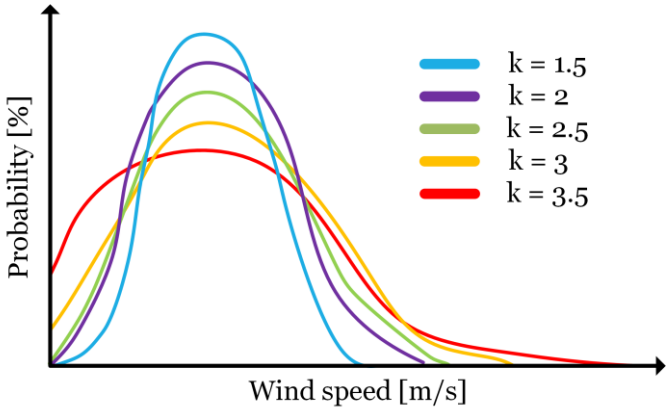

Figure 23: Weibull distribution plot for different k_Weibull scale factors

The statistical model represents the results of the wind simulation across the studied area since it is based on the topographical analysis and wind climate data.

Since the statistical model of wind distribution is done, the turbine selection could be the next step in determining of generated energy from the wind.

4.3.3 Wind turbine selection and onsite positioning

It is important to choose the correct wind turbine since all turbines differ in terms of power curves, cut-in and cut-off wind speeds, power control. [85] Different models but with similar nominal output power would, therefore, show different energy production.

4.3.3.1 Wind turbine operation principles

Wind turbines can be divided into two different types, depending on the axis of rotation: horizontal or vertical. [71]

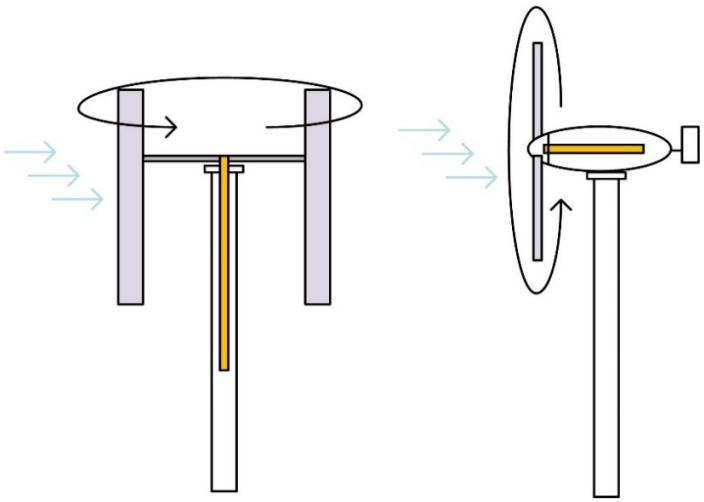

Figure 24: Schematic drawing of VAWT (left) and HAWT (right)

Vertical axis wind turbines (VAWT) are usually designed for the urban usage only since they do not need to be positioned in the direction of the wind flow and produce less noise. Nevertheless, the total energy production of VAWT is below HAWT. Figure 24 on left shows the HAWT's schematic drawing.

Horizontal axis wind turbines (HAWT). Figure 24 on right shows the HAWT's schematic drawing. The propeller-type rotor is installed on a horizontal axis. The rotor must be placed into the wind direction by the use of a tail or a yaw motor. HAWTs are sensitive to the changes in wind flow direction and turbulence, produce noise but in overall can generate more electricity than vertical axis turbines.

The wind turbine generates electricity by extracting the power of the airflow from the swept area of the rotor disk [85] Power in the airflow is given by the Equation 8. It is clearly seen that the airflow power most of all depends on the speed since it is a cubic value.

$$P_{air} = \frac{1}{2}\rho A U_w^3 \tag{8}$$

The wind turbine cannot extract all airflow energy so a power coefficient (C_p) is defined which is the ratio of power extracted by the rotor to the power in the airflow. [71] Power coefficient C_p is given by the equation:

$$C_p = \frac{P_{wt}}{P_{air}} \tag{9}$$

The power that could be generated by the wind turbine given by the equation: [71]

$$P_{wt} = C_p P_{air} = C_p \frac{1}{2}\rho A V_w^3 \tag{10}$$

Given by the Betz limit, it states for every fluid turbine, as so as for wind turbine, the maximum power that can be extracted will not exceed the 59% [71] of the airstream power:

$$C_{pmax} = \frac{16}{27} = 0.59 \quad (11)$$

The generated power as a function of the wind speed at hub height is called the *power curve*. Figure 25 shows a power curve.

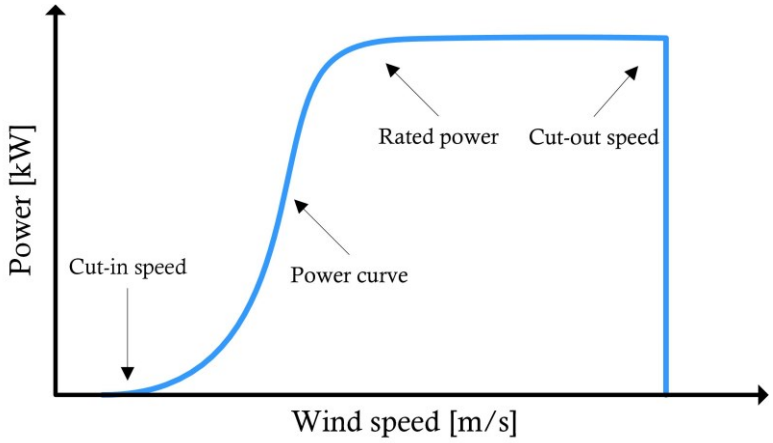

Figure 25: Power curve example

Below the *cut-in wind speed*, the wind generator stays suspended, since the power in the wind flow is not enough for practical electricity generation. During energy generation phase, the output increases by early stated in Equation 8 cubic relationship with wind speed until achieved *rate wind power at rated speed*. Above rated wind speed, the aerodynamic rotor blades are designed in a way to limit the power derived from the wind flow. In case of extremely high wind speeds, called *cut-out speeds*, the turbine will be shut down and will not produce electricity. [89]

The wind turbine electricity generation calculation is based on the turbine power curve, and wind speed on the height of the turbine's tower at a standard air density under the specified temperature and pressure. If the wind speed at the turbine tower is higher than the cut-out speed of the turbine, the turbine does not produce electricity, following the assumption that wind turbine does not produce electricity bellow cut-in and above cut-out speeds.

4.3.3.2 Wind turbine selection comparison

In order to select the best turbine for a particular studied site, 17 different SWTs were studied. All turbines were certified under international standard IEC 61400-2 and in some particular EU countries but still may not be certified in Finland, since there is but no EU unified standards. [72]. All compared below SWTs could be installed on the roof with a specially designed tower. Since there are not many SWTs manufactures on market, five different turbines were selected based on such criteria:

- Skystream 3.7 manufactured by Southwest Windpower, USA. It is one of the most selling SWT on the market.
- Proven6 manufactured by Kingspan Wind, United Kingdom. It is designed for work in the aggressive environment, such as gusts of wind, blade icing, and low temperatures.
- AV-7 manufactured by Aventa, Switzerland, is designed for a low-wind-speed.
- Qr6 manufactured by Quietrevolution, United Kingdom, is the example of VAWT design designed for the aggressive environment.
- SA40 manufactured by Ropatec, Italy. The VAWT has a highest rated capacity for the on-roof turbine.

Appendix 7 provides detailed information for comparison according to their technical characteristics which are based on manufacturer datasheets and corresponding websites.

The type of the rotor has a huge effect on the power curve of the turbine. [89] Figure 26 shows, that VAWTs can operate in high wind speeds, but this feature cannot be utilized at the studied site, since, according to Section 4.3.2.4 the probability of high wind speeds is too low. In this case, the HAWT turbines are a better choice, but the main drawback is the noise from the rotating blades that is why the installation approval in an urban area could be a challenge.

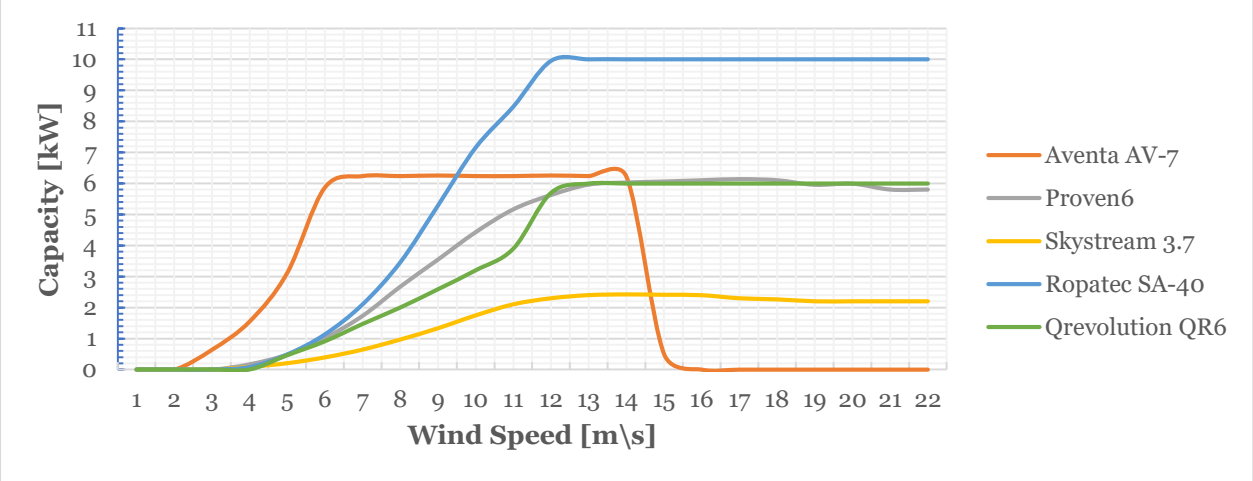

Figure 26: Power curve of compared wind turbines

The tower height, since the turbulence and separation bubble should be avoided by installing turbines on highest tower possible. The tower height is important according to Equation 10, where the speed is proportional to height.

Since almost all wind turbines utilize PWM inverters, that allow turbine speed to fluctuate without the influence of the output voltage. Therefore, the I-V parameters of the generator are not so important. [93]

Since the average wind speed at the studied site is 4.45 m/s, turbines with higher cut-in speeds are useless. Figure 26 illustrates the power curves of each reference turbine.

It is clearly seen that all turbines except Aventa AV-7 have a cut-in speed of 3.0 – 4.0 m/s, so according to Section 4.3.2, some of the wind flow energy will be extracted.

By analyzing the competitors, the AV-7 is the best choice for the study site. The turbine differs substantially with respect to their output at studied site average speed, their rotor surfaces, and their costs. Because of the huge swept area of rotor A, the AV-7 shows the highest output at studied site wind speed. The AV-7 turbine also have the lowest cut-in speed and its working conditions can help to achieve maximum possible electricity generation among other compared turbines. The AV-7 can be installed on the high tower, which lead to a better wind flow and lower turbulence disturbances. The degradation of energy conversion is set to 1.6% every year. [94]

4.4 SIMULATION RESULTS

4.4.1 Wind climate analysis results

Based on the Wind Atlas data, the average wind speed at a 50m height at the studied site sector is 4.5 – 5 m/s. The highest speed 5.5- 6.0 m/s occurs on January and the lowest 4.0 – 4.5 m/s occurs on April. Since the 250 by 250 m² grid resolution data is lack of the wind directions, 2500 by 2500 m² grid will be used in the simulation. The data consists of monthly wind speed at 50 meters' height under 12 wind directions. Should be noted that the results of the Wind Atlas are represented by average wind conditions in a certain area, not in a single geographical point, so they should be interpolated for a particular studied site.

4.4.2 Wind speed estimation results

The results of the statistical model simulation are shown in Figure 27. The left side describes annually $k_{weibull}$ factor distribution for all wind directions. The studied site is red colored ($k_{weibull}$ = 2.18), which correspond to narrower wind speed distribution compared to the neighbor area. The right side of the Figure 27 describes the $A_{weibull}$ scale parameter for all wind directions, shows that that the studied area could be utilized for the wind power generation, since minimum speed equals to 4.39 m/s. and maximum equals to 4.87 m/s. The minimum $A_{weibull}$ factor at the site equals to 5.0 m/s and maximum equals to 5.5 m/s. It could be noted, that west buildings have even better opportunities for wind energy generation, since their $A_{weibull}$ factor equals to 5.5 m/s.

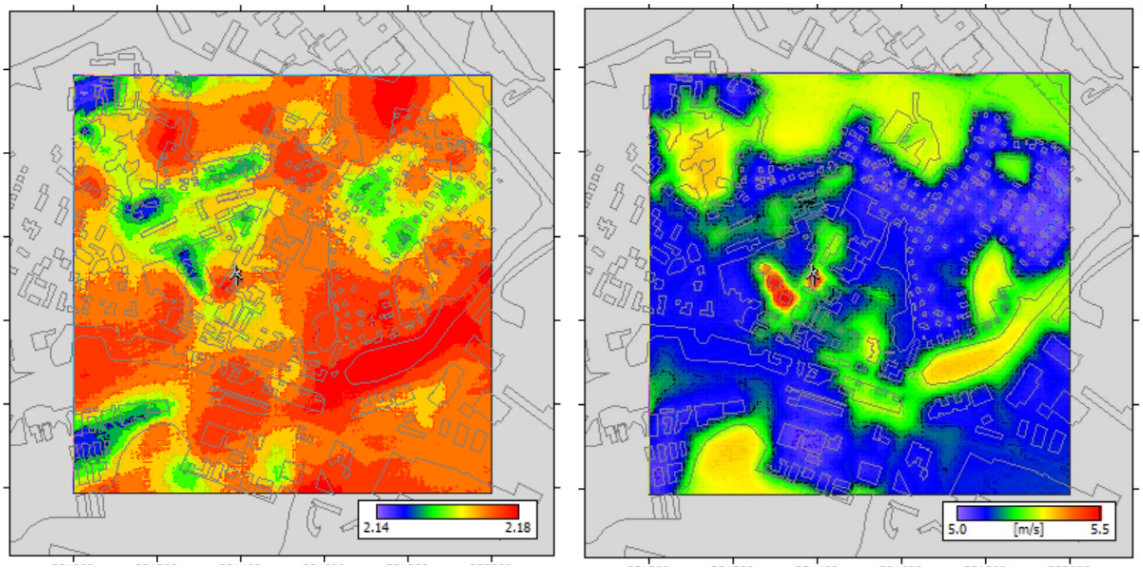

Figure 27 Weibull distribution k (left) and A (right)

Appendix 8 describes the results of the simulation in a more detailed way, including wind parameters and the power density per twelve sectors, where each sector differs by 30° from the previous one.

The highest wind speed is reached at 210 and 240 sector which is the side where no tall structures are situated. The opposite could be stated for the 30 and 60, where the lowest wind speed and are three tall and steepness buildings are situated. Wind in the speed range of 2.5 – 4 m/s is available from every direction, however, wind speed of 4.5 – 5.5 m/s most of the time is available from the north-east directions. Nevertheless, all sectors are suitable for wind energy generation. Based on Weibull wind speed distributions, the hourly wind speed model was built.

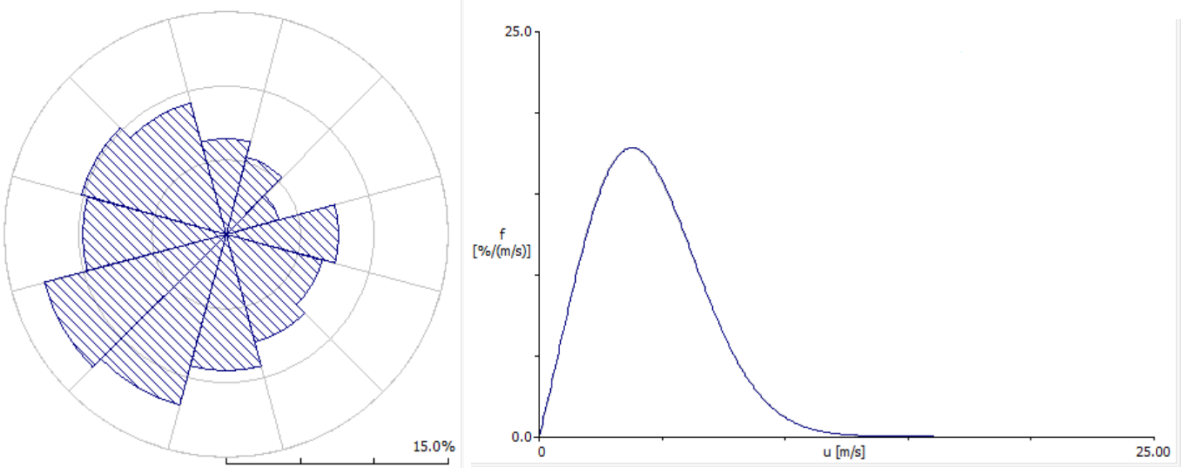

Figure 28: Histogram (left) and Weibull (right) wind speed distribution at study site

Figure 28 on left shows the sector histogram wind distribution, for a studied site. It shows the percentile of occurrence for every range of wind speed. The top sector is defined as 0° and the rest are defined clockwise. The sector histogram is defined as a variation of wind speed relating to climatological variations at the studied site of

turbine installation. Figure 28 on right represents the Weibull distribution curve for all sectors, where $A_{weibull}$ factor equals to 5.0 and $k_{weibull}$ factor equals to 2.13.

4.4.3 System simulation results

During the Chapter, it was found that the southern part of Finland is suitable for wind energy generation. The mean wind speed at the height of the turbine's tower equals to 4.45 m/s, with the strongest wind from the North. The Venta-AV 7 was selected as the best choice for onsite installation. The height of the tower to which the wind turbine will be installed is 15 meters. The amount of electricity generated during the year, without taking into account the degradation equals to 23606 kWh. The CF equals to 43.1%. The average produced energy equals to 10.34 kWh/kWp/day. The highest energy generation occurs in November is 2.911 kWh. The lowest energy production occurred in June is 2.483 kWh. The averaged distribution of energy generation during the year is shown in Figure 29. The degradation of energy conversion is 1.6% every year [94].

Installation and use of a wind turbine may be difficult or impossible due to a lack of withstand calculations of static and dynamic forces produced by a wind turbine on the roof, and also noise, vibration, and flicker that can lead to discomfort of the local residents.

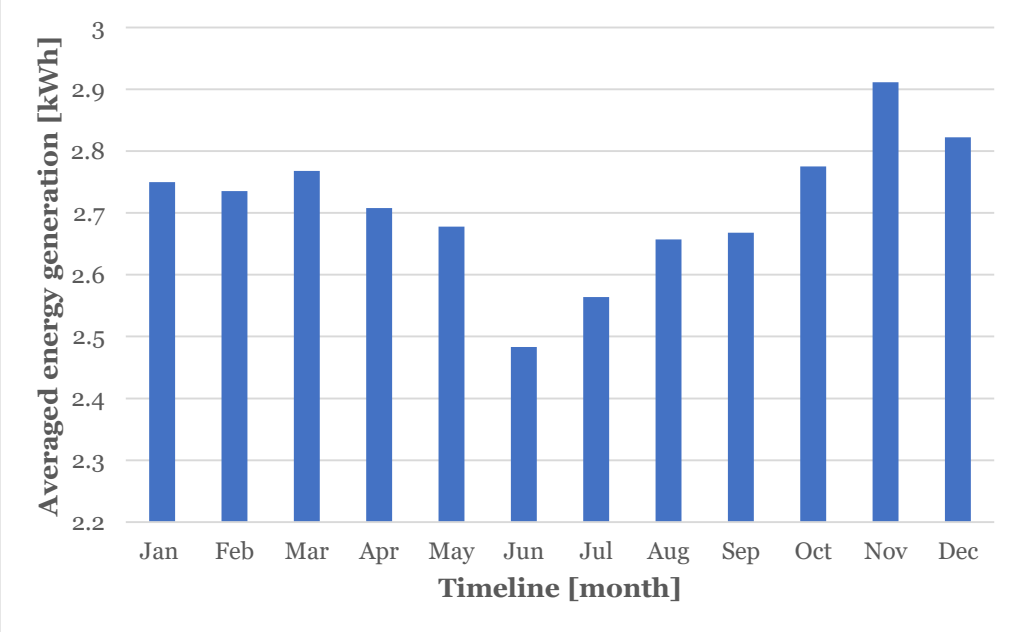

Figure 29: Distribution of energy generation of wind turbine

5 CONSUMPTION ANALYSIS AND FORECAST

5.1 CHAPTER INTRODUCTION

The feasibility analysis of different RESs cannot be processed without a study of the demand site. The onsite generation capacity is always limited, and in case of PV panels due to panel degradation, it will be decreasing every year. The energy consumption is growing at 1.5% every year [8], so the equilibrium between the generation capacity costs and the onsite generated electricity should be achieved in a reasonable way. At the same time, the demand response is important for energy consumption forecast, since solar and wind electricity is not a reliable source. [95]

This section develops a model for forecasting the energy consumption of the studied site for the next 25 years. It is based on time-series regression historical data analysis. [96] [97] [98] It will be examined for energy repetitive seasonal energy consumption patterns. Consequently, these patterns will be used for forecasting of electricity usage at the studied site. The process is divided into three stages of time-series analysis and interpretation: [96]

- descriptive evaluation and data preparation of electricity consumption;
- time series modeling of electricity consumption;
- forecasting of electricity consumption.

In this section, the nature of the time series is discovered. The data will be analyzed for a trend in and energy consumption and whether or not there are hourly, daily weekly or seasonal trend is present in energy consumption data. Based on this analysis, the basic components of the electrical energy consumption forecast will be derived. [97]

5.2 METHODOLOGY

5.2.1 Descriptive evaluation and data preparation of electricity consumption

The demand response is represented by hourly resolution load profiles of the studied site. Each measured point corresponds to the total electricity consumption. Since heating at the studied site is done by the district heating system, it will not be taken into consideration of energy demand response. The load profiles are supplied by Talokeskus Oy and consist of 13998 data points, measured from 2015 to 2017.

However, there are 6% of data points missing from the total measured data. The lacking data was patched by ARIMA model. [97] The ARIMA model is based on the concept of transforming the time series to be stationary. [99] Thus, the ARIMA model is a linear problem, represented by equation:

$$y_t = const + \varphi_1 y_{t-1} + \varphi_2 y_{t-2} + \cdots + \varphi_p y_{t-p} + \varepsilon_t \quad (12)$$

The ARIMA model was executed by Oracle Cristal Ball software, with Automatic model selection criteria so all forecasted models are fitted to each series. [99] Care was taken to ensure that missing hours are restored with the corresponding hours, i.e., missing data for 12:00 are replaced with the forecasted data at 12:00. Similarly, weekday hours are replaced with other weekday hours and weekend hours are replaced with the corresponding weekend hours. The final dataset has 11256 observations, starting at 2015 and finishing at 2016.

5.2.2 Time series modeling of electricity consumption

A time series is an ordered combination of values over similar periods of time. The general method in studying time series is to decompose the series into the following three elements [96] :

- the trend is the overall yearly movement that the data demonstrates throughout the period without adjustments for seasonality or other unevenness;
- seasonality is the routine fluctuation of the data, that contains indicators which might be constant in time, magnitude and direction;
- residuals are the stochastic component of the time series data.

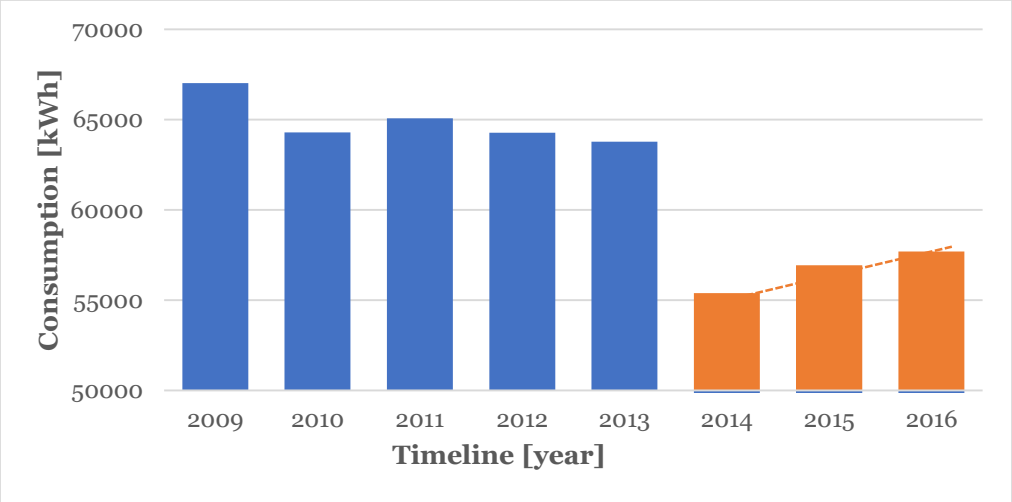

Figure 30: The annual consumption of study site

Figure 30 shows the annual consumption of study site from 2009 to 2016. Started from 2014 lighting renovation was done, so the electricity consumption of previous years with incandescent lamps usage is not relevant. Based on the 2014-2016 linear trend, the average energy consumption will grow 2.02% annually.

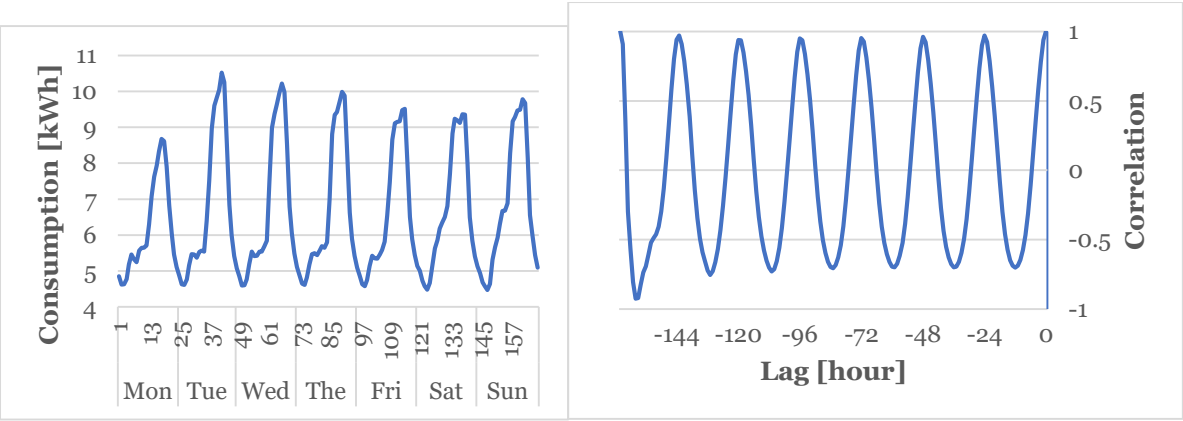

Figure 31: Weekly average consumption (left) and the autocorrelation of consumption (right)

Figure 31 on the left shows the yearly average consumption of the studied site over one week, averaged over time for all 64 apartments. Each day is clearly recognizable and shows seasonality. It is interesting to notice, that Monday has the lowest peak across the whole week, since students spend more time at the university classes at the beginning of the week. Nevertheless, it is easy to distinguish Saturday and Sunday weekends, when students wake up later, compared to the studying days. On the top of that, every different hour of the day follows a unique pattern. This is convenient, since the consumption is minimal at night, when only a fridge, some lights, and the electrical appliances are in standby mode. The consumption grows to its peak at around 20:00.

Figure 31 on the right confirms the seasonality statement, showing the autocorrelation of electricity consumption aggregated over the whole building. Figure 31 on the right shows that the consumption of any single hour is highly related to the same hour of the day before or even seven days before. Furthermore, the electricity consumption is highly correlated with the consumption from four hours before. This indicates that consumption hours and the days of the week are seasonal, repeating elements.

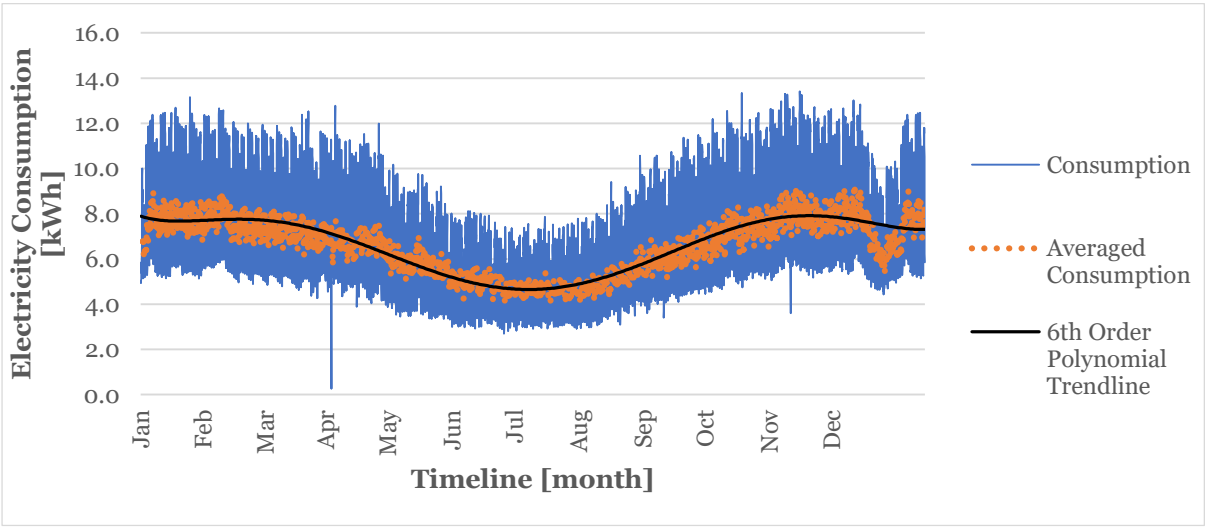

Figure 32: Yearly consumption of study site

Figure 32 shows the hourly consumption of studied site at 2016. It is clearly seen that the highest consumption occurs from November to February. This is explained by the fact that these months are the coldest, so electric heaters are used during these

months. Another factor of higher consumption is the short length of light day during winter days, so lights inside are used for a longer period. The drawdowns are clearly seen during summer and winter holidays when students usually are not staying at the dormitory. Given the data on hand, the best fit for yearly seasonality is described by the 6th polynomial equation. The visual inspection of Figure 32 proves that the chosen yearly seasonality equation is corresponds to the real data.

5.2.3 Data segmentation

The energy consumption patterns depend on the segmentation by features that are correlated with the consumption. [97] [98] The segmentation will utilize the periodic patterns for identifying the consumption tendencies in the time series data thus the consumption patterns will be segmented into different groups. [96]

During the time series analysis, two consumption patterns were found: climate and study-year based patterns. The climate pattern was divided into two groups with respect to climate conditions. In other words, there is a difference between the warm and light period (summer) and the cold and dark period (winter). Figure 33 shows winter and summer electricity consumption, in comparison to the average annual consumption. The summer period was defined for the weeks from 22nd to 31st, while the winter period from 36th to 17th week. The weeks that are between the mentioned periods are defined as transitional weeks.

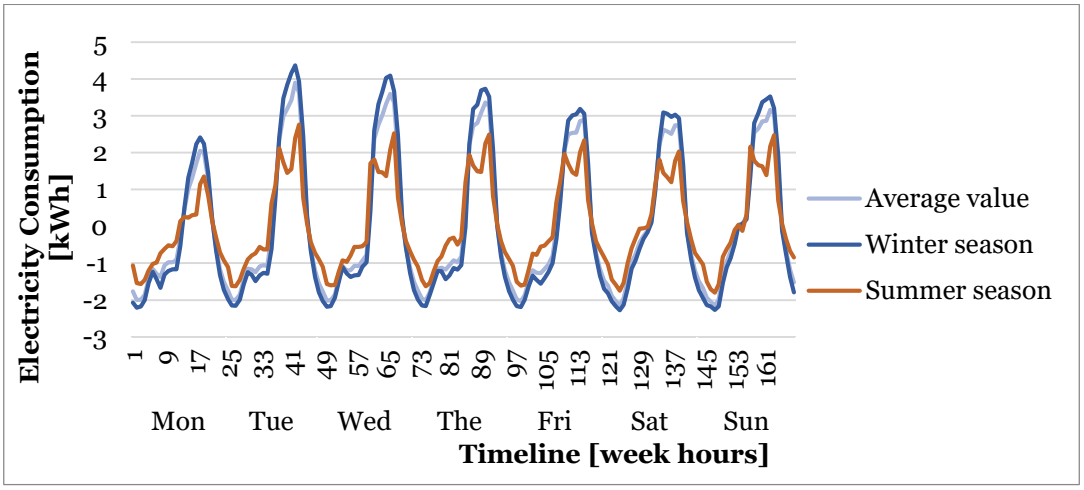

Figure 33: Average summer and winter electricity consumption

The study-year pattern was divided into two following groups: vacation and studying period. As it can be seen in Figure 34 the patterns of those groups differ, since during university study period students are staying at their apartments and using the electric appliances, while during the vacation period the consumption pattern is decreases due to student being away. The study period was defined for the periods of from 1st to 17th and from 35th to 52nd week, while the vacation period is defined from 18th to 35th week.

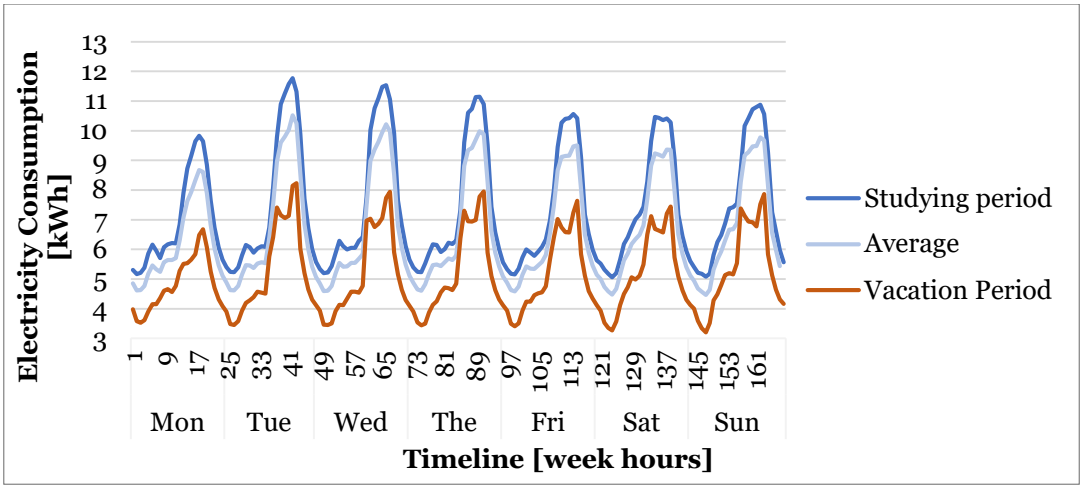

Figure 34: Average studying and vacation electricity consumption

5.2.4 Validation of consumption model

To be able to ensure that the consumption model is relevant and could be used for electricity consumption forecasts, the synthetic data should be compared to the real statistical data. [100] Figure 35 shows the comparison between the synthetic and 2017 historical data divided by for seasons. The annual correlation equals to 0.90. Furthermore, the model is matching the Finnish consumption trend. [101]

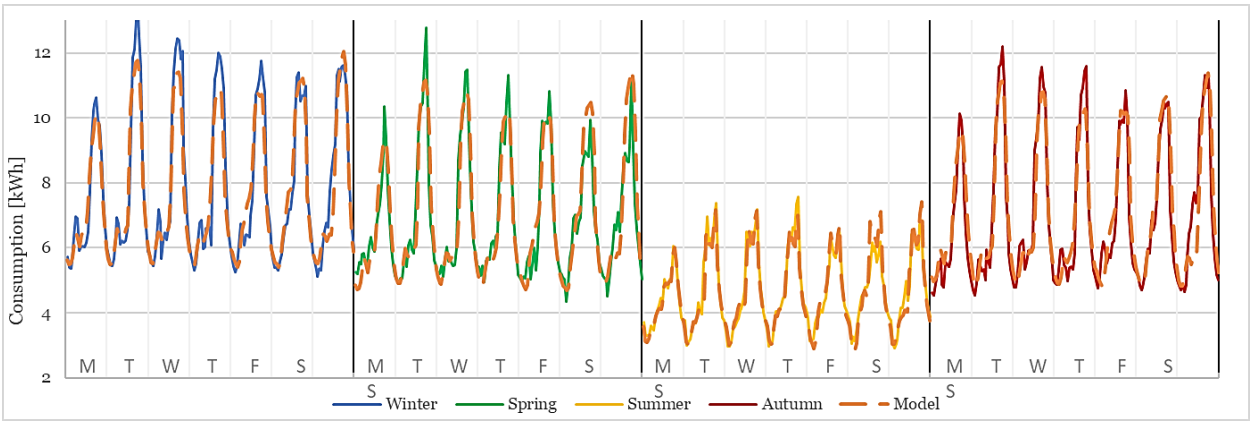

Figure 35: Comparison between the historical consumption data and the model, divided according to season

There is still some slight variation in synthetic and real consumption data. Such variations occur due to a stochastic residual component of the time series. Thus, according to the mentioned above factors, the electrical consumption time series are quite accurate.

The electricity consumption is highly correlated to the consumption of previous hours, which leads to daily and weekly repeating elements. The electricity demand of the studied site is generally driven by the climate and the educational process. Due to the seasonality in weather conditions and educational process following the yearly cycle, the total electricity consumption presents a seasonal pattern with higher demand during winter and lower demand during summer. The seasonality affects not only the

consumption patterns but also the yearly trend, which forms the overall seasonality fluctuations. The overall trend is driven by the annual consumption forecast.

The built model was validated to the historical data, and demonstrated rather high correlation, so the model can be utilized in further studies and calculations.

5.3 CONSUMPTION FORECAST RESULTS

During the Chapter, it was found that the site consumption has different seasonal variations and long-term trend. The consumption of study site will grow 2.02% annually. based on the created consumption model, the 25-year forecast was built, which will be used during the feasibility study. Understanding the power consumption helps to calculate the system capacity and use it as efficiently as possible.

6 ELECTRICITY PRICE ANALYSIS AND FORECAST

6.1 CHAPTER INTRODUCTION

Due to seasonal nature of solar and wind-generated energy, and energy security, the studied site should be connected to the grid. [46] [31] [89] The grid connection allows not only to buy, but also, under certain conditions, to sell the surplus electricity back to the grid. Generally, the electricity prices have a high influence on the consumption, but, at the same time, can greatly affect the overall need for the onsite generation capacities. [71] [31] Based on this conclusion, this Chapter will describe the energy price forecast for the next 25 years. Two different electricity trading approaches will be compared: pool-based market and bilateral contracts. Pool-based electricity price is formed by the market supply and demand equilibrium. Bilateral contracts allow directly going into short-term and long-term contracts between the supplier and consumer. As for the studied site, it is possible to buy electricity on the terms the contracts or at the market prices. This chapter will investigate both alternatives in terms of long-term forecasting and feasibility for the end user.

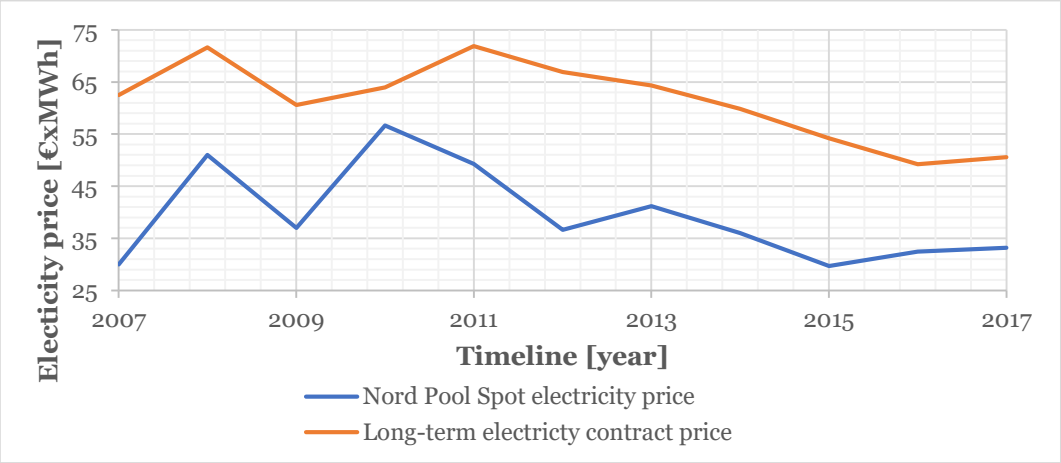

Figure 36: Comparison between Finnish NPS market and ling-term contracts

Figure 36 shows the comparison between Finnish Nord Pool Spot (NPS) power market price and the averaged long-term contracts electricity prices during 2007 – 2016. As seen from the figure, the prices of the long-term contracts are followed by the market prices, since the government is not controlling the retail electricity prices. The long-term contracts are partially tied to the NPS electricity prices. Long-term contracts can smooth the electricity price, but at the same time deprive the flexibility of the consumption control.

Based on stated above, both pricing principles will be used during the study.

6.2 METHODOLOGY

6.2.1 Electricity price formation

The overall electricity price for the end consumer consists of three following components:

- *Electricity price* is the price for the consumed electricity that the seller will receive. The electricity market price grew by 10.6% between 2008 and 2017 while the difference between market price and the long contract price decreased by 46.5% between 2008 and 2017. [102]
- *Transmission and distribution costs* include all costs related to the transport and distribution of electricity. The distribution tariff is set to 2.91 c/kWh excl. VAT with a basic charge 4.44 EUR/month excl. VAT by government-owned Helen Sähköverkko Oy's distribution network. [103] The transmission and distribution costs forecast is based on a multiple linear regression of last 10 year period averaged transmission and distribution monthly prices, obtained from StatFin database [102] :

$$y_{distr\ price} = 0.0558x + 2.91 \quad (13)$$

- *Taxes*. According to the Act on Excise Duty on Electricity and Certain Fuels (1260/96) [104], electricity tax is divided into two categories:
  - Tax class I, 2.253 c/kWh.
  - Tax class II, 0.703 c/kWh.

Tax class I is used for private households, tax class II is used in industry or server rooms. Since the studied site is the apartment building, the I tax class will be used. Electricity price, transmission and distribution costs, and electricity tax are subject to value-added tax (VAT), which equals to 24 %, assuming that AYY does not get VAT paid for the electricity refunded, for simplicity. The forecasted tax class I value is based on a multiple linear regression with 10 data points of 10-year period:

$$y_{tax} = 0.1266x + 2.253 \quad (14)$$

6.2.1.1 Feed-in tariff

The power plants with a rated output power of less than 100 kVA are exempted from the duty. At the same time, if the annual sales will not exceed 10 000 EUR, the VAT charge is not collected but a small brokers fee will be charged. Transmission and distribution cost is also not collected from the power plants with less than 100 kVA output power. [103] [104]

Based on stated above, the consumption of onsite-generated electricity can save on the transmission and distribution fee. At the same time, feed-in tariffs allow selling electricity without any extra charges and lower the tax burden on the studied site.

Since electricity could be bought in two different ways by signing the bilateral contract or at market prices, both electricity price forecasts should be modeled.

6.2.2 Long-term bilateral contract electricity price forecast

The most common type of the bilateral contracts in Finland is two-year long-term general distribution contract. [105] The contract is signed for a fixed electricity price for two years, so the electricity price will stay fixed at any time during the contract time. According to Finnish regulations and liberalized market principles, electricity sellers may not be producers of that electricity, but shall trade electricity that is bought on the market or elsewhere. [106] The consumer electricity market has, therefore, numerous participants.

Fifteen electricity sellers were examined to find the best fitting long- term contract. The selection was not only based on the hourly electricity price but also on the availability of sell-in the surplus electricity. Appendix 9 describes the compared electricity sellers.
Based on this comparison, the chosen electricity seller is Helen Oy, since it offers a reasonable electricity price, that equals to 4.79 c/kWh, a monthly fee 3.84 EUR/month and no trade-in fee. This means that Helen Oy undertakes to buy the surplus electricity for the NPS Finnish region price. The Helen two-year contract will be used as the initial value for long-term contract model.

The bilateral contract prices are based on the NPS prices. [107] The bilateral contract electricity prices are correlated at 0.77 with the spot electricity prices. [108] Based on this, the trend of bilateral contract electricity prices will be based on multiple linear regression of the spot price, that will be discussed in Section 6.2.3.

6.2.3 Electricity spot and futures price forecast

Since 1995 the electricity supply chain was deregulated in Finland. After 1998 Finnish electricity market became a part of the interconnected Nordic market, NPS. During last decade, the households were introduced to hourly pool-based market-driven price formation. [109] The core idea is that a consumer can buy the electricity at the real-time prices with some small fee introduced. In this case, the demand side management can decrease the total energy costs. This section will study the electricity pool-based market price formation and will introduce the pool-based market price forecasting model.

In the NPS market, the electricity trading is introduced to complimentary marketplaces. Elbas stands for intra-day trading and Elspot, for next-day trading. The Elspot marketplace forms the system price which is used as a reference for financial contracts and for pool-based market-based contracts. The system price is based on the equilibrium between the supply and demand. [110]

As a complimentary part of Elspot and Elbas marketplaces, a huge role is played by the financial electricity market, hosted by NASDAQ OMX Commodities exchange marketplace. [111]

The financial electricity market allows to hedge the future electricity deliveries with the use of electricity futures and forwards contracts. The difference between futures and forwards is in standardization of futures, while forwards are tailored individually and are traded over the counter. The prices for future contracts can be openly observed on NASDAQ OMX Commodities. Hence it is the futures that are used in the further discussion. [112]

The NPS system price is the reference for all future contracts. Since the correlation between short-term (only few weeks long) and long-term futures is low [111], the short-term contracts are not relevant for the forecasting purposes. Hence, a minimum one-year future contracts will be used in the forecasting model for the pool-based electricity market price.

Since the NASDAQ OMX Commodities exchange marketplace is trading the electricity generated by imperfectly storable fuels, such as hydropower, wind or photovoltaic, future prices on that electricity can provide the spot price formation. [112]

Furthermore, electricity futures prices consist of anticipated spot prices and risk premium. [113] For this reason, the relationship could be expressed by the equation:

$$F_{t,T} = E_t(S_t) + P_{t,T} \tag{15}$$

A market where supply and demand coincide is called a balanced market. Under such conditions, $P_{t,T}$ equals to zero. [114] In this study, it is assumed that the NPS market is a balanced market, therefore, the futures prices are equal to the spot prices at the same period of time. Based on that, the futures electricity prices will be a base for the electricity spot price linear trend for the forecasting model.

6.2.4 Time series modeling of electricity spot price

The spot price forecasting model will be build based on time series decomposition, that was discussed in Section 5.2.2. The time series are decomposing in three elements: trend, seasonality, and residuals.

Since the futures prices are showing the spot prices in future, they will be used as a trend line for the model. The futures prices dataset was taken from Thomson Reuters DataStream financial database [115] and consists of yearly futures from 2017 to 2027 with 11578 system price data points and 5066 Finland region data points. According to the futures pricing, the spot market price will rise by 0.56% every year.

The seasonality was studied by historical time series analysis of the NPS market data. This set of Nord Pool historical price data includes Elspot historical price data for the NPS system price, consisting of hourly price observations for the NPS system price from 1.1.2007 to 31.12.2016, total 87 672 hourly observations.

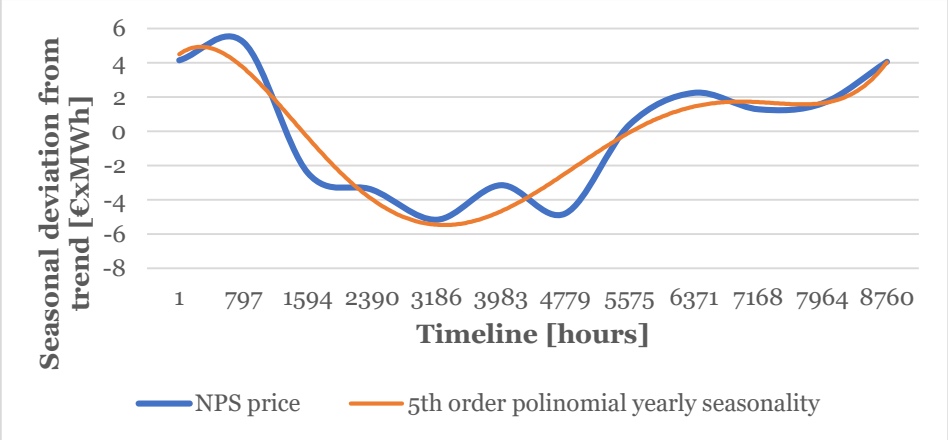

Figure 37:Yearly averaged electricity PNS price

Figure 37 shows the average electricity spot price averaged for ten years. It is clearly seen that the electricity price will go down in summer when the vacation time and most of the manufactures are not working. The highest price occurs during the winter season, since some buildings use electric heating systems. The peaks are smooth due to a high hydropower plans capacity in the system, that can regulate the generation on short notice. Based on that, it could be stated that electricity spot price has a yearly seasonality. Consequently, yearly seasonality will be described by the 5th polynomial equation.

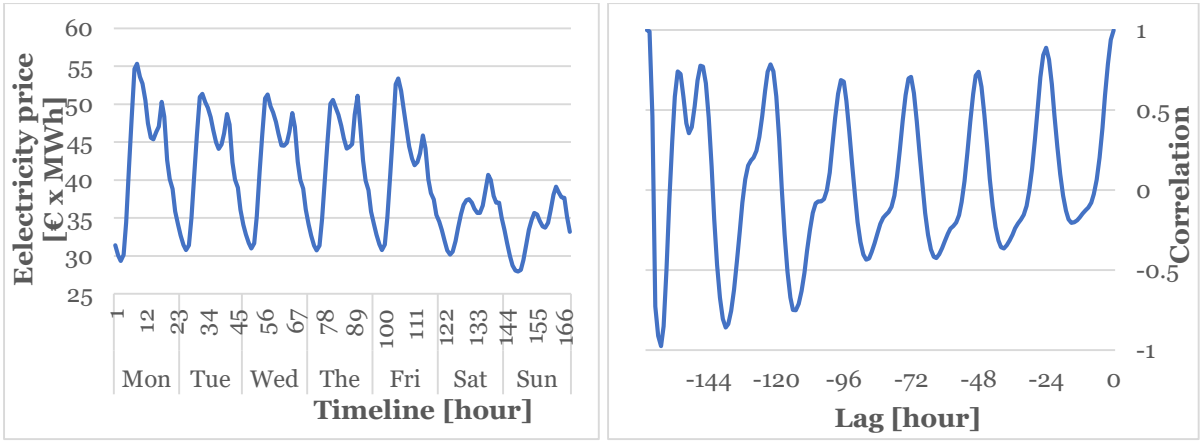

Figure 38: Yearly average NPS electricity price (left) and autocorrelation of NPS electricity price (right)

Figure 38 to the left shows the yearly average spot price at NPS market over one week, averaged over last ten years. Each day is clearly recognizable and demonstrates seasonality. It is clearly seen that the highest price occurs during working days, while the cheapest electricity could be bought during nights. This happens due to the fact that the largest consumers are manufactures, and they drive the demand up. Hence, the demand is low at night, so the price is also low during the night.

Figure 38 to the right confirms the seasonality statement, showing the autocorrelation of electricity spot price for the 168 hours. The price volatility is high at the spot market. Figure 38 (to the right) shows that the price of any single hour is highly related to the

same hour at the day before. This indicates that consumption hours and the days of the week are seasonal, repeating elements.

6.2.5 Validation of electricity spot price model

To be able to ensure that spot market electricity price forecasting model is relevant and could be used for electricity price forecasting, the synthetic data is compared to the real NPS hourly data. [96] Figure 39 shows the comparison of synthetically generated data with real data. The yearly correlation equals to 0.49 which can be viewed as a good accuracy, with acceptable deviation. [96]

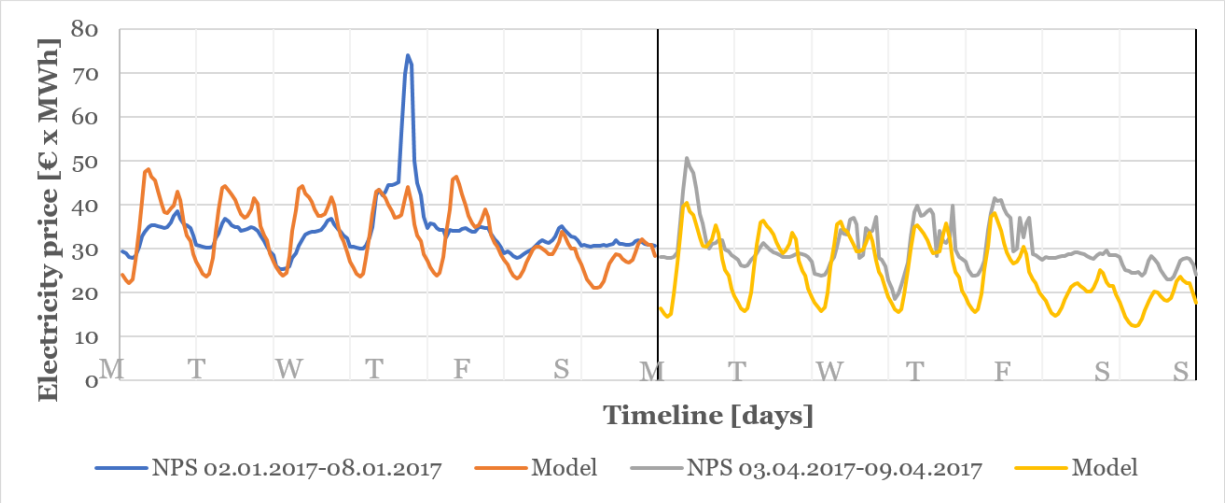

Figure 39: Synthetic and real data comparison

Based on the stated above, the synthetically generated electricity spot market price could be used for further study.

6.3 ELECTRICITY PRICE FORECAST RESULTS

During the Chapter, it was found that the two-year long-term contract electricity price will be increased up to 0.76 % every second year during the 25-year period. The electricity spot market price has a year seasonality. The futures electricity prices are a base for the electricity spot price linear trend. The sell-in electricity price is based on electricity market price model, developed in Section 6.2.4 since it is in direct dependence on the equilibrium electricity market prices. The trade fee will remain zero for the whole duration of the study. The electricity price forecast was validated and will be used in feasibility analysis.

7 FEASIBILITY ANALYSIS

7.1 CHAPTER INTRODUCTION

The main selection criterion of any feasibility analysis is economic analysis [116], in other words, the study should answer the question, is the system feasible or not. If the answer is yes, how much will it cost.

The system is assumed to be feasible when the electric part of the system can be properly served. The next step is to quote the overall installation and maintaining costs of the whole system during the lifetime of the project. Three main stages will be done during this chapter.

- *System simulation* procedure will analyze different operational approaches to calculate the energy balance between system elements over the project lifetime. The simulation will compare the energy supply from different sources with the demand and energy storage.
- *System optimization*. Several most feasible system configurations will be compared, thus, based on the economy and generation feasibility the optimal configuration will be selected.
- *System sensitivity* analysis will denote the weaknesses and threats of the selected configuration.

7.2 METHODOLOGY

Chapter 7 study procedure is based on the Homer PRO [117] software's guideline.

The Homer PRO software selection is based on a comparison of three different software that are able to simulate RES system.

RETScreen Expert is an Excel-based freeware product developed by the Government of Canada. It can compute the financial analysis of the project but cannot optimize the system layout. Homer PRO 3.11 by Homer Energy is a shareware software with trial period. It can carry out the time-series calculations and do the simulation analysis of various system layouts. SAM 2017.9.5, by the National Renewable Energy Laboratory, can calculate basic financial parameters, but cannot analyze system configurations in order to find the most optimal configuration.

Homer PRO has more depth calculations and a system configuration analyzer tool, so it will be selected for overall feasibility analysis.

7.2.1 System simulation

The simulation will model specific generation system configurations, based on previous chapters, generation, consumption and grid interactions. The overall electricity utilization strategy is set to generate maximum energy and consume the

cheapest energy available. In other words, if it will be cheaper to consume electricity from the grid and sell the onsite generated energy, the system will do that. The surplus generated energy will be sold to the grid or will charge the storage, depends what way is more economically justified.

Roof-mounted PV system will be installed for 25 years. The degrading of energy generation is based on the manufacturer's datasheet and equals to 2% every year [44]. The maintenance should be held every season and the costs are stated as 3.5% annually. [30] Wall-mounted PV system panels are same as roof-mounted, so previous statements for roof-mounted PV system are true for wall-mounted panels as well.

The wind turbine system is designed for 25 years of use. The generation degradation of the wind turbine is stated as 1.6% each year. [94] Since wind turbine should be installed on the roof, as well as roof-mounted PV panels, the installation and usage of both systems simultaneously could be complicated.

In addition, taking into account that PV roof simulations were obtained without shadows from turbine tower, the simultaneous usage of both systems will not be considered in the simulation.

The model takes into account an increase in consumption of 2.02% each year. Different seasonal effects were included in the model. The consumption model is not considering the heat load of the studied building.

Grid interactions are introduced by two buying tariffs and one feed-in tariff. Buying tariffs introduced by 2 years fixed price contract and NPS hourly price. The feed-in tariff is an NPS hourly price plus a broker's fee. The electricity price will increase by 2.03% every year. The yearly grid usage fee is 113,01 €.

To investigate the behavior of the system with storage capacity, the storage option was added in the simulation. The Tesla Powerwall 2.0 of 13.5 kWh capacity, 5000-lifetime cycles and 10 years of operation warranty and 6,500 € prices will be used in simulation as a reference for the storage option. The optimum number of batteries will be calculated during the simulation processes. The storage utilization strategy is set to charging a storage bank only by renewable energy when it is beneficial than sell electricity to the grid.

The shipping costs for system components are based on the distance between the seller and the studied site, size, weight, and volume of components. Total shipping costs were estimated and averaged among three different service providers. [118] [119] [120]

Based on a number of reports [7] [33] [121] and personal phone conversations with local PV and turbine installers [122] [123], the installation costs are assumed to be a percentage of the overall system price. Roof-mounted PV installation costs equal to 35%. Since the wall-mounted PV system requires additional installation equipment, the installation costs for these are equal to 40%. The wind turbine installation costs are assumed at 20% of the system fixed costs. The cabling and PV tables prices are source from the corresponding manufacturer websites. [124] [125] As was discussed

in Chapters 3 and 4, all renewable generation systems are eligible for the government subsidy as the percentage of the initial capital costs. The overall price breakdown is shown in Appendix 11, where all prices are in € and 24% VAT included.

The total cost of wind turbine system is stated as 91676.03 € and its annual maintenance costs 2350.00 €. The overall roof-mounted PV system costs 41175.66 €, the maintenance expenses are 1921.53 € every year. The wall-mounted PV system costs equal to 29212.25 €, maintenance will cost 1363.24 €.

Every part of the simulation is presented by 8760 data points for each element. The discount rate is used to attribute a weight to future cash flows. [126] The discount rate is based on Energy Efficiency Directive [127] and relevant research papers [128] [129] [130], with the average rate of 5.75%, The expected inflation rate equals 1.5% is based on a long-term forecast of Bank of Finland. [131] The total number of simulations that was done is 828.

7.3 SYSTEM OPTIMIZATION ANALYSIS

The main purpose of the optimization analysis is to find the most efficient configurations that meet the lowest the levelized cost of energy (LCOE). [117]

After simulating 828 possible system iterations, 24 system configurations were found to be the most effective. Those system configurations are compared by the lowest total net present cost values (NPC) and LCOE values. In addition, the system configurations will be compared by the ratio of renewable sources to the grid, the volume of sold and purchased energy.

The outcomes of system optimizations are shown in Appendix 12, where each row represents a possible system configuration. All presented configurations could be used for implementation. However, the most preferable variant should be selected.

NPC is the sum of discounted expenses and earnings during the whole project duration and calculated by Equation 16. [117] The total NPC contains the initial costs, maintenance and the costs of electricity, bought from the grid. The income, gained from selling electricity to the grid, will decrease the total NPC.

$$C_{NPC} = \frac{C_{annual,total}}{CRF(\,i,R_{poject}\,)} \tag{16}$$

The capital recovery factor (CRF), the series of discounted equal annual cash flows [117], is calculated by equation:

$$CRF(\,i,R_{poject}\,)\,\frac{i(1+i)^{R_{project}}}{(1+i)^{R_{project}-1}} \tag{17}$$

The LCOE is the average price per kWh of onsite-generated electricity for the duration of the project [117] and calculated by the equation:

$$LCOE = \frac{CRF(i,R_{project}) \times C_{NPC}}{E_{served}} \quad (18)$$

Where the E_{served} is the total electric load that was served by the project time life [117], which is calculated by the equation:

$$E_{served} = E_{load} + E_{defferable} + E_{grid\ sales} \quad (19)$$

Based on system optimization analysis, only-grid configuration with the NPS market price contract is the cheapest option with the lowest NPC costs that are equals to 147552.80 € for the whole project period. This configuration does not require any initial capital costs.

In the case of the selection between the fixed contract electricity price or the market-driven contract, the best choice is to select the NPS hourly contract, since it saves up to 12040.7 € during the project lifetime compared to a fixed contract. The LCOE difference between fixed contract and the NPS-driven contract is equaled to 0.01 €/kWh.

The usage of storage is unfeasible due to the high NPC. Initial price and operational costs are high, since batteries should be changed every 10 years. The LCOE value for any storage configuration is much higher compared to any other system configuration. Charging the batteries during summer and, then consume this energy later is not as beneficial as selling generated electricity to the grid. In addition, the usage of storage can increase the renewable fraction only by up to 1.5%. The renewable fraction could be achieved 100%, but this, in its turn, will lead to even higher NPC and LCOE values.

Any wind energy generation configurations are the worst case. Due to the highest initial costs in in combination with a low output, the NPC and LCOE values are the highest. Standalone, the wind system can generate only 26% of consumed energy, when almost all generated energy is consumed on site, with minimal opportunities for energy selling.

The wall-based PV panels can supply up to 29% of the total consumption for the project period. The roof-based PV panels can generate up to 41% of the total consumption. By installing roof and wall PV panels together, the renewable fraction can rise up to 55%, while, during the first operational year, it will be up to 75%. Even due to moderate NPC costs, the combination of wall and roof PV installation can achieve 0.11 €/kWh LCOE, which is the lowest among the compared configurations.

Based on the stated above, *the combination of wall and roof-mounted PV panels with the hourly NPS-driven contract is selected to be the most feasible configuration for the nZEB.*

Taking into account the fact that the uncertainty of external parameters may influence the project implementation and the overall feasibility, inputs sensitivity analysis will be performed in the following section.

7.4 SYSTEM SENSITIVITY ANALYSIS

The sensitivity analysis is widely used in identifying the input parameters of the model that could have an influence on the output of the model as well as calculate the impact of input parameters on the output. [96] [117] The sensitivity analysis can help to evaluate the confidence of the system model and reduce the uncertainty for further research.

Four different input parameters will be studied during the sensitivity analysis, therefore six system outputs that can cause significant uncertainty for the output parameters will be determined. The analysis will be carried out by changing the input parameters of the model by ±5% with 1% step and observing changes in the output parameters of the system. The annual consumption growth for the base case scenario is set at 2%, and this is the proxy for the sensitivity analysis, i.e. the 1% steps are added/subtracted from these 2%, ranging the cases generated by the sensitivity analysis between -3% and 7% of annual consumption growth.

This layout leads to 40 performed simulations during the sensitivity analysis.

Four parameters with low correlation were determined:

- the *nominal discount rate* represents the overall expectations of the growth of the national economy. Changes in the development of economic and production potential of the country can significantly affect the project.
- weather and climatic factors can significantly affect the amount of *generated electricity*.
- changes in the *electricity consumption* should affect the volume of purchased and sold electricity, and, as a consequence, the economic indicators of the project.
- since the cost of electricity for the consumer depends on *electricity price* in the NPS market, the factor of price change can affect the implementation of the project during the lifetime of the project.

7.5 RESULTS

Appendix 12 shows the generation and consumption profiles for each system during different seasons for the first year of installation. The upper left graph shows the week 15, represents the middle of the spring. During that period, the peak generation of PV-based systems three times exceeds the consumption, while the peak wind generation is not exceeding the minimal consumption through the day. The upper right graph shows the summer week 26 profile. During this period, the consumption is the lowest, while the solar generation achieves the highest generation. The lower left graph shows the profile of week 38 during Autumn when the wind generation is on the highest level during the year. The lower right graph shows the profile at week 3 during Winter, when solar systems cannot generate the base load and when the consumption is on the highest level during the year.

Overall, wind generation seems more stochastic throughout the day, but seems more reliable during winter, compared to solar systems. The average wind system generation does not change radically throughout the year. The peak generation of solar systems occurs with 1-2-hour lag behind the consumption peak. The highest generation rate of solar system is achieved during the summer season when the consumption is the lowest and the selling tariffs are the lowest.

The detailed summary of the sensitivity analysis is shown in Appendix 13, where different graphs represent different input parameters.

An increase in the discount rate by 5% of the base-case will reduce the NPC to 73%, even though all fixed assets will be purchased at the beginning of the project. The increase in the discount rate will also reduce operating costs but will lead to an increase in the LCOE. The reduction of the discount rate will lead to a significant increase in NPC by 64%, increase in operating costs and reduce in LCOE.

A five percent increase in electricity production of the base-case will lead to an 8% increase in electricity sales to the grid, but, at the same time, will reduce the volume of purchase by 1%. Also, a slight decrease will occur in LCOE, NPC, and in fraction of the use of renewable energy sources. Five percent reduction in electricity production will reduce sales to 92% and the ratio of renewable energy to 97%. By reducing production by 5% of the base-case, the volume of purchased electricity will increase by 1%. The LCOE and NCP values will increase, respectively, by 4% and 1%.

With an increase in electricity consumption at the studied site by 5% (i.e. 7% of annual growth rate), the amount of energy that will be purchased should increase by 225%, while the volume of sales of electricity should decrease to 69%, and the ratio of renewable energy should decrease by one third. These changes might look rather dramatic, but they are easily explained by the fact that a growth rate is a cumulative value (also often referred to as “compounded annual growth rate”), meaning that it is compounded each year, leading to rather substantial effects over a long period of time.

Also, operating costs and NPC will increase by more than a half, while LCOE will increase by only 9%. Reduction of electricity consumption by 5% of the base-case, will reduce the volume of purchased electricity twice, will reduce the NPC to 76% by reducing operating costs, and the LCOE will decrease to 93%.

An increase in the cost of electricity in the NPS market by 5% of the base-case will increase the NPC and LCOE by almost a half. Reducing the cost of electricity on the market by 5% will reduce NPC and LCOE to 79%.

During the sensitivity analysis, it was found that the discount rate has the greatest impact on the NPC, as it will essentially affect the present value of all income and costs. Changes in production volumes will mostly affect the volume of electricity sold. Changes in consumption volumes will have the greatest impact on the purchase of electricity and, consequently, on overall project costs. Based on the stated above, it should be concluded that the price change will not affect the volume of purchased and sold electricity. Production peaks during the day do not coincide with consumption

peaks, which in case of changes in production volumes, will lead to an increase in sales of surplus energy, but will not significantly affect the change in the ratio of use of onsite production.

It follows that the successful implementation of the project is mostly dependent on external economic factors. In addition, due to certain consumption patterns, the increase in electricity production will not affect the increase in consumption of onsite-generated electricity. Finally, the volume of purchased electricity may decrease with the increase of efficiency of electrical appliances.

8 CONCLUSIONS

Based on the study described throughout this research, its scope, the available data, the theory and methodology used, the following results have been obtained and verified.

- The most efficient configuration of RES for the studied site, in terms of maximum onsite generation consumption, is the use of wall and roof-installed panels.
- The energy storage option is not feasible for any simulated configurations.
- The electricity contract must be based on NPS market price formation.
- This configuration requires 70387.97 € of initial costs.
- The total NPC will equal to 201503.00 €, whereas the LCOE will equal to 0.117 €.
- During the project implementation, 50344.48 kWh will be purchased from the grid and 36461.58 kWh will be sold, yielding 13882.90 kWh of net purchase.
- The renewable fraction in the overall consumption during the project will be 55.16%.
- Changes in consumption and discount rate will be the most sensitive for the project.

In terms of economic feasibility, the installation of RES is not feasible. The payback period of the system configuration exceeds the project period. The idea of on-site electricity production will not be able to convince the owners of the building to make renovation with RES simply for the sake of it. To increase such interest, the government should introduce special tariffs for the green on-site electricity generation. Moreover, a reduction of energy storage prices may lead to an increase in the consumption of own electricity. This will make the system less dependent on the network, and in the future bring us to the point of refusing of purchasing of energy produced from fossil fuels.

The most effective type of renovation of the building in nZEB will be focusing on increasing efficiency of its energy consumption; this also includes its heating system. Consumption management will help to increase the fraction of renewables in the consumed energy. The latter could become a possible direction for further development of this research.

9 REFERENCES

[1] "Directive 2009/28/EC of the European Parliament and of the Council on the promotion of the use of energy from renewable sources," 23 04 2009. [Online]. Available: http://data.europa.eu/eli/dir/2009/28/oj. [Accessed 12 04 2018].

[2] "Buildings-European Comission," [Online]. Available: https://ec.europa.eu/energy/en/topics/energy-efficiency/buildings. [Accessed 12 04 2018].

[3] E. P. a. o. t. Council, "Directive 2010/31/EU," 19 04 2010. [Online]. Available: http://data.europa.eu/eli/dir/2010/31/oj. [Accessed 12 04 2018].

[4] M. o. t. Environment, "The National Building Code of Finland," 19 01 2017. [Online]. Available: http://www.ym.fi/en-US/Land_use_and_building/Legislation_and_instructions/The_National_Building_Code_of_Finland. [Accessed 12 04 2018].

[5] M. o. t. Environment, "Land Use and Building Act," 30 07 2013. [Online]. Available: http://www.ym.fi/en-US/Land_use_and_building/Legislation_and_instructions/The_Land_Use_and_Building_Act. [Accessed 12 04 2018].

[6] M. D. A. a. R. Hill, Clean electricity from photovoltaics, Imperial College Press, 2001.

[7] Solar Energy Industries Association, "Solar Market Insight Report 2015," Q1 2015. [Online]. Available: https://www.seia.org/research-resources/solar-market-insight-report-2015-q1. [Accessed 2 5 2018].

[8] IEA, (2015), OECD/IEA, Paris, "Medium-Term Renewable Energy Market Report," 2015. [Online]. Available: https://www.iea.org/bookshop/708-Medium-Term_Renewable_Energy_Market_Report_2015. [Accessed 22 03 2018].

[9] "Energy Aid. Climate and Environment Friendly Investment and Investigation projects," [Online]. Available: https://www.businessfinland.fi/en/for-finnish-customers/services/funding/sme/energy-aid/]. [Accessed 02 05 2018].

[10] K. Auvinen, "Solar & Wind Exchange Vaasa Energy Week, Solar power in Finland," Vaasa, Finland, 22 March 2017.

[11] M. Niininen, "Renewable energy sources produced 45 per cent of electricity and 57 per cent of heat," Statistics Finland, 2 11 2017. [Online]. Available: https://www.stat.fi/til/salatuo/2016/salatuo_2016_2017-11-02_tie_001_en.html. [Accessed 02 05 2018].

[12] Timo Hakkarainen, Eemeli Tsupari, Elina Hakkarainen & Jussi Ikäheimo VTT Technical Research Centre of Finland Ltd , "The role and opportunities for solar energy in Finland and Europe," 2015. [Online]. Available: http://www.vtt.fi/inf/pdf/technology/2015/T217.pdf . [Accessed 02 05 2018].

[13] U.-A. Hugo Ahlenius, "Solar insolation," [Online]. Available: http://old.grida.no/graphicslib/detail/solar-insolation_83d8. [Accessed 02 04 2018].

[14] "PVSyst 6 Manual," [Online]. Available: http://files.pvsyst.com/help/index.html. [Accessed 02 05 2018].

[15] "System Advisor Model (SAM)," NREL SAM U.S. Department of Energy Office of Energy Efficiency and Renewable Energy, [Online]. Available: https://sam.nrel.gov/. [Accessed 15 02 2017].

[16] W. F. Holmgren, "PVLib-python," [Online]. Available: https://github.com/pvlib/pvlib-python/. [Accessed 15 02 2017].

[17] J. L. H. Z. L. M. X. Z. F. Zhang, "On the relationship between direct and diffuse radiation," *Journal of Quantitative Spectroscopy and Radiative Transfer,* vol. 115, pp. 60-65, 2013.

[18] T. Haukkala, "Does the sun shine in the High North?Vested interests as a barrier to solar energy deployment in Finland," *Energy Research & Social Science,* vol. 6, pp. 50-58, 2015.

[19] H. H. Yinghong Qin, "A new simplified method for measuring the albedo of limited extent targets," *Solar Energy,* vol. 157, pp. 1047-1055, 2017.

[20] "Seasons in Finland," Finnish Metrological Institute, [Online]. Available: http://en.ilmatieteenlaitos.fi/seasons-in-finland. [Accessed 02 05 2018].

[21] "Meteonorm Software," [Online]. Available: http://www.meteonorm.com/en/downloads. [Accessed 02 05 2018].

[22] M. C.-P. R.J. Aguiar, "Time-dependent, Autoregressive, Gaussian Model for Generating Synthetic Hourly Radiation," *Solar Energy,* vol. 49, no. 3, pp. 167-174, 1992.

[23] M.-N. F. F. B. L. Scartezzini, "Compression of Multi-Year Meteorological Data," OFEN, Bern, 1990.

[24] A. D. Fontanini, "Contaminant transport at large Courant numbers using Markov matrices," *Building and Environment,* vol. 112, pp. 1-16, 2017.

[25] B. Marion, "A model for deriving the direct normal and diffuse horizontal irradiance from the global tilted irradiance," *Solar Energy,* vol. 112, pp. 1037-1046, 2015.

[26] F. D. Mehmet Emin Meral, "A review of the factors affecting operation and efficiency of photovoltaic based electricity generation systems," *Renewable and Sustainable Energy Reviews,* vol. 15, no. 5, pp. 2176-2184, 2011.

[27] C. S. C. E. R. M. C. Köhnke, " Observation of a 27-day solar signature in noctilucent cloud altitude," *Advances in Space Research,* vol. 61, no. 10, pp. 2531-2539, 2018.

[28] H. P. L. Dijkstra, "Regional typologies: a compilation," *Regional Focus,* vol. 1, 2011.

[29] H. M. R. K. a. E. D. H. Ossenbrink, "Standards in Photovoltaic Technology, In Comprehensive Renewable Energy," *Elsevier,* vol. Oxford, pp. 787-803, 2012.

[30] T. G. E. Society, Planning and installing photovoltaic systems: a guide for installers, architects, and engineers., Berlin: Deutsche Gesellshaft fur Sonnenenergie, 2008.

[31] A. L. a. S. Hegedus, Handbook of photovoltaic science and engineering, John Wiley & Sons, 2011.

[32] M. R. a. J. Royer, Photovoltaics in cold climates., James and James Science Publishers Ltd, 1999.

[33] F. I. f. S. E. Systems, "PHOTOVOLTAICS REPORT," ISE with support of PSE Conferences & Consulting GmbH, Freiburg, 26 February 2018.

[34] M. A. G. M. E. W. R. C. a. A. S. S. R. Wenham, "Applied photovoltaics," *Routledge,* vol. 2011.

[35] S. A. Kalogirou, "Solar energy engineering: processes and systems," *Academic Press,* 2009.

[36] Bruce, "Investigation of Cost and Performance Characteristic of Photovoltaic Panels," ENG 4111/4112, 2011.

[37] O. H. K. S. Yılmaz S, "The analysis of different PV power systems for the determination of optimal PV panel and system installation-A case study in Kahramanmaras," *Renewable and Sustainable Energy Reviews,* vol. 2015, no. 52, p. 1015–1024..

[38] L. Ş. Figen Baloa, "3rd International Conference on Power and Energy Systems Engineering," in *The selection of the best solar panel for the photovoltaic system design by using AHP*, Kitakyushu, 8-12 September 2016.

[39] "ENF List of Solar Companies and Products," [Online]. Available: https://www.enfsolar.com. [Accessed 24 03 2018].

[40] "Photocoltaic Trade Germany," [Online]. Available: http://www.photon-solar.eu/. [Accessed 22 03 2018].

[41] "GWL Power - Photovoltaic poly Mono and flexible solar panels," [Online]. Available: https://www.ev-power.eu/Solar-Panels/. [Accessed 22 03 2018].

[42] "PV solar panels, inverters, charge controllers," [Online]. Available: http://pvshop.eu/. [Accessed 23 03 2018].

[43] A. Ibrahim, "Effect of Shadow and Dust on the Performance of Silicon Solar Cell," *Journal of Basic and Applied Sciences Research,* vol. 1, no. 3, pp. 222-230, 2011.

[44] Axitec, "AXIpremium AC-290M/156-60S Datasheet," [Online]. Available: https://www.axitecsolar.com/data/solarpanels_documents/DB_60zlg_mono_premium_MiA_EN.pdf. [Accessed 25 01 2017].

[45] M. A. M. I. Saeed Edalati, "Comparative performance investigation of mono- and poly-crystalline silicon photovoltaic modules for use in grid-connected photovoltaic systems in dry climates," *Applied Energy,* vol. 160, p. 255–265, 2015.

[46] Ö. T. Ö. N. T. O. K. Erdem Elibol, "Outdoor performance analysis of different PV panel types," *Renewable and Sustainable Energy Reviews,* vol. 67, p. 651–661, 2017.

[47] A. M. e. ,. M. A. A. Guenounou, "Comparative performance of PV panels of different technologies over one year of exposure: Application to a coastal Mediterranean region of Algeria," *Energy Conversion and Management,* vol. 114, p. 356–363, 2016.

[48] J.-B. S. Matthias Eichelbrönner, "German Experience on the Support Mechanism and Technical Aspects of Grid Connectivity of Solar PV Rooftop-Systems," Deutche Gasellschaft fur Internationale Zusammenarbeit, 2012.

[49] J. M. D. Hay, " Estimating solar irradiance on inclined surfaces: a review and assessment of methodologies," *Int. J. Solar Energy ,* vol. 3, p. 203–240, 1985.

[50] S. M. D. Hamid Moghadam, "Determination of optimum location and tilt angle of solar collector on the roof buildings with regard to shadow of adjacent neighbors," *Sustainable Cities and Society,* vol. 14, pp. 215-222, 2015.

[51] X. Y. D. Y. D. Q. Chengquan Xiao, "Impact of solar irradiance intensity and temperature on the performance of compensated crystalline silicon solar cells," *Solar Energy Materials and Solar Cells,* vol. 128, pp. 427-434, 2014.

[52] " Sun position and elevation online tool," [Online]. Available: https://www.sunearthtools.com/dp/tools/pos_sun.php. [Accessed 28 04 2018].

[53] K. N. Y. H. J. S. H. W. D. Y. Ruidong Xu, "Analysis of the optimum tilt angle for a soiled PV panel," *Energy Conversion and Management,* vol. 148, pp. 100-109, 2017.

[54] D. P. S. I. G. N. C. S. R. Potnuru, "Positioning of PV panels for reduction in line losses and mismatch losses in PV array," *Renewable Energy,* vol. 78, pp. 264-275, 2015.

[55] L. P. Z. J. P. G. Chamberlin CE, "Effects of mismatch losses in photovoltaic arrays," *Solar Energy Elsevier,* vol. 54(3), pp. 165-71, 1995.

[56] R. B. B. S. d. l. C. J. A. J. Picault D, "Forecasting photovoltaic array power production subject to mismatch losses," *Solar Energy,* vol. 84, no. 7, 2010.

[57] R. A. Kaushika ND, "An investigation of mismatch losses in solar photovoltaic cell networks," *Energy ,* vol. 32, no. 5, 2007.

[58] G. D. L. S. A. Acciari G, "Higher PV module efficiency by a novel CBS bypass," *IEEE Trans Power Electron,* vol. 26, no. 5, 2011.

[59] "Municipal Register of the City of Helsinki," [Online]. Available: https://asiointi.hel.fi/arska/. [Accessed 12 01 2017].

[60] "Helsinki City Plan," [Online]. Available: kartta.hel.fi/yleiskaava. [Accessed 15 01 2017].

[61] T. M. U. W. P. R. Ned Mohan, Power Electronics. Converters, Applications and Design, John Wiley and Sons, Inc, 2003.

[62] R. V. E. F. F. .M. Rodrigo, "DC/AC conversion efficiency of grid-connected photovoltaic inverters in central Mexico,," *Solar Energy,* vol. 139, pp. 650-665, 2016.

[63] G. Marsh, "Partner in power: Part two: Whilst the micro-inverter revolution looks set to spread, central and string inverters remain the mainstream," *Renewable Energy Focus,* vol. 12, no. 3, 2011.

[64] H. S. K. D. B. Joydip Jana, "A review of inverter topologies for single-phase grid-connected photovoltaic systems," *Renewable and Sustainable Energy Reviews,,* vol. 72, pp. 1256-1270, 2011.

[65] N. D. R.-B. M. I. M.-P. Héctor Báez-Fernández, "Selection and configuration of inverters and modules for a photovoltaic system to minimize costs," *Renewable and Sustainable Energy Reviews,* vol. 58, pp. 16-22, 2016.

[66] G. D. M. A. D. V. Witold Marańda, "Optimization of the master–slave inverter system for grid–connected photovoltaic plants," *Energy Conversion and Management,,* vol. 39, no. 12, pp. 1239-1246, 1998.

[67] A. T. A. T. Özgür Çelik, "Overview of micro-inverters as a challenging technology in photovoltaic applications," *Renewable and Sustainable Energy Reviews,* vol. 82, no. 3, pp. 3191-3206, 2018.

[68] "AE 1TL 1.8-4.2 kW Datasheet," 2017. [Online]. Available: https://cdn.enfsolar.com/Product/pdf/Inverter/53ce0ecb58d98.pdf. [Accessed 28 11 2017].

[69] "Climate Elements," Finnish metrological Institute, [Online]. Available: http://en.ilmatieteenlaitos.fi/climate-elements. [Accessed 02 05 2018].

[70] Timothy Dierauf, Aaron Growitz, Sarah Kurtz National Renewable Energy Laboratory, "Weather-Corrected Performance," 04 2013. [Online]. Available: https://www.nrel.gov/docs/fy13osti/57991.pdf. [Accessed 13 07 2017].

[71] D. P. Sadh, Studies About Wind Energy, Porto Alegre: Department of Mechanical Engineering, 1983.

[72] A. Barbieri, "Small wind turbines: navigating the 'jungle'," 14 03 2017. [Online]. Available: https://cordis.europa.eu/news/rcn/139275_en.html. [Accessed 06 05 2018].

[73] "Press Releases Statistics," World Wind Energy Association, 12 02 2018. [Online]. Available: http://www.wwindea.org/2017-statistics/. [Accessed 03 05 2018].

[74] "Lag om stöd till produktion av el från förnybara energikällor," 10 12 2010. [Online]. Available: http://www.finlex.fi/sv/laki/alkup/2010/20101396. [Accessed 03 05 2018].

[75] "World Energy Balances 2017: Overview," International Energy Agency (IEA), 4 08 2017. [Online]. Available: https://webstore.iea.org/world-energy-balances-2017-overview. [Accessed 03 05 2018].

[76] T. I. E. Commission, "IEC 61400-2 standard. Part 2: Design requirements for small wind turbines".

[77] F. School, "Global trends, the urban usage of small turbines," UNEP Centre, Frankfurt am Main, 2016.

[78] N. D. H. O. R. a. M. N. Mortensen, Wind Atlas Analysis and Application Program: WAsP 11 Help Facility, Roskilde: Department of Wind Energy, Technical University of Denmark (DTU), 2014.

[79] P. A. T. H. W. Taylor, "The Askervein Hill project: Overview and background data," *Boundary-Layer Meteorology,* vol. 39, no. 1, pp. 15-39, 1987.

[80] "File service of open data," National Land Survey of Finland, [Online]. Available: https://tiedostopalvelu.maanmittauslaitos.fi/tp/kartta?lang=en. [Accessed 04 05 2018].

[81] M. Zhang, Encyclopedia of Atmospheric Sciences , Coupled Ocean-Atmosphere Models: Physical Processes, Academic Press, 2015.

[82] Alphabet Inc., "Google Maps," [Online]. Available: https://www.google.com/maps. [Accessed 05 08 2017].

[83] "Windpotentieel en de bebouwde omgeving," Turby, [Online]. Available: https://www.turby.nl/windenergie/wind-en-omgeving/. [Accessed 16 02 2017].

[84] L. B. R. S. S. M. J. N Meroney R, "Wind-tunnel and numerical modeling of flow and dispersion about several building shapes," *Wind Eng Ind Aerodyn,* vol. 81, no. 1, p. 333, 1999.

[85] S. Ş. Ayhan D, "A technical review of building-mounted wind power systems and a sample simulation model," *Renew Sustain Energy,* vol. 16, no. 1, p. 1040, 2012.

[86] H. N. D. S. Abohela I, "Effect of roof shape, wind direction, building height and urban configuration on the energy yield and positioning of roof mounted wind turbines," *Renew Energy,* p. 1106–1118, 2013.

[87] A. a. N. M. Bowen, "Exploring the limits of WAsP: the Wind Atlas Analysis and Application Program," in *European Union Wind Energy Conference*, Goteborg, 1996.

[88] J. L. H. Z. L. M. X. Z. Feng Zhang, "On the relationship between direct and diffuse radiation," *Journal of Quantitative Spectroscopy and Radiative Transfer,,* vol. 115, pp. 60-65, 2013.

[89] B. Fox, D. Flynn, L. Bryans, N. Jenkins, D. Milborrow, M. O'Malley, R. Watson and O. Anaya-Lara, Wind Power Integration: Connection and system operational aspects, 2014.

[90] Technical University of Denmark (DTU Wind Energy), "Global Solar Atlas," [Online]. Available: https://globalwindatlas.info/. [Accessed 22 07 2017].

[91] B. e. a. Tammelin, "Production of the Finnish Wind Atlas," *Wind Energy,* no. doi: 10.1002/we.517, 2011.

[92] J. S. R. a. V. Nelson, Wind Characteristics: An Analysis for Generation of Wind Power, Canyon: Alternative Energy Institute, West Texas A&M University, 1994.

[93] M. M. J. U. A. A. Alo Allik, "Optimization of the inverter size for grid-connected residential wind energy systems with peak shaving,," *Renewable Energy,* vol. 99, pp. 1116-1125, 2016.

[94] R. G. Iain Staffell, "How does wind farm performance decline with age?," *Renewable Energy,* vol. 66, pp. 775-786, 2014.

[95] J. K. L. M. A. H. Clara M St. Martin, "Variability of interconnected wind plants: correlation length and its dependence on variability time scale," *Environmental Research Letters,* vol. 10, no. 4, 2015.

[96] A. F. Siegel, Practical Business Statistics (Seventh Edition), Seattle: Elsevier, 2016.

[97] F. Z. J. Y. S. E. L. K. W. S. Chirag Deb, "A review on time series forecasting techniques for building energy consumption,," *Renewable and Sustainable Energy Reviews,* vol. 74, pp. 902-924, 2017.

[98] "Electricity load forecasting for residential customers: Exploiting aggregation and correlation between households," *Sustainable Internet and ICT for Sustainability,* pp. 30-31, 2013.

[99] "Crystal Ball Reference and Examples Guide," Oracle , [Online]. Available: https://docs.oracle.com/cd/E57185_01/CBREG/ch06s03s04s01.html. [Accessed 26 01 2018].

[100] C. F. T. A. a. B. S. H. Meier, "Representative VDEW-Last profile," *VDEW,* 1999.

[101] "Energy supply and consumption," Finland Statistics, [Online]. Available: https://www.stat.fi/til/ehk/index_en.html. [Accessed 16 08 2017].

[102] "Statistical databases," [Online]. Available: http://stat.fi/tup/tilastotietokannat/index_en.html. [Accessed 04 03 2018].

[103] "Electricity distribution tariffs," 07 01 2016. [Online]. Available: https://www.helensahkoverkko.fi/globalassets/hinnastot-ja-sopimusehdot/hsv---enkku/distribution-tariffs.pdf. [Accessed 21 08 2016].

[104] "Energy taxation," Vero, 29 12 2016. [Online]. Available: https://www.vero.fi/en/detailed-guidance/guidance/56206/energy_taxation/. [Accessed 13 08 2017].

[105] E. Lehto, "Electricity prices in the Finnish retail market," *Energy Policy,* vol. 39, no. 4, pp. 2179-2192, 2011.

[106] "Electricity market," Ministry of Economic Affairs and Employment, [Online]. Available: http://tem.fi/en/electricity-market.

[107] L. S. Genaro Longoria, "Nash-equilibrium electricity portfolios in the smart grid: A genetic annealing solution," in *Smart Grid and Cities Congress and Fair*, Istambul, 2017.

[108] "Electricity price statistics," Eurostat, 11 2017. [Online]. Available: http://ec.europa.eu/eurostat/statistics-explained/index.php/Electricity_price_statistics. [Accessed 03 08 2017].

[109] E. L. S. Karkkainen, "Liberalisation of the electricity market in Finland as a part of Nordic market," *IEE Proceedings - Generation, Transmission and Distribution ,* vol. 148, no. 2, pp. 194-199, 2001.

[110] "Trading," Nord Pool AS, [Online]. Available: https://www.nordpoolgroup.com/TAS/. [Accessed 29 07 2017].

[111] F. O. Steen Koekebakker, "Forward curve dynamics in the Nordic electricity market Norway," *Norwegian School of Economics and Business Administration,* 2001.

[112] M. K. Ronald Huisman, "Futures Prices: Indirect Storability, Expectations, and Risk Premiums," *Energy Economics,* vol. 43, pp. 892-898, 2012.

[113] E. F. F. a. K. R. French, "Commodity Futures Prices: Some Evidence on Forecast Power," *Premiums, and the Theory of Storage ,* vol. 60, no. 1, pp. 55-73, 1987.

[114] O. &. B. T.-L. Gjolberg, "The biased short-term futures price at Nord Pool: can it really be a risk premium?," *Energy Res. Mark,* vol. 4, 2011.

[115] "Thomson Reuters Datastream," [Online]. Available: https://financial.thomsonreuters.com/en/products/tools-applications/trading-investment-tools/datastream-macroeconomic-analysis.html. [Accessed 17 05 2017].

[116] M. S. Islam, "A techno-economic feasibility analysis of hybrid renewable energy supply options for a grid-connected large office building in southeastern part of France," *Sustainable Cities and Society,* vol. 38, pp. 492-508, 2018.

[117] "HOMER Pro 3.11 User Manual,," 28 11 2017. [Online]. Available: https://www.homerenergy.com/products/pro/docs/3.9/index.html. [Accessed 06 03 2018].

[118] "Freight Calculator," World Freight Rates , [Online]. Available: http://worldfreightrates.com/en/freight. [Accessed 05 03 2018].

[119] "Sea Rates," [Online]. Available: https://www.searates.com/. [Accessed 05 03 2018].

[120] "Freight Rate Calculator," [Online]. Available: https://www.freightos.com/portfolio-items/freight-rate-calculator-free-tool/. [Accessed 05 03 2018].

[121] Fraunhofer-Institute for Solar Energy Systems , "Current and Future Costs of Photovoltaics," 02 2015. [Online]. [Accessed 08 03 2017].

[122] "Aurinkopaneelin asennus," [Online]. Available: https://solarvoima.fi/aurinkopaneelin-asennus/. [Accessed 08 03 2017].

[123] "Aurinkopaneelit," Fortum, [Online]. Available: https://www.fortum.fi/aurinkopaneelit. [Accessed 16 03 2017].

[124] "djustable Roof Mounting System," ENF, [Online]. Available: https://www.enfsolar.com/pv/mounting-system-datasheet/4047?utm_source=ENF&utm_medium=mounting_system_list&utm_campaign=enquiry_product_directory&utm_content=41359. [Accessed 01 05 2018].

[125] "Industrial Cable," Belden, [Online]. Available: https://www.belden.com/products/industrial/cable. [Accessed 02 05 2018].

[126] W. B. &. C. Hepburn, "Ethics of the Discount Rate in the Stern Review on the Economics of Climate Change," *World Economics,* vol. 8, no. 1, pp. 190-190=2, 2007.

[127] "Impact Assessment accompanying the Communication from the European Commission: A policy framework for climate and energy in the period from 2020 to 2030," European Commission, 2014.

[128] R. E. T. F. M. K. B. P. M. R. e. a. S. Braungardt, "Study evaluating the current energy efficiency policy framework in the EU and providing orientation on policy options for realising the cost-effective energy efficiency / saving potential until 2020 and beyond," raunhofer ISI, TU Vienna, PWC on behalf of DG ENER, Vienna, 2014.

[129] M. Dupuy, "Hidden Barriers to Efficiency. The Treatment of Discount Rates and Energy Efficiency Costs in EU Policy Scenarios.," 15 05 2015. [Online]. Available:

http://www.raponline.org/knowledge-center/hidden-barriers-to-efficiency-the-treatment-of-discount-rates-and-energy-efficiency-costs-in-eu-policy-scenarios/. [Accessed 05 05 2018].

[130] "Discount rates for low-carbon and renewable generation technologies," Oxera, 2011. [Online]. Available: https://www.oxera.com/Latest-Thinking/Publications/Reports/2011/Discount-rates-for-low-carbon-and-renewable-genera.aspx. [Accessed 02 05 2018].

[131] "Upswing more broadly based – Improved chances for balanced growth in Finland," 05 2017. [Online]. Available: https://www.bofbulletin.fi/en/2017/5/forecast-upswing-more-broadly-based-improved-chances-for-balanced-growth-in-finland/. [Accessed 03 05 2018].

10 APPENDIXES

Appendix 1: Thesis organization chart

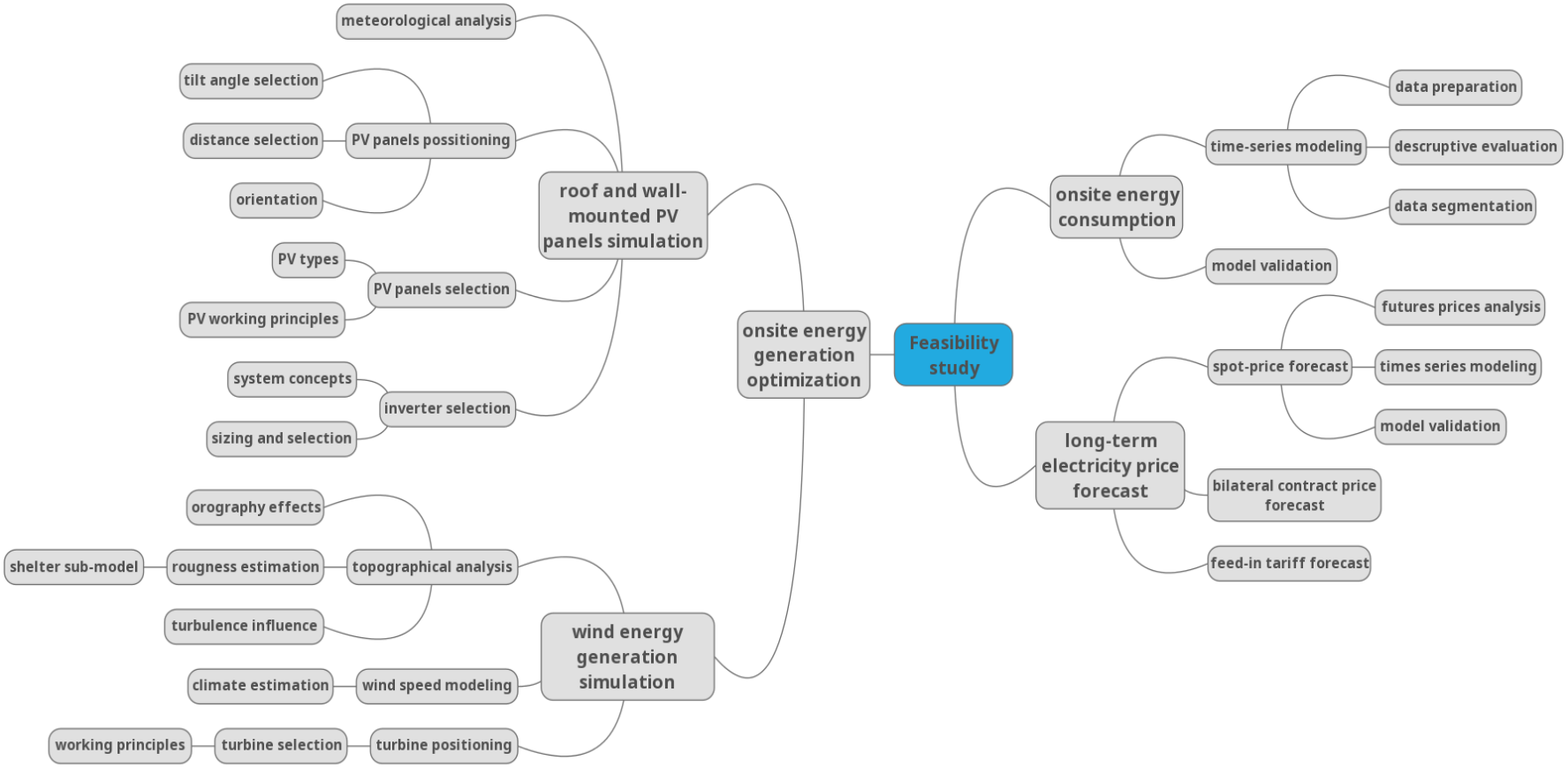

Appendix 2: PV panels characteristics comparison table

Model	Cell type	Rated power [W]	Efficiency at STC [%]	V_{oc} at STC [V]	I_{sc} at STC [A]	Price [€/W]	Dimensions [mm]	Performance warranty (min 80%) [years]	Rated Power characteristic (400 W/m², t=25C°) [W]
AXIpremium AC-290M/ 156-60S	mono-Si	290	17.83	39.7	9.7	0.38	1360x954x35	25	109
Q.Plus BFR-G4.1 275-285	poly-Si	275	16.5	38.7	9.35	0.53	1670x1000x32	25	98
AXIpremium AC-265M/ 156-60S	mono-Si	265	15.98	38.3	9.06	0.38	1360x954x35	25	95
SCM-FB-280	mono-Si	280	17.11	39.5	9.2	0.52	1640x992x40	30	109
Sunny-320P	poly-Si	320	16	45.5	9.01	0.4	1956x992x45	25	69
SC-270	poly-Si	270	18.5	38	9.26	0.41	1640x992x40	30	100
TM-660265/ 285	mono-Si	285	17.53	39.0	9.26	0.33	1640x992x35	30	102
P-60 LX-265P	poly-Si	265	15.08	37.5	8.87	0.5	1682x1000x41	30	92
LX-275M	mono-Si	275	17.42	38.4	9.3	0.42	1658x990x51	25	101
AS-6P30	poly-Si	270	16.9	38.4	9.06	0.48	1640x992x40	25	105

Appendix 3: System concepts: central inverter (upper left), master-slave (upper-right), module inverter (lover left) and subarray string inverter (lover right)

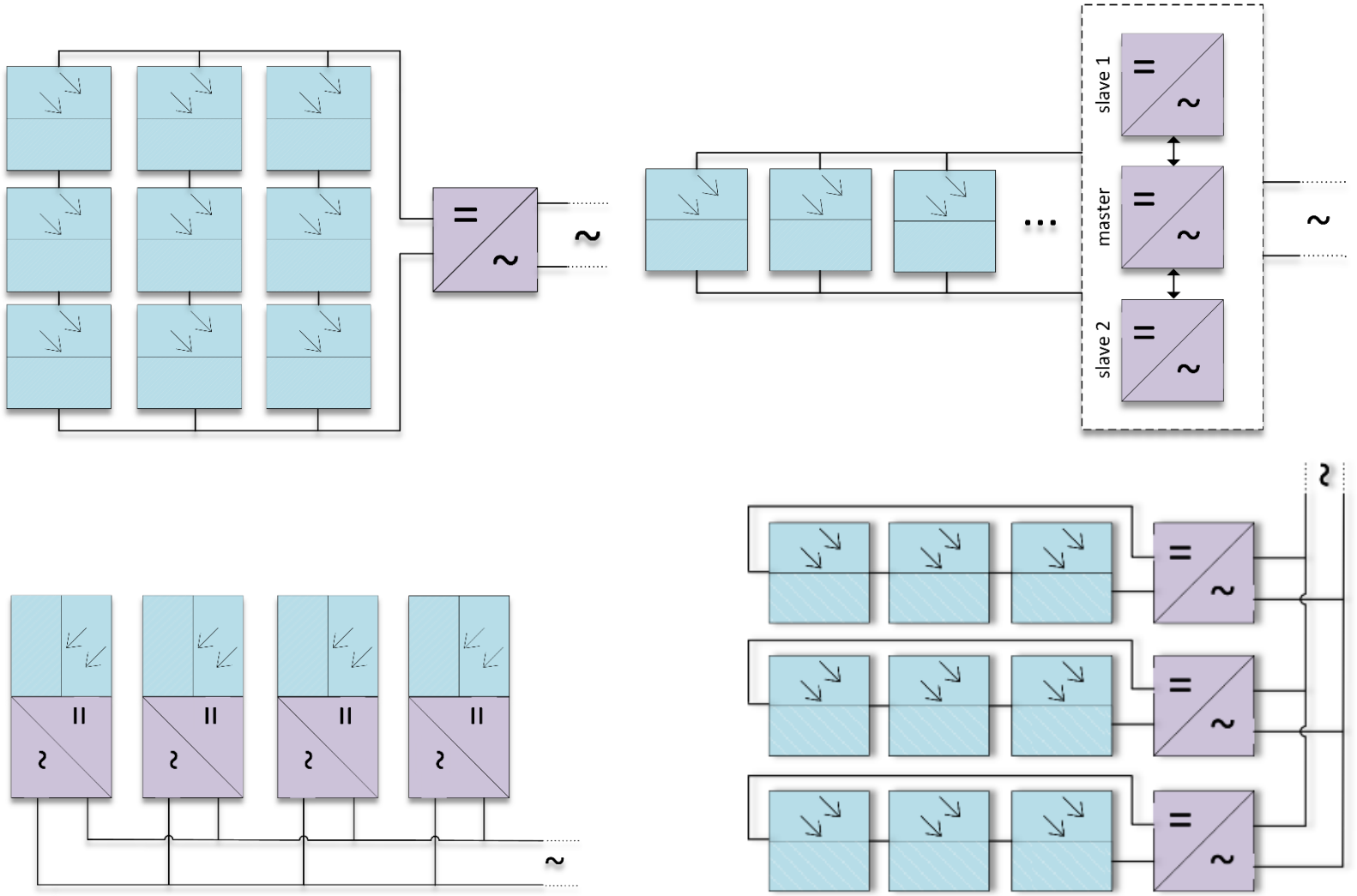

Appendix 4: Electrical layout between wall-mounted panels and inverters

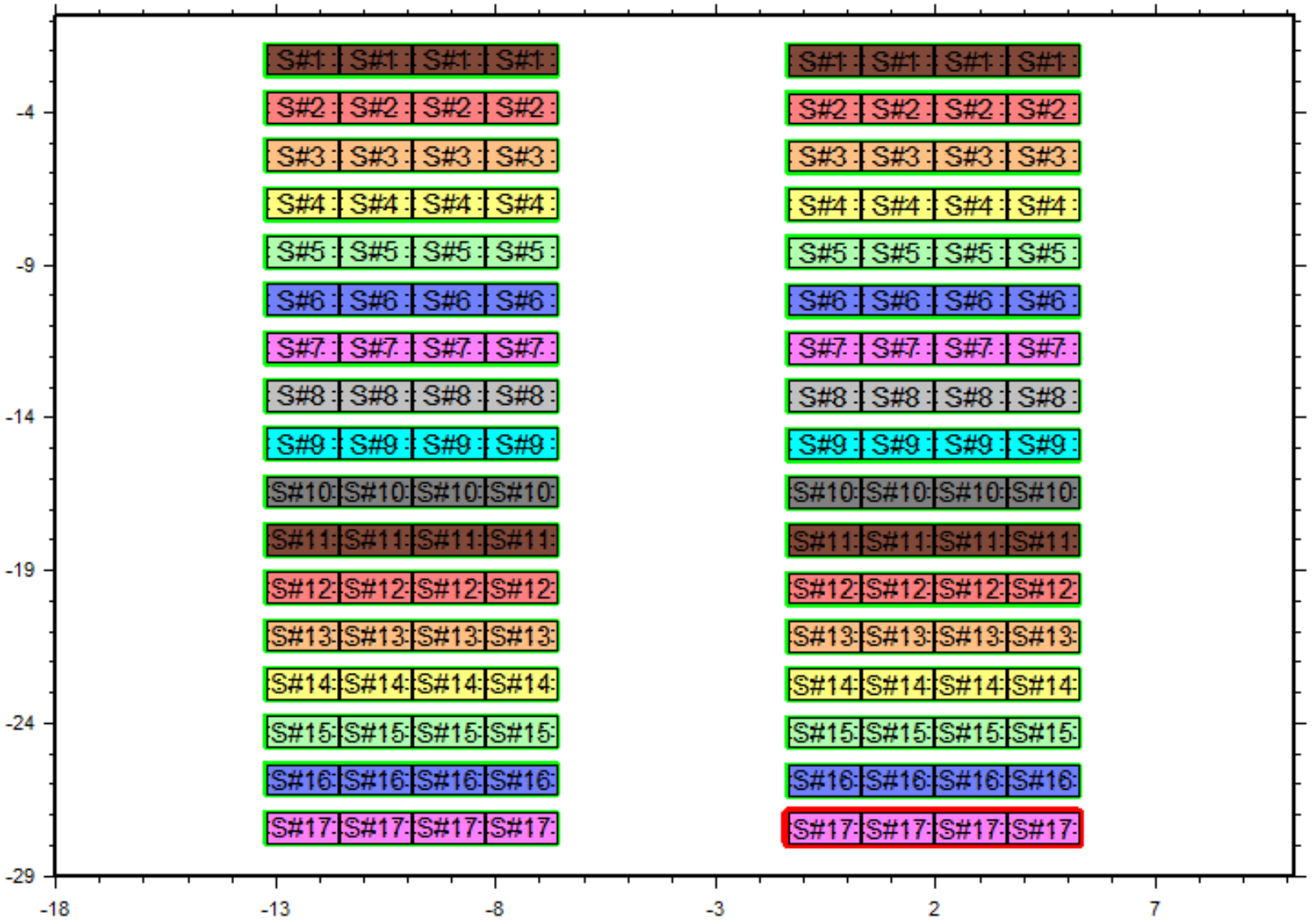

Appendix 5: Electrical layout between roof-mounted panels and inverters

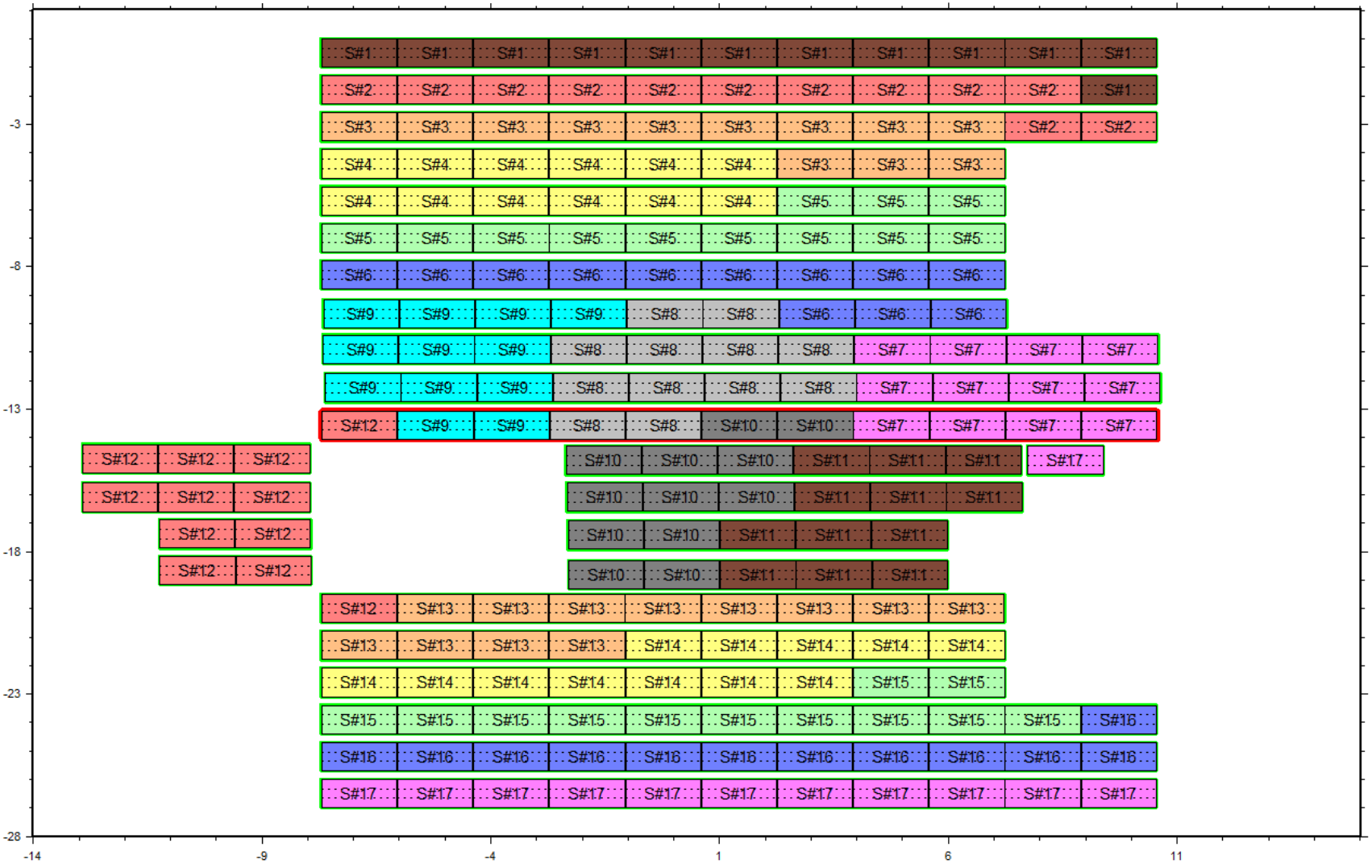

Appendix 6: Landscape roughness classes

RC	Roughness Length, Z_0 [m]	Energy Index [%]	Landscape description
0	0.0001	100	Water, sea surface
0.5	0.0024	73	Open terrain with a glazed surface, e.g. airport runway
1	0.03	52	Farmland
1.5	0.055	45	Farmland with short structures within a 1.25 km radius
2	0.1	39	Farmland with short structures within a 0.5 km radius
2.5	0.2	31	Farmland with many structures, trees, and bushes within a 250-meter radius.
3	0.3	24	Suburbs or small town with may structures, rough and uneven terrain
3.5	1	18	Large cities, tall structures.
4	1.6	13	Very large cities, very tall structures

Appendix 7: Wind turbine characteristics comparison table

Model	AV-7	Qr6	SA40	Skystream 3.7	Proven6
Rotor type	HAWT	VAWT	VAWT	HAWT	HAWT
Rated capacity [kW]	6.253	7.5	10	2.1	6
Wind speed at nominal capacity [m/s]	7.5	13	15	11	11
Cut in wind speed [m/s]	2	4.5	4.5	3	2.5
Swept area [m^2]	129	16	40	20.1	23.7
Power at 5 m/s wind speed [kW]	3.1	0.5	0.5	0.2	1.1
Noise (wind speed = 8m, distance =30m) [dBA]	40	n\a	40	41.2	45
On roof max tower height [m]	15	6	12	11	9
Price [€]	93000	41510	28600	13500	24400
Maintenance [€]	2350	750	800	300	600
Generator type	Permanently excited	Permanently excited	Permanently excited	Permanently excited	Permanently excited
Inverter	Preinstalled	Preinstalled	Preinstalled	Preinstalled	Preinstalled

Appendix 8: Wind turbine simulation results

Sector		**Wind climate**				**Power**
#	angle, [°]	frequency, [%]	$A_{weibull}$	$k_{weibull}$	mean speed, [m/s]	power density, [W/m²]
1	0	6.4	4.8	2.27	4.22	78
2	30	5.4	4.4	2.24	3.91	63
3	60	3.7	4	2.27	3.57	48
4	90	7.6	5.5	2.33	4.91	121
5	120	6.7	4.7	1.9	4.14	88
6	150	7.5	4.6	1.69	4.12	99
7	180	9.1	5	1.97	4.41	102
8	210	11.9	5.5	2.46	4.88	114
9	240	12.7	4.9	1.97	4.38	100
10	270	9.6	4.9	2.15	4.35	90
11	300	10.1	5.4	2.31	4.78	112
12	330	9.2	5.3	2.63	4.73	99
	All (emergent)				4.45	97

Appendix 9: Electricity price comparison

Seller	Monthly fee [EUR]	Long-term (2 year) contract electricity price [c\kWh]	Market-based contract fee [c\kWh]	Trade in fee [c\kWh] excl. VAT
Vattenfall Oy	2.7	4.72	0.29	n/a
Lumme Energia Oy	2.99	4.67	0.25	n/a
Pori Energia Oy	2.5	5.2	0.35	n/a
Jyväskylän Energia Oy	0.89	4.59	0.3	n/a
Kokkolan Energia Oy	2.5	4.96	0.31	n/a
Oulun Sähkönmyynti Oy	3.5	5.08	0.25	n/a
Fortum Oy	4.02	4.99	0.3	0.24
Lappeenrannan Energia Oy	2.7	4.65	0.35	0.3
Savon Voima Oyj	3.98	4.98	0.25	n/a
Valkeakosken Energia Oy	3.5	4.85	0.33	0.35
Sallila Energia Oy	3.6	4.77	0.4	n/a
Helen Oy	3.84	4.79	0.24	0
Imatran Seudun Sähkö Oy	2.5	5.05	0.31	0.2
Porvoon Energia Oy	3	4.74	0.25	0.3
Korpelan Energia Oy	1.24	5.01	n/a	n/a

Appendix 10: RES price breakdown

	Wind turbine	**Roof-mounted PV**	**Wall-mounted PV**
Number of generation units [pcs]	1	204	136
Price per unit	93000.00	136.65	136.65
Sipping costs	10557.26	2787.66	1858.44
Total generation costs	**102300.00**	**30664.26**	**20442.84**
Number of invertors [pcs]	-	17	17
Price per unit	-	342.99	262.95
Shipping costs	-	874.62	670.52
Total inverter costs	**-**	**6705.45**	**5140.67**
Number of PV tables [pcs]	**-**	30	17
Price per unit	**-**	52.00	52.00
Shipping costs	**-**	156.00	88.40
Total tables costs	**-**	**1716.00**	**972.40**
Total cabling costs	**231.59**	**1581.60**	**1265.28**
Installation costs	**14122.48**	**14233.56**	**11128.48**
Overall costs	117911.33	54900.87	38949.67
Government subsidy [%]	22.25	25.00	25.00
Subsidized overall costs	**91676.06**	**41175.66**	**29212.25**
Maintenance annual costs	**2350.00**	**1921.53**	**1363.24**

Appendix 11: System optimizations breakdown

Type of contract	Grid	Wind Turbine	Roof-mounted PV	Wall-mounted PV	Energy storage	Cost/LCOE [EUR kWh]	Cost/NPC [EUR]	Operating costs [EUR/yr]	Initial capital [EUR]	System/ Ren Frac [%]	Storage/ Annual Throughput [kWh/yr]	Grid/ Energy Purchased [kWh]	Grid/ Energy Sold [kWh]
Fixed	1					0.143	159593.50	10419.02	0.00	0.00		75780.38	0.00
Fixed	1			1		0.140	171597.20	9295.56	29212.25	29.22		58659.93	6383.97
Fixed	1				1	0.157	174334.90	10950.53	6600.00	0.00	0.54	75779.86	0.00
Fixed	1		1			0.127	178483.80	8964.13	41175.66	41.62		54740.88	17353.56
Fixed	1			1	1	0.152	180938.90	9474.55	35812.25	29.83	2064.94	56700.96	4207.91
Fixed	1		1		1	0.137	187252.80	9105.73	47775.66	42.58	2507.79	52361.79	14710.69
Fixed	1		1	1		0.122	210100.70	9121.11	70387.91	55.16		50344.48	36461.58
Fixed	1		1	1	1	0.131	217673.80	9184.64	76987.91	56.64	3307.33	47206.88	32975.92
Fixed	1	1				0.221	246856.00	10131.00	91676.00	26.70		56366.00	165.00
Fixed	1	1			1	0.233	259185.00	10505.00	98276.00	26.80	149.00	56225.00	9.41
Fixed	1	1		1		0.203	263430.00	9306.00	120888.00	50.70		43061.00	10365.00
Fixed	1	1		1	1	0.218	271778.00	9420.00	127488.00	52.20	2722.00	40479.00	7497.00
NPS	1					0.133	147552.80	9632.94	0.00	0.00		75780.38	0.00
NPS	1			1		0.132	161919.80	8663.77	29212.25	29.22		58659.93	6383.97
NPS	1				1	0.146	162294.30	10164.46	6600.00	0.00	0.54	75779.86	0.00
NPS	1		1			0.120	169467.00	8375.46	41175.66	41.62		54740.88	17353.56
NPS	1			1	1	0.144	171584.20	8863.83	35812.25	29.82	2034.10	56730.21	4240.42
NPS	1		1		1	0.131	178825.00	8555.52	47775.66	42.53	2404.68	52459.60	14819.37
NPS	1		1	1		0.117	201503.00	8559.81	70387.91	55.16		50344.48	36461.58
NPS	1		1	1	1	0.126	209779.40	8669.26	76987.91	56.57	3180.41	47327.29	33109.71
NPS	1	1				0.213	238355.00	9576.00	91676.00	26.90		56110.00	0.00
NPS	1	1			1	0.326	363121.00	13478.00	156676.00	26.90	187.00	56109.21	3.81
NPS	1	1		1		0.200	255161.00	8766.00	120888.00	51.40		41989.00	9408.00
NPS	1	1		1	1	0.319	371622.00	12126.00	185888.00	55.20	6299.00	36014.00	2425.00

Appendix 12: Generation and consumption of studied site during week 15 (upper left), week 26 (upper right), week 38 (lover left) and week 3 (lower right)

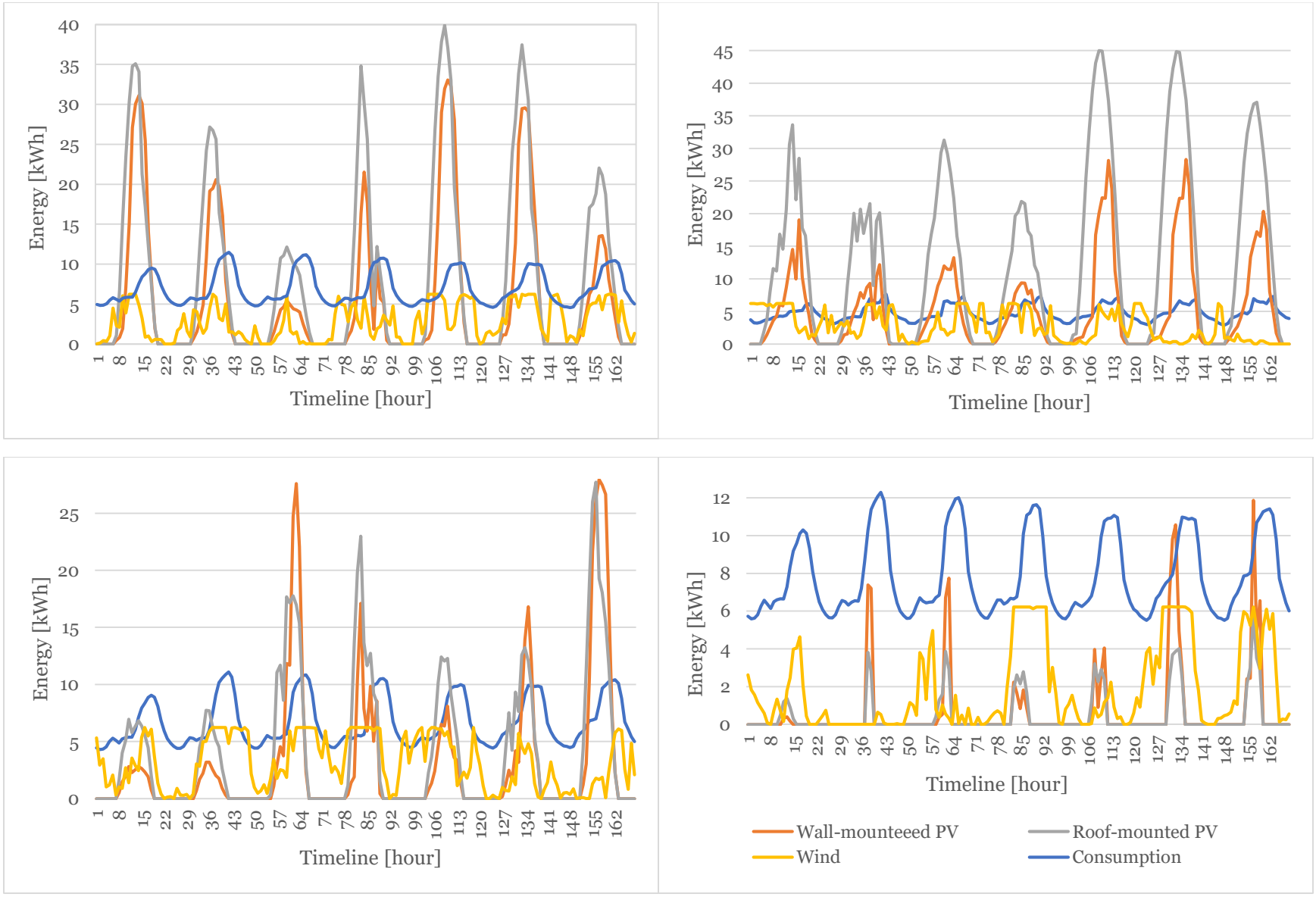

Appendix 13: System sensitivity analysis results